

# **Spreader-bar Technology: A Strategy for Formation of Stable Nanostructured Surfaces**

Dissertation zur Erlangung des Doktorgrades der Naturwissenschaften

(Dr. rer. nat.)

an der Fakultät für Chemie und Pharmazie

der Universität Regensburg



vorgelegt von

Thomas Hirsch

aus Pocking (Landkreis Passau)

Juni 2008

This work was performed at the Institute of Analytical Chemistry, Chemo- and Biosensors of the University of Regensburg between September 2000 and May 2008 in the frame of a DFG project (two years) and a Volkswagen project (one year) under the supervision of Prof. Dr. Otto Wolfbeis.

Promotionsgesuch eingereicht am: 13. Juni 2008

Kolloquiumstermin: 15. Juli 2008

Prüfungsausschuss:	Vorsitzender:	Prof. Dr. Jörg Daub
	Erstgutachter:	Prof. Dr. Otto S. Wolfbeis
	Zweitgutachter:	Prof. Dr. Vladimir M. Mirsky
	Drittprüfer:	Prof. Dr. Werner Kunz

# Acknowledgements

I want to express my most profound gratitude to the following people who contributed to the completion of my dissertation:

First of all, I am very grateful to my supervisor Prof. Dr. Otto S. Wolfbeis, who gave me the opportunity to carry out my thesis at the Institute of Analytical Chemistry, Chemo- and Biosensors of the University of Regensburg. He offered help and support whenever I needed it.

I gratefully acknowledge the extensive help of Prof. Dr. Vladimir M. Mirsky, his helpful ideas, largely contributing to the completion of this thesis, and his open-minded personality during many discussions on or off matters of chemistry.

I gratefully appreciate financial support of the Volkswagen Foundation and the DFG making this thesis possible.

I am likewise thankful to the following people for the help and support of this work:

Hubert Kettenberger and Mamantos Prodromidis for numerous measurements of receptor properties of the spreader-bar systems.

Joachim Stahl of the Institute of Experimental and Applied Physics, University of Regensburg, for SEM measurements.

PD Dr. Michael Zharnikov from Institute of Applied Physical Chemistry (IAPC), University of Heidelberg for doing the X-ray and NEXAFS spectroscopy.

Dr. Edith Schnell from the Institute of Physical and Theoretical Chemistry, University of Regensburg for the accomplishment of the AFM studies.

Dr. Vladimir Portnov for the theoretical modeling of the binding site.

Furthermore, I would like to thank Angela Haberkern and Joachim Rewitzer for technical assistance during this work and the wonderful personal assistance in any adverseness of everyday life. I want to thank Edeltraud Schmid for her friendly assistance in any official or personal business.

I very much enjoyed working at the Institute of Analytical Chemistry, Chemo- and Biosensors with its unique familiar atmosphere and generous working conditions. I would like to thank all the people who worked at this institute during the course of my PhD studies and made it a pleasure for me to be there!

# Table of Contents

<b>1. Introduction.....</b>	<b>1</b>
1.1 References .....	6
<b>2. Aim of the work.....</b>	<b>11</b>
<b>3. Ultrathin layers adsorbed on substrates.....</b>	<b>13</b>
3.1 Ultrathin layers.....	13
3.2 Monomolecular layer .....	14
3.3 Alkanethiol monolayers on gold .....	16
3.3.1 Adsorption kinetics .....	17
3.3.2 Order and geometry .....	19
3.3.3 Defects in and stability of the monolayer .....	20
3.4 Mixed monomolecular layers .....	21
3.5 Spreader-bar system.....	21
3.5 Summary .....	25
3.6 References .....	25
<b>4. Methods of surface characterization.....</b>	<b>32</b>
4.1 Contact angle measurement.....	34
4.2 Electrochemistry of monomolecular surfaces .....	36
4.2.1 Electrochemical impedance spectroscopy.....	36
4.2.2 Cyclic voltammetry .....	41

4.3 X-ray photoelectron spectroscopy (XPS).....	42
4.4 NEXAFS spectroscopy .....	45
4.5 Infrared spectroscopy.....	46
4.6 Surface plasmon resonance .....	50
4.7 Ellipsometry.....	51
4.8 Atomic force microscopy .....	53
4.9 Scanning electron microscopy .....	55
4.10 References .....	58
<b>5. Results and discussion .....</b>	<b>62</b>
5.1 Characterization of mixed monolayers formed by the spreader-bar technique .....	66
5.1.1 Formation of mixed monolayers .....	66
5.1.2 Distribution of molecules in the mixed monolayer .....	77
5.1.3 Stability of mixed monolayer.....	83
5.1.4 Kinetics of the analyte binding in spreader-bar systems.....	85
5.2 Applications.....	89
5.2.1 Spreader-bar systems as molecular receptors .....	89
5.2.2 Spreader-bar systems as chiral selectors .....	95
5.2.3 Spreader-bar systems as templates for metallic nanoparticles .....	101
5.2.4 Spreader-bar systems used as support for studying ionic pumps .....	105
5.3 References .....	109
<b>6. Summary .....</b>	<b>112</b>

<b>7. Zusammenfassung</b> .....	<b>115</b>
<b>8. Experimental methods</b> .....	<b>118</b>
8.1 Sample preparation .....	118
8.1.1 Materials.....	118
8.1.2 Preparation of monolayers on gold .....	119
8.1.3 Electrodeposition of platinum .....	121
8.2 Analytical methods.....	121
8.2.1 Contact angle measurements.....	121
8.2.2 Electrochemical measurements .....	122
8.2.3 SPR measurements .....	123
8.2.4 NEXFAS, XPS Studies .....	124
8.2.5 Other techniques.....	125
8.3 Chemicals .....	125
8.4 References .....	127
<b>9. Appendix</b> .....	<b>128</b>
9.1 Fundamental physical constants .....	128
9.2 Symbols .....	128
9.3 Abbreviations .....	130
<b>10. Curriculum Vitae</b> .....	<b>133</b>
<b>11. List of publications</b> .....	<b>134</b>

## **1. Introduction**

The last years were marked by essential progress in formation and application of nanostructures, and this field of science has become a promising technology for applications in material science, biotechnology, medicine or chemical analysis. A development of nanotechnology is determined not only by technical possibilities to form practically useful nanostructures, but also by their temporal stability: a struggle between chaos and order is especially hardened in the nanoworld, where local concentration gradients are very high and diffusion processes extremely fast.

It is typical for many systems ordered in the nanometer scale that even small structural changes lead to a total loss of function of the whole system. The stabilization by cross-linking leads to other problems, like complicated chemistry



and/or poor compatibility of subsequent preparation steps resulting in strong limitations in the selection of molecules which can be used.

The known techniques to form micro structured ultra thin layers include photolithography [1, 2], electron beam lithography [3] or microcontact printing ( $\mu$ -CP) [4, 5] and soft lithography [6, 7] are limited in their resolution and cannot reproducibly achieve stable patterns with dimensions at the nanometer scale. The LANGMUIR-BLODGETT technology which has a renaissance in 1980's posses such essential disadvantages as low stability in liquid phases, huge defect density [8 - 10], expensive fabrication devices and poor compatibility with industrial requirements and therefore can hardly be considered as a perspective technology for structures working in liquids. A very interesting system based on alternatively charged polyionic layers [11, 12], is limited by using of polyelectrolytes only. The  $\mu$ -CP technique is inherently limited by the physical interaction of a macroscopic stamp with the surface, often leading to a less structured organic layer with significant defect density; moreover, very precisely structures achieved with microcontact printing ( $\mu$ -CP) are only described up to now by using of long chain alkanethiols [13, 14]. Therefore, success of the *top down* approach breaks down, when molecular precision is desired.

This challenge was a strong motivation for the development of *bottom-up* approaches based on subsequent assembly of complete structures molecule by molecule. Single-molecule manipulation has been successfully demonstrated using scanning probe microscopy, but this technique is extremely time consumable and therefore too expensive for any industrial and many laboratorial applications [14 - 19].

A combination of the speed and versatility of lithographic techniques with the resolution of single-molecule manipulation can be realized by introducing a technique using the way which biological systems explore: self assembly. Moreover, according to the current state of technology, the self-assembly is probably the only possible way to fabricate nanoscale assemblies simply and economically effective.

The natural phenomenon of self-assembly has been recently explored for producing supramolecular alignments and has been adapted to form even nanoscale patterns [20 - 24]. The best studied systems are self-assembled monolayers (SAMs) formed spontaneously by chemisorption of the thiol-terminated molecules, onto gold surface [25 - 27]. The high stability and low defect density of these molecular arrangements is the consequence of the attractive VAN DER WAALS forces between the methylene groups and the covalent bond between gold and sulfur. The chain length of the alkanethiol determines the insulating properties of the SAM. Cyclic voltammograms show that electrodeposition of silver is kinetically hindered depending on the chain length of the alkanethiol [28].

Multi-component SAMs formed by co-deposition of two or more adsorbates from solution have been investigated for their patterning potential [21, 22, 29 - 32]; it has been shown that depending on the molecules used, the resulting monolayer content a homogeneous mixture or separated phases of these compounds [30, 33]. The mixed monolayers comprising electro-inactive insulating long-chain thiols and conductive aromatic thiols were also used to demonstrate a template directed growth of polymer nanostructures: a subsequent electropolymerisation of aniline occurred at the places occupied by the latter sort of thiols only [34].

Self-assembled monolayers of thiolated molecules are used for development of different systems which are important not only for technology and applied science, but for basic research too. Namely these systems were used as a support for investigation of analyte-receptor-binding in the case of antigen-antibody systems [35 - 37], bioreceptor-lipoprotein binding [38] or G-protein dependent receptors [39]. The range of maximal stability of alkanethiol monolayers on gold electrodes is between about -0.3 V and 0.6 V versus a saturated calomel electrode (SCE). The open circuit potential of the gold electrode during thiol deposition is within this stability range [40]; that is why it is usually possible to obtain self-assembled monolayers even without application of external potential. However, control of the electrode potential during deposition of monolayers allows one to obtain monolayers with better insulating properties and much faster [40]. Decrease of the electrical potential of gold electrodes coated by thiols leads to

some loss of insulating properties detected by impedance measurement [40 - 43]. The effect is comparatively small and reversible. At more negative potentials, a reductive desorption occurs. This desorption was measured electrochemically, by quartz crystal microbalance (QCM), X-ray photoelectron spectroscopy or IR reflection spectroscopy [44 - 54]. The potential of reductive desorption depends on the type of thiol derivative and on the properties of metallic surfaces [46, 49, 55, 56]. For alkanethiol monolayers on silver electrodes, the reductive desorption occurs at more negative potentials [49]. The dependence of the desorption potential on the alkanethiol type can be used for selective substitution of one type of thiol by another one [51]. The dependence of this potential on the electrode metal, as well as a formation of islands of atomic monolayers of silver during its underpotential deposition on octanethiol coated gold electrodes [57], provides a technology for electrochemical formation of nanopores in self-assembled monolayers [58].

According to the results of BARTHLOTT and NEINHUIS describing the so called "lotus"-effect, formation of lateral microstructures decreased adsorption of particles that are larger than these structures [59]. These results were explained by a decrease of interaction area. However, all the works exploit only the anchor function of the self-assembled monolayers as a "molecular glue" or just opposite, a formation of adsorption resistive surfaces [60, 61] and in some works their insulating properties; an exploring of the high potential of laterally nanostructured self-assembled monolayers in combination with bio molecules is just in the beginning.

The introduction of in-situ synthesis on surface of solid substrates has resulted in essential progress in different fields of science and technology. Immobilized metallic nanoparticles are of particular interest. Their applications include electrocatalysis, data storage systems, new electronic devices, electrochemical chemo- and biosensors, refractometric and fluorescent sensors based on plasmon effects and many other fields of science and high technology [3 - 8]. The strategies for preparation of these systems are mostly based on the deposition of pre-synthesized nanoparticles with [9] or without [10, 11] further treatment. So far the

deposition was mostly performed by electrospray technique [12] or adsorption [10, 13] while only a few techniques based on the in-situ synthesis of nanoparticle were tested. Such a synthesis can be performed by electroless deposition or by electroplating. The electroless deposition of nanoparticles was used for deposition of gold, silver, nickel, palladium, copper and cobalt nanoparticles onto different substrates [3, 6, 14, 15]. Deposition by electroplating was used for formation of bulk phases of nanocrystalline metals by reduction of corresponding salts in ionic liquids [16, 17]. Formation of metallic nanoparticles by electrochemical reduction on the tip of scanning tunneling microscope (STM) followed by transfer to planar metal electrodes was reported [18, 19] and then reproduced by other groups [20], which gives one a powerful tool for composing desired surface characteristics.

Molecular interactions at surfaces play an important role in many biochemical processes and they are of great interest for medical purposes. These processes are often rapid and complex in nature under physiological conditions and therefore they are very difficult or impossible to study. One of the most exciting applications of nanotechnology is a formation of hybrid structures including conductive solid supports, laterally nanostructured organic layer of a definite design and biological ion pump. Such systems can be used for fundamental biological study (investigation of mechanisms of ion transport, measurement of kinetic or thermodynamic properties), for drug discovery (high-throughput screening to find effective pharmacological ways to control these ion pumps and ion fluxes through biological membranes) in technology (to form nanodevices for energy and information conversion and storage). Several such supported systems have been described in literature [62 - 65], however they provide only capacitive electrical coupling with bio molecules and cannot be used for direct measurements of steady-state ion fluxes and thermodynamic properties.

Electrogenic ionic pumps like Na,K-ATPase are important house-keeping protein in most animal cells for the maintaining of the intracellular high  $K^+$  and low  $Na^+$  concentrations by active ion transport. Recent extensive studies led to a substantial progress in the understanding of the transport mechanism of the ion pump [66]. It was found that the transport of ions by Na,K-ATPase is performed through wells

or ion access channels which connect water solutions with the binding sites inside the protein. The information about the size of access channels and the kinetics of the active transport with Na,K-ATPase was obtained by electrical and optical studies which allowed the identification of the electrogenic reaction steps of the transport cycle and of the determination of their characteristic parameters [66 - 73]. However, further investigations on these systems are considerably restricted due to several problems typical for these systems. The main problem arising with patch clamp investigations on cells is that the cells contain many other proteins besides of Na,K-ATPase. It restricts the experimental conditions of measurements. Net electrical signal from Na,K-ATPase in such systems can be measured as a result of subtracting of electric currents before and after inhibition of the protein. The problem cannot be solved in model system based on bilayer lipid membranes with adsorbed membrane fragments where direct measurements of electric current through the membrane fragment and the control of voltage across it are impossible. However, these problems can be solved by formation of hybrid nanostructured systems with reversible nanoelectrodes.

## 1.1 References

- [1] Moreau, W.M.; *Semiconductor Lithography: Principles and Materials*, **1988**, Plenum, New York.
- [2] Brambley, D.; Martin, B.; Prewett, P. D.; *Adv. Mater. Opt. Electron.* **1994**, 4, 55 - 74.
- [3] Rai-Choudhury, P.; *Handbook of Microlithography, Micromachining, and Microfabrication*, **1997**, SPIE, London.
- [4] Xia, Y.; Zhao, X.-M.; Whitesides, G. M.; *Microelectron. Eng.* **1996**, 32, 255 - 268.
- [5] Xia, Y.; Kim, E.; Whitesides, G.M.; *J. Electrochem. Soc.* **1996**, 143, 1070 - 1079.
- [6] Xia, Y.; Whitesides, G. M.; *Angew. Chem. Int. Edn. Engl.* **1998**, 37, 550 - 575.
- [7] Zhao, X. M.; Xia, Y.; Whitesides, G.M.; *J. Mater. Chem.* **1997**, 7, 1069 - 1074.

- [8] Peterson, I. R.; *J. Mol. Electron.* **1986**, 2(2), 95 - 99.
- [9] Peterson, I. R.; *J. Chim. Phys.-Chim. Biol.* **1988**, 85(11-12), 997 - 1001.
- [10] Garnaes, J.; Schwartz, D. K.; Viswanathan, R.; Zasadzinski, J. A. N.; *Synth. Met.* **1993**, 57(1), 3795 - 3800.
- [11] Shimomura, M.; Sawadaishi, T.; *Current Opinion in Colloid & Interface Science* **2001**, 6, 11 - 16.
- [12] Shimomura, M.; *Thin Solid Films* **1985**, 132, 243 - 248.
- [13] Jeon, N. L.; Finnie, K.; Branshaw, K.; Nuzzo, R. G.; *Langmuir* **1997**, 13, 3382 - 3391.
- [14] Xia, Y.; Qin, D.; Yin, Y.; *Current Opinions in Colloid & Interface Science* **2001**, 6, 54 - 64.
- [15] Becker, R. S.; Golovchenko, J. A.; Swartzentruber, B. S.; *Nature* **1987**, 325, 419 - 421.
- [16] Eigler, D. M.; Schweizer, E. K.; *Nature* **1990**, 344, 524 - 526.
- [17] Weiss, P. S.; Eigler, D. M.; *NATO ASI Series E: Applied Sciences* **1993**, 235, 213 - 217.
- [18] Gimzewski, J. K.; Joachim, C.; *Science* **1999**, 283, 1683 - 1699.
- [19] Hla, S.-W.; Bartels, L.; Meyer, G.; Rieder, K.-H.; *Phys. Rev. Lett.* **2000**, 85, 2777 - 2780.
- [20] Allara, D. L.; *Biosens. Bioelectron.* **1995**, 10, 771 - 783.
- [21] Bain, C. D.; Evall, J.; Whitesides, G.M.; *J. Am. Chem. Soc.* **1989**, 111, 7155 - 7164.
- [22] Bain, C. D.; Whitesides, G. M.; *Langmuir* **1989**, 5, 1370 - 1378.
- [23] Ulman, A.; *An Introduction to Ultrathin Organic Films: from Langmuir-Blodgett to Self-Assembly*, **1991**, Academic, San Diego.
- [24] Ulman, A.; *Chem. Rev.* **1996**, 96, 1533 - 1554.
- [25] Dubois, L. H.; Nuzzo, R. G.; *Annu. Rev. Phys. Chem* **1992**, 43, 437 - 463.
- [26] Poirier, G. E.; *Chem. Rev.* **1997**, 97, 1119 - 1122.
- [27] Mirsky, V. M.; *Trends in Analytical Chemistry* **2002**, 21(6+7), 439 - 450.
- [28] Hagenström, H.; Esplandiú, M. J.; Kolb, D. M.; *Langmuir* **2001**, 17, 839 - 848.

- [29] Bain, C. D.; Whitesides, G. M.; *J. Am. Chem. Soc.* **1988**, *110*, 6560 - 6561.
- [30] Folkers, J. P.; Laibinis, P. E.; Whitesides, G. M.; Deutch, J.; *J. Phys. Chem.* **1994**, *98*, 563 - 571.
- [31] Stranick, S. J.; Attre, S. V.; Parikh, A. N.; Wood, M. C.; Allara, D. L.; Winograd, N.; Weiss, P. S.; *Nanotechnology* **1996**, *7*, 438 - 442.
- [32] Stranick, S. J.; Parikh, A. N.; Tao, Y.-T.; Allara, D. L.; Weiss, P. S.; *J. Phys. Chem.* **1994**, *98*, 7636 - 7646.
- [33] Hayes, W. A.; Kim, H.; Yue, X.; Perry, S. S.; Shannon, C.; *Langmuir* **1997**, *13*, 2511 - 2518.
- [34] Hayes, W. A.; Shannon, C.; *Langmuir* **1998**, *14*, 1099 - 1102.
- [35] Dong, Y.; Shannon, C.; *Analytical Chemistry* **2000**, *72*(11), 2371 - 2376.
- [36] Blonder, R.; Katz, E.; Cohen, Y.; Itzhak, N.; Riklin, A.; Willner, I.; *Anal. Chem.* **1996**, *68*(18), 3151 - 3157.
- [37] Duschl, C.; Sevin-Landais, A.-F.; Vogel, H.; *Biophys. J.* **1996**, *70*(4), 1985 - 1995.
- [38] Bajari, T. M.; Lindstedt, K. A.; Riepl, M.; Mirsky, V. M.; Nimpf, J.; Wolfbeis, O. S.; Dresel, H. A.; Bautz, E. K. F.; Schneider, J. W.; *Biological Chemistry* **1998**, *379*(8/9), 1053 - 1062.
- [39] Heyse, S.; Ernst, O. P.; Dienes, Z.; Hofmann, K.-P.; Vogel, H.; *Biochemistry* **1998**, *37*(2), 507 - 522.
- [40] Ma, F.; Lennox, R. B.; *Langmuir* **2000**, *16*, 6188 - 6190.
- [41] Riepl, M.; Mirsky, V. M.; Wolfbeis, O. S.; *Mikrochim. Acta* **1999**, *131*, 29 - 34.
- [42] Boubour, E.; Lennox, R. B.; *J. Phys. Chem. B* **2000**, *104*, 9004 - 9010.
- [43] Boubour, E.; Lennox, R. B.; *Langmuir* **2000**, *16*, 7464 - 7470.
- [44] Kawaguchi, T.; Yasuda, H.; Shimazu, K.; Porter, M. D.; *Langmuir* **2000**, *16*, 9830 - 9840.
- [45] Wong S. S.; Porter, M. D.; *J. Electroanal. Chem.* **2000**, *485*, 135 - 143.
- [46] Zhong, C. J.; Zak, J.; Porter, M. D.; *J. Electroanal. Chem.* **1997**, *421*, 9 - 13.

- [47] Weisshaar, D. E.; Walczak, M. M.; Porter, M. D.; *Langmuir* **1993**, *9*, 323 - 329.
- [48] Walczak, M. M.; Popenoe, D. D.; Deinhammer, R. S.; Lamp, B. D.; Chung, C.; Porter, M. D.; *Langmuir* **1991**, *7*, 2687 - 2693.
- [49] Widrig, C. A.; Chung, C.; Porter, M. D.; *J. Electroanal. Chem. Interfacial Electrochem.* **1991**, *310*, 335 - 359.
- [50] Yang, D. F.; Wilde, C. P.; Morin, M.; *Langmuir* **1997**, *13*, 243 - 249.
- [51] Yang, D. F.; Morin, M.; *J. Electroanal. Chem.* **1998**, *441*, 173 - 181.
- [52] Yang, D. F.; Morin, M.; *Can. J. Chem.* **1997**, *75*, 1680 - 1686.
- [53] Yang, D. F.; Al Maznai, H.; Morin, M.; *J. Phys. Chem. B* **1997**, *101*, 1158 - 1166.
- [54] Vinokurov, I. A.; Morin, M.; Kankare, J.; *J. Phys. Chem. B* **2000**, *104*, 5790 - 5796.
- [55] Beulen, M. W. J.; Kastenbergh, M. I.; van Veggel, F. C. J. M.; Reinhoudt, D. N.; *Langmuir* **1998**, *14*, 7463 - 7467.
- [56] Imabayashi, S. I.; Hobara, D.; Kakiuchi, T.; Knoll, W.; *Langmuir* **1997**, *13*, 4502 - 4504.
- [57] Oyamatsu, D.; Kuwabata, S.; Yoneyama, H.; *J. Electroanal. Chem.* **1999**, *473*, 59 - 67.
- [58] Oyamatsu, D.; Kanemoto, H.; Kuwabata, S.; Yoneyama, H.; *J. Electroanal. Chem.* **2001**, *497*, 97 - 105.
- [59] Fuerstner, R.; Barthlott, W.; Neinhuis, Ch.; Walzel, P.; *Langmuir* **2005**, *21*, 956 - 961.
- [60] Harder, P.; Grunze, M.; Dahint, R.; Whitesides, G. M.; Laibinis, P. E.; *J. Phys. Chem. B* **1998**, *102*, 426 - 436.
- [61] Valiokas, R.; Svedhem, S.; Oestblom, M.; Svensson, C. T.; Liedberg, B.; *J. Phys. Chem. B* **2001**, *105*, 5459 - 5469.
- [62] Naumann, R.; Jonczyk, A.; Hampel, C.; Ringsdorf, H.; Knoll, W.; Bunjes, N.; Graeber, P.; *Bioelectrochemistry and Bioenergetics* **1997**, *42(2)*, 241 - 247.
- [63] Naumann, R.; Baumgart, T.; Graber, P.; Jonczyk, A.; Offenhausser, A.; Knoll, W.; *Biosensors & Bioelectronics* **2002**, *17(1-2)*, 25 - 34.
- [64] Steinem, C.; Janshoff, A.; Hoehn, F.; Sieber, M.; Galla, H.-J.; *Chemistry and Physics of Lipids* **1997**, *89(2)*, 141 - 152.



- [65] Pintschovius, J.; Fendler, K.; Bamberg, E.; *Biophysical Journal* **1999**, 76(2), 827 - 836.
- [66] Apell, H.-J.; Karlisch, S. J.; *J. Membrane Biol.* **2001**, 180, 1 - 9.
- [67] Heyse, S.; Wuddel, I.; Apell, H.-J.; Sturmer, W.; *J. Gen. Physiol.* **1994**, 104, 197 - 240.
- [68] Wuddel, I.; Apell, H.-J.; *Biophys. J.* **1995**, 69, 909 - 921.
- [69] Clarke, R. J.; Kane, D. J.; Apell, H.-J.; Roudna, M.; Bamberg, E.; *Biophys. J.* **1998**, 75, 1340 - 1353.
- [70] Sokolov, V. S.; Ayuan, A. G.; Apell, H.-J.; *European Biophysics Journal* **2001**, 30, 515 - 527.
- [71] Holmgren, M.; Wagg, J.; Bezanilla, F.; Rakowski, R. F.; De Weer, P.; Gadsby, D. C.; *Nature* **2000**, 403, 898 - 901.
- [72] Cornelius, F.; *Biophys. J.* **1999**, 77, 934 - 942.
- [73] Sokolov, V. S.; Apell, H.-J.; Corrie, J. E. T.; Trentham, D. R.; *Biophys. J.* **1998**, 74, 2285 - 2298.

## **2. Aim of the work**

The aim of this work was the development of a new technology for simple formation of nanostructured organic monolayers. The resulting structures should be stable and exhibit different abilities like working as chemoreceptor or dealing as template for creating metallic nanoparticles. This should confirm the generality of this new technique.

The technology is based on combination of self-assembly of thiol compounds on metals, by co-adsorption of different types of molecules: linear ones (matrix) and large rigid planar ones (template or molecular spreader-bar). This results in the fabrication of heterogeneous structured monomolecular film with so called spreader-bar moieties imbedded in the matrix.

In contrast to two-dimensional molecular imprinting, realized by formation of a monolayer in presence of an analyte and washing out the analyte after the self assembly, the structures formed by spreader-bar technique are temporary stable, because the spreader-bar molecules remain in the monolayer.

Different types of spreader-bar molecules like purines and pyrimidines as well as thiol modified porphyrins was planned to investigate. The resulted structures should be characterized in their phenomenology by different surface sensitive methods like, contact angle measurements, electrical impedance studies, infrared spectroscopy, ellipsometry, atomic force microscopy, scanning electron microscopy, X-ray photon spectroscopy and NEXAFS.

With this approach a formation of stable artificial receptors for different purines and pyrimidines was planned. The concept of this new type of receptors should be also tested by a formation of enantioselective receptors with thiol modified R- and S-stereoisomers of 1,1'-binaphthyl-2,2'-diamine.

In a further step the spreader-bar approach should be used to design a nanostructured self-assembled monolayer consisting of insulating matrix (long chain alkanethiols) with incorporated conductive islands (large, planar adsorbed molecules). Reduction of metal onto such heterogeneous films was planned. Since a density of the electrical current through the spreader-bar molecules could be much higher than through the insulating alkanethiol environment, the formation of metallic nanoparticles was expected.

Another application of nanostructured spreader-bar systems includes a formation of such new hybrid structures providing not only capacitive but also ohmic electrical contacts with Na,K-ATPase. Therefore it was tested, if the hybrid nanostructured systems with reversible nanoelectrodes, are suitable for adsorption of membrane fragments with Na,K-ATPase, detected by measurement of electrochemical properties.

## **3. Ultrathin layers adsorbed on substrates**

### **3.1 Ultrathin layers**

Ultrathin layers cover a substrate with a film of a thickness in the range from ångströms to micrometers. These layers can be of organic or inorganic nature, in the case they are as thin as their molecular dimensions they are called monolayer. Since the past 30 years there has been great interest in monolayers (more than 100.000 references found by SciFinder), resulting in the development of surface analytical techniques [1, 2] to understand the phenomena of these layers in order to exploit them for surface modification, e.g., control of wetting [3 - 6], creation of bio-compatible materials [7 - 9], in development of solid-state electronic devices [10], for tuning the optical properties of lenses [11], as inhibitors for corrosion [12,

13], in lubrication [14], as adhesion materials [15 - 18], for passivation [19], or as biosensors [20 - 28].

There are many ways to cover substrates by ultrathin layers. The most common techniques are such as physical vapor deposition (PVD) [29], chemical vapor deposition (CVD) [30], plasma deposition [31] or molecular beam epitaxy (MBE) [32]. These techniques recommend relative complicated equipment and therefore they are cost intensive. Another strategy to form ultrathin layers is adsorption from solution. This versatile technique is one of the best ways to assembly monolayers of organic nature on a solid substrate. Furthermore, as described below, it gives the possibility to produce layers of controlled order, composition and properties without need of any expensive equipment.

### **3.2 Monomolecular layer**

Thin films at the water-air interface attract the interest of scientists since the 18<sup>th</sup> century [33]. AGNES POCKELS was the first who describes a monolayer at this interface [34 - 37] and this type of monolayer are classified as LANGMUIR films after IRVING LANGMUIR, who has extensively studied the behavior of amphiphilic molecules at a liquid-gas-interface [38]. In a next step, KATHARINE BLODGETT developed a technique to deposit multilayer of long chain carboxylic acids from a LANGMUIR film to solid substrates by means of glass, silver, chromium, brass or steel. These thin layers are known as LANGMUIR-BLODGETT (LB) films [39, 40]. By this way it was possible to get a good controlled film with the disadvantage of poor time stability, because of thermodynamic disequilibrium of this deposited film on the substrate. This drawback of physisorbed layers was overcome by chemical binding of the molecules to the substrate, which is often the case by using the self-assembly (SA) technique.

The first monolayers created by self-assembly resulted by dipping a glass surface into a solution of long-chain alcohols dissolved in hexadecane [41]. These well

oriented monomolecular films alter the wetting properties of the glass. It was demonstrated that self-assembly of monolayers could be extended to various metal and metal oxide surfaces in combination with different molecules like long-chained amines, carboxylic acids and primary amides [42, 43]. The process of self-assembly in these systems is driven by the large interfacial energy between the substrate and the nonpolar solvent phase, which will be decreased by spontaneous adsorption of the amphiphilic species. The polar head group adsorbs to the substrate and the hydrophobic part of the molecules is oriented away from the substrate.

Monolayers of silanes on glass, described by SAGIV [44], were the first self assembled monolayers (SAMs) with driving force of the chemical binding of the monolayer compound to the substrate. This binding occurs, if an organosilane, like octadecyltrichlorsilane (OTS) is exhibited to surface hydroxyl groups (-OH) of the glass. Different  $\omega$ -substituted alkyl silanes have been used to form SAMs on  $\text{SiO}_2$ , like such as amines [45, 46], cyanides and thiocyanides [46], halogens [46 - 50], methyl ether and acetate [47], thioacetate [47, 51],  $\alpha$ -haloacetate [48], vinyl [52 - 55], (trimethylsilyl)ethynyl [56], methyl ester [57, 58], and *p*-chloromethylphenyl [48, 59 - 61]. All these systems of monolayer based on organosilanes show enhanced stability and allow generating a wide variation of SAMs with different functional groups on top of the surface. It is reported that the controlling of the amount of water in the coating solution makes the production still difficult [52, 62, 63]. The exclusion of water leads to incomplete monolayer formation [53, 64], and an excess of water results in polymerization in solution and deposition of polysiloxane at the surface [65]. An easier and more perspective way to get very stable monolayer can be reached by the use of organosulfur compounds instead of organosilanes.

### 3.3 Alkanethiol monolayers on gold

The first report on monomolecular assemblies of alkanethiols on a gold surface was given in 1983 [66] and it describes that dialkyldisulfides adsorb in an oriented direction to the gold surface, with the alkane moiety at the interface to the air. The reason for that is the strong interaction of the sulfur to the gold [67 - 71]. Because sulfur exhibits also this strong interaction to other metals, monolayers of alkanethiols can also be formed on silver [72], copper [73 - 75], palladium [76], and platinum [77]. An overview about different systems of molecules self assembled on solid substrates is given in table 3.1. For most applications and investigations most of these metal surfaces are incompatible because they form, in contrast to gold, stable oxides.

Beside different metal surfaces, many other organosulfur compounds have been investigated in their ability to form SAMs on gold. Among others alkanethiols [78], dialkyldisulfides [77, 79], cysteines [80, 81], thiocarbamates [82] and xanthates [83] were used. If it is desired to get a well ordered, dense packed monolayers, investigations by studying the contact angle of water and hexadecane at the monolayer air interface, small head groups give better results compared to bulky groups, by similar length of the alkane chain [84].

**TABLE 3.1.** Overview of combinations of self assembled monolayers on solid substrates. R stands for an organic, Ar for an aromatic moiety. X symbolizes a halogen [85].

<b>Substrate</b>	<b>Monolayer forming molecule</b>	<b>Binding</b>	<b>Reference</b>
Au	RSH, ArSH	-S-Au	[86]
Au	RS-SR'	-S-Au	[87]
Au	RSR'	-S-Au	[77]
Au	RSO <sub>2</sub> H	-O <sub>2</sub> S-Au	[88]
Au	R <sub>3</sub> P	-P-Au	[89]
Ag	RSH, ArSH	-S-Ag	[90]
Cu	RSH, ArSH	-S-Cu	[91]
Pd	RSH, ArSH	-S-Pd	[69]
Pt	RNC	-NC-Pt	[92]
GaAs	RSH	-S-GaAs	[93]
InP	RSH	S-InP	[94]
SiO <sub>2</sub>	RSiCl <sub>3</sub> , RSi(OR') <sub>3</sub>	-O-Si	[95]
Si/Si-H	(RCOO) <sub>2</sub>	C-Si	[96]
Si/Si-H	RCH=CH <sub>2</sub>	C-Si	[97]
Si/Si-Cl	RLi, R-MgX	C-Si	[98]

### 3.3.1 Adsorption kinetics

Self-assembly of alkanethiols on a gold surface is characterized by two steps with different kinetics. By dipping a clean gold surface into a solution of an alkanethiol in millimolar concentration a monolayer is formed within several seconds. Measurements of contact angles demonstrate that there is no further change in these values after this process. Studies in thickness of the resulting layer as a function of coating time show that thickness reaches only 80 - 90% of its final value



after the first rapid step [99]. This behavior is explained by a fast adsorption of the thiols to the gold surface by formation of an imperfect monolayer. In a second process lasting for several hours, the packing density of the monolayer is increased, lateral diffusion on the surface reduces defects, and a well ordered monolayer is formed (figure 3.1).

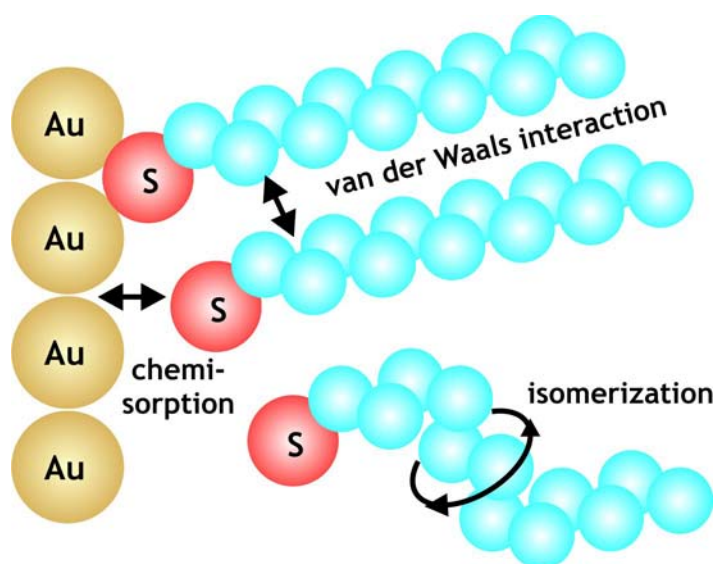


**FIGURE 3.1.** Self-assembly of alkanethiols on gold surfaces. In a fast process the sulfur binds to the gold. In a second step the alkyl chain get well oriented and a dense monolayer is formed.

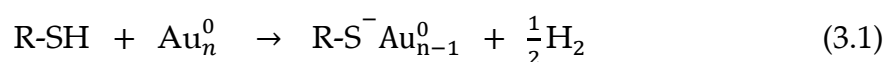
The adsorption kinetics is also influenced by the concentration of the alkanethiol in the solution. For concentrations less than  $1 \text{ mmol}\cdot\text{L}^{-1}$  a slower kinetic for the first step is reported [99]. By the use of very high concentrations it was found that functionalized alkanethiols like 1-mercapto-11-undecanol form monolayer with excessive thickness. An explanation could be that additional adsorption or incorporation of ethanol used as solvent for the alkanethiols will occur [100].

As mentioned above, not only alkanethiols form self assembled monolayer on gold surfaces. For molecules with other organosulfur headgroups it needs a time up to several days to get a well-oriented, densely packed monolayer [84].

For alkanethiols with different chain length it is described that the kinetics of monolayer formation for the long chain 1-octodecanethiol  $\text{HS}-(\text{CH}_2)_{17}-\text{CH}_3$  are faster than for the 1-decanethiol  $\text{HS}-(\text{CH}_2)_9-\text{CH}_3$  [101]. An increase of the chain

length is attended by an increase of the VAN DER WAALS interaction in the resulting monolayer, which might enhance the assembly of long chains.

One important step in the formation of the self assembled monolayer of thiols on the gold surface is the chemisorption of the organosulfur compound to the metal surface. The resulting bonding is described by a Au(I)-thiolate species [2]. The commonly accepted mechanism is considered as an oxidative addition of the S-H bond to the gold surface and a reductive elimination of hydrogen. This is indicated by the fact that monolayers can be formed from gas phase [102 - 104] even in the absence of any oxygen:



The reaction (3.1) is exothermic and the bonding of the thiolate group is very strong. For homolytic dissociation of the Au-S bond an energy of approximately 40 kcal·mol<sup>-1</sup> has been estimated [67].

### 3.3.2 Order and geometry

The order of the monolayer is affected by VAN DER WAALS interaction between the alkyl chains. Studies of the thickness of the monolayer by varying the chain length of alkanethiols HS-(CH<sub>2</sub>)<sub>n</sub>-CH<sub>3</sub> by ellipsometry [78] show two linear regions, one for short alkanethiols up to  $n < 8$  and second one for long alkanethiols beginning from  $n \geq 9$ , with a slope of 1.5 Å for every CH<sub>2</sub>-unit. The intercept was determined to 3.8 Å. Short-chain alkanethiols exhibit a lower slope. From infrared spectroscopy it was found [78] that long-chain alkanethiols are tilted 20 - 30° from surface normal. These results show that alkanethiols with more than nine CH<sub>2</sub>-groups form nearly perfect monolayer with fully extended alkyl chains in trans-configuration, densely packed and with high order.

Investigation of the symmetry of the monolayer on the gold surface has been done by electron diffraction studies [91, 105, 106], helium diffraction [106], and atomic force microscopy [107]. On Au (111) the sulfur occupies not all hollow sites due to

its size (figure 3.2). The sulfur layer can be described by hexagonal symmetry with a distance between two sulfur atoms of about 5 Å [108].

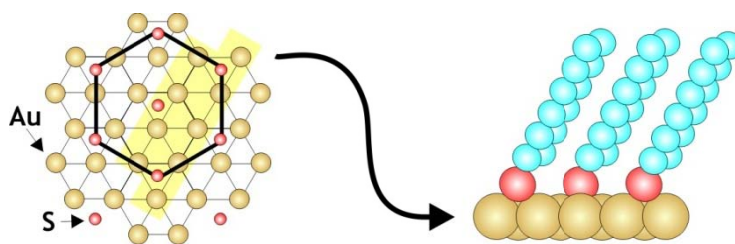


**FIGURE 3.2.** Orientation of a self assembled monolayer of alkanethiols on gold. The symmetry of sulfur atoms is hexagonal with an S—S distance of 4.97 Å and a calculated area per molecule of 21.4 Å<sup>2</sup> [1].

### 3.3.3 Defects in and stability of the monolayer

Beside easy formation and good reproducibility, the number of defects in and the stability of a monolayer is one of the main criterions for using it in applications.

By using a perfect flat Au(111) substrate and by immersion until thermodynamic equilibrium is reached one can expect to get a well ordered monolayer without any defects. Both cannot be achieved for practical applications. To minimize the amount of gold, and therefore the costs, only a thin film of gold is evaporated to glass or silicon surfaces. By this production usually polycrystalline gold is obtained. The surface exhibits terraces at different atomic levels. The self assembly of alkanethiols leads to a slightly declined geometry of the single molecules (figure 3.2). On each border of these terraces on the gold surface the orientation of the declination can be changed and defects will occur.

To test the stability of SAMS, a molecular film of 1-dodecanethiol on gold, heated to temperatures of 100 °C for 10 h in air, did not show any loss of thiols [106]. At higher temperatures XPS data indicate a loss of sulfur and carbon.

Even in solvents self-assembled monolayer of alkanethiols on gold are relatively stable. Desorption in solutions of hydrocarbons starts at about 70 °C, the desorption rate depends not only on the temperature but also on the chain length

of the alkanethiol and the characteristics of the solvent. By using hexadecane as solvent at 83 °C, a decrease of desorption rate with increase of the chain length was found [99].

A self-exchange of radio labeled 1-octadecanethiol molecules from a monolayer exposed to a solution containing the same thiol was observed and its kinetics were described by first order [91].

### **3.4 Mixed monomolecular layers**

To increase the possibilities to design surfaces with certain properties it is also possible to obtain mixed monolayer, consisting of different molecules. This mixed SAMs can be prepared by immersing the gold substrate into a solution of different molecules with thiol moieties. The composition of the resulting monolayer depends on the concentration ratio of these molecules in solution, the type of the molecules and the solubility of them in the solvent. It has to be stressed out that the concentration of one thiol in the mixed monolayer is in general not the same as in the solution used for self assembly [109 - 114].

### **3.5 Spreader-bar system**

A new type of mixed self assembled monolayers is described by the spreader-bar technique. As for known systems, the mixed monolayer is not formed by similar alkanethiols which only differs in their length and the headgroup. The spreader-bar system describes the self assembly of two different molecules.

The basic idea was from the work of SAGIV [115]. He describes a monolayer of *n*-octadecyltrichlorosilane (OTS) on glass, assembled together with a dye, characterized by a polar moiety at one end of the molecule and a nonpolar part. A

mixed monolayer of OTS with incorporated dye molecules is formed. After treatment of the surface by chloroform the physisorbed dye was washed out and the silane remains on the substrate. By immersion of this silane covered glass substrate to a solution of the dye a re-adsorption of this molecule was found. And it was found that not only the molecule, which was present during the self assembly of the silane, was able to adsorb to this surface, although other molecules which have the same geometrical properties like the displaced molecule could be entrapped (figure 3.3).

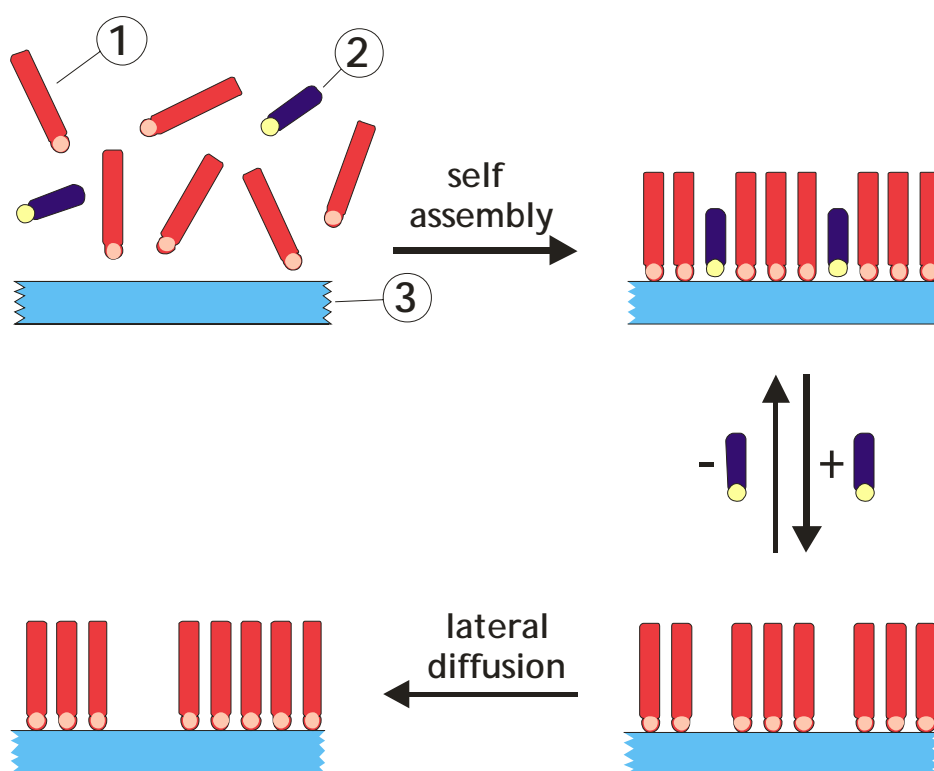


**FIGURE 3.3.** Adsorption of a silane (1) together with a polar molecule (2) onto a glass surface (3). A memory effect for the surface was found. The polar molecules could be washed out and rebound. This characteristics get lost with time, because of lateral diffusion of the molecules within the monomolecular film.

One drawback of this concept is that after desorption the stability of this structured monolayer is weak, because of lateral diffusion of the molecules forming the SAM. Another limitation is in the choice of molecules which can be used for this memory effect. They have to be from the same type like the monolayer forming compound with a small polar and a large non-polar moiety.

The spreader-bar technique provides a stable nanostructured mixed self-assembled monolayer and is based on creation of mixed monolayers of two different compounds, none of them exhibiting recognition properties alone. One component, called matrix, is an alkanethiol, the second component called spreader-bar molecule (template), is similar to the analyte in shape and chemical structure. The matrix molecule must be able to form a monolayer thicker than a monolayer of the template molecules. Both types of molecules are chemisorbed to the gold surface. The structures formed should be able to interact with analyte molecules in a solution and these structures are stable against lateral diffusion, because the template will remain in the surface (figure 3.4).

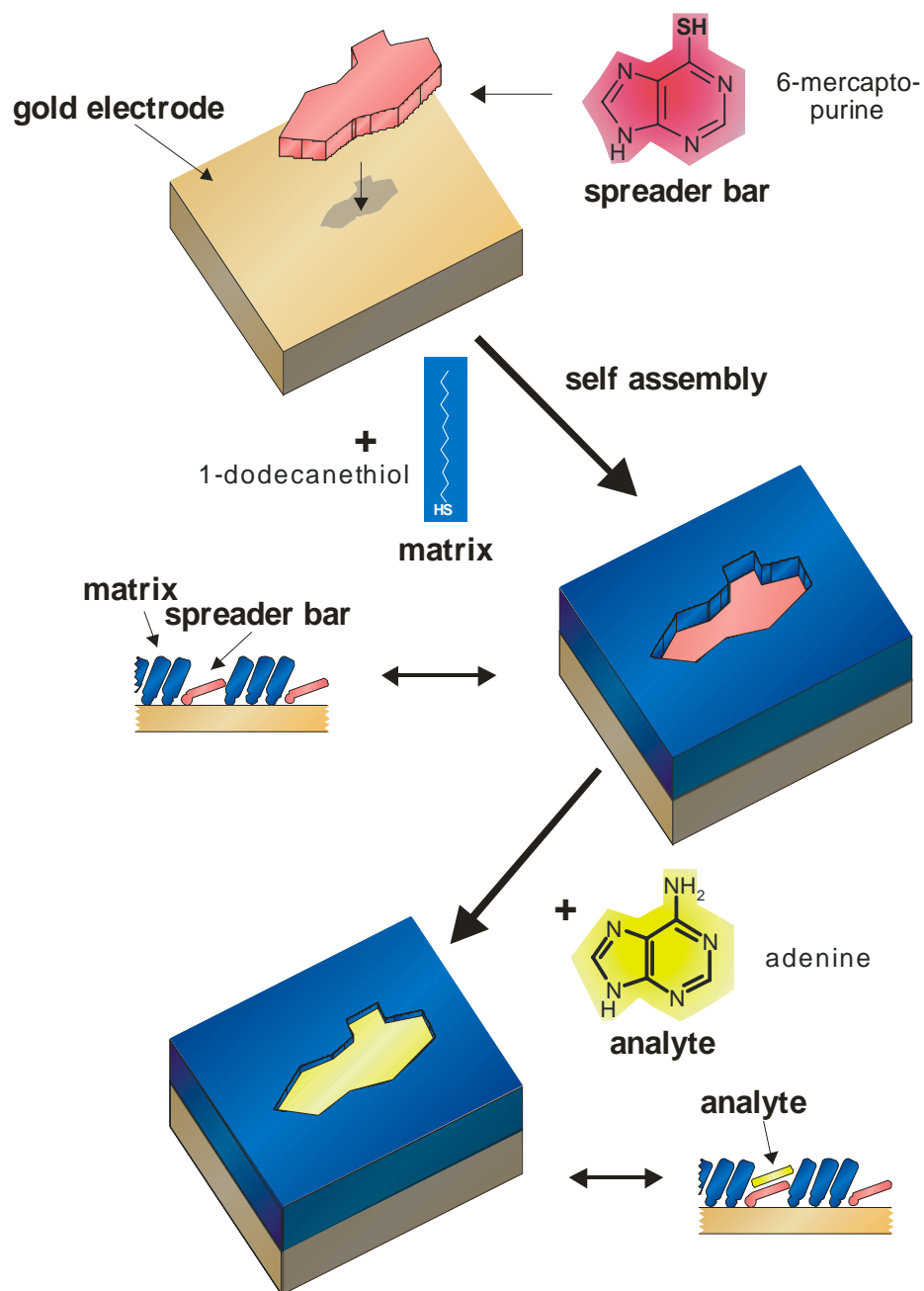


FIGURE 3.4. Principle of a spreader-bar stabilized, nanostructured monolayer.

### 3.5 Summary

Beside other possible systems for testing the concept of spreader-bar structured monomolecular films, the self assembly of alkanethiol on gold has been chosen because of the following reasons:

- The general inertness of gold to nearly all chemical species in ambient conditions makes it sure that only the organosulfur compound will be assembled. A concurrent chemisorption of any non-sulfur based moiety can be excluded.
- Monolayer on gold can be easily investigated by a lot of techniques, including electrochemistry, STM, SEM, or SPR. Experimental approaches to study organosilanes on glass are very limited.
- Alkanethiols and thiols containing heteroaromatic systems are available in large variations, and therefore no special synthesizing is necessary.
- Monolayers of thiols on gold are easy in preparation and can be formed high reproducible.
- SAMs of alkanethiols on gold are known for the low density of defects and their high stability under ambient conditions.

### 3.6 References

- [1] Ulman, A.; *Chem Rev.* **1996**, 96, 1533 - 1554.
- [2] Ulman, A.; *An Introduction to Ultrathin Organic Films*, **1991**, Academic Press, Boston.
- [3] Whitesides, G. M.; Laibinis, P. E.; *Langmuir* **1990**, 6, 87 - 96.
- [4] Laibinis, P. E.; Whitesides, G.M.; *J. Am. Chem. Soc.* **1992**, 114, 1990 - 1995.



- [5] Laibinis, P. E.; Whitesides, G. M.; Allara, D. L.; Tao, Y.-T.; Parikh, A. N.; Nuzzo, R. G.; *J. Am. Chem. Soc.* **1991**, *113*, 7152 - 7167.
- [6] Laibinis, P.E.; Bain, C.D.; Nuzzo, R. G.; Whitesides, G.M.; *J. Phys. Chem.* **1995**, *99*, 7663 - 7676
- [7] Prime, K. L.; Whitesides, G. M.; *Science* **1991**, *252*, 1164 - 1166.
- [8] Singhvi, R.; Kumar, A.; Lopez, G. P.; Stephanopolus, G. N.; Wang, D. I. C.; Whitesides, G. M.; Ingber, D. E.; *Science* **1994**, *264*, 696 - 698.
- [9] Wirth, M. J.; Fairbank, R. W.; Fatunmbi, H. O.; *Science* **1997**, *275*, 44 - 47.
- [10] Collier, C. P.; Matterstei, G.; Wong, E. W.; Luo, Y.; Beverly, K; Sampaio, J.; Raymo, F. M.; Stoddart, J. F.; Heath, J. R.; *Science* **2000**, *289*, 1172 - 1175.
- [11] Goldenberg, L. M.; Wagner, J.; Stumpe, J.; Paulke, B.-R.; Goernitz, E.; *Langmuir* **2002**, *18*, 5627 - 5629.
- [12] Feng, Y.; Siow, K.-S.; Teo, W.-K.; Tan, K.; Hsieh, A.-K.; *Corrosion* **1997**, *53*, 546 - 555.
- [13] Ramachandran, S.; Tsai, B. L.; Blanco, M.; Chen, H.; *Langmuir* **1996**, *12*, 6419 - 6428.
- [14] Xiao, X.; Hu, J.; Charych, D. H.; Salmeron, M.; *Langmuir* **1996**, *12*, 235 - 237.
- [15] Stewart, K. R.; Whitesides, G. M.; Godfried, H. P.; Silvera, I. F.; *Rev. Sci. Instrum.* **1986**, *57*, 1381 - 1383.
- [16] de Gennes, P. G.; *Langmuir* **1996**, *12*, 4497 - 4500.
- [17] Zhuk, A. V.; Evans, A. G.; Hutchinson, J. W.; Whitesides, G. M.; *J. Mat. Res.* **1998**, *13*, 3555 - 3564.
- [18] Choi, G. Y.; Kang, J. F., Ulman, A.; Zurawsky, W.; Fleischer, C.; *Langmuir* **1999**, *15*, 8783 - 8786.
- [19] Lunt, S. R.; Ryba, G. N.; Santangelo, P. G.; Lewis, N. S.; *J. Appl. Phys.* **1991**, *70*, 7449 - 7467.
- [20] Gooding, J. J.; King, G. C.; *J. of Mat. Chem.* **2005**, *15*, 4876 - 4880.
- [21] Andreescu, D.; Andreescu, S.; Omowunmi, A.; *Compr. Anal. Chem.* **2005**, *44*, 285 - 327.

- [22] Davis, F.; Higson, S. P. J.; *Biosens & Bioelectron.* **2005**, *21*, 1 - 20.
- [23] Schuhmann, W.; *Rev. in Mol. Biotechnol.* **2002**, *82*, 425 - 441.
- [24] Vijayamohanan, K.; Aslam, M.; *Appl. Biochem. and Biotechnol.* **2001**, *96*, 25 - 39.
- [25] Ferretti, S.; Paynter, S.; Russell, D. A.; Sapsford, K. E.; Richardson, D. J.; *TrAC, Trends in Anal. Chem.* **2000**, *19*, 530 - 540.
- [26] Willner, I.; Katz, E.; Willner, B.; *Sensors Update* **1999**, *5*, 45 - 102.
- [27] Everhart, D. S.; *Chemtech* **1999**, *29*, 30 - 37.
- [28] Mrksich, M.; Whitesides, G. M.; *Trends in Biotechnology* **1995**, *13*, 228 - 235.
- [29] Mahan, J. E.; *Physical Vapor Deposition of Thin Films*, **2000**, John Wiley & Sons, New York.
- [30] Crowell, J. E.; *J. Vac. Sci. Technol. A* **2003**, *21*, S88 - S95.
- [31] Kinloch, A. J.; *Adhesion and Adhesives*, **1987**, Chapman and Hall, London.
- [32] Schneider, H. G.; Ruth, V.; Kormany, T.; *Advances in Epitaxy and Endotaxy*, **1990**, Elsevier, Amsterdam-Budapest.
- [33] Franklin, B.; *Phil. Trans. R. Soc.* **1774**, *64*, 445 - 460.
- [34] Pockels, A.; *Nature* **1891**, *43*, 437 - 439.
- [35] Pockels, A.; *Nature* **1892**, *46*, 418 - 419.
- [36] Pockels, A.; *Nature* **1893**, *48*, 152 - 154.
- [37] Pockels, A.; *Nature* **1894**, *50*, 223 - 224.
- [38] Langmuir, I.; *J. Am. Chem. Soc.* **1917**, *39*, 1848 - 1906.
- [39] Blodgett, K. A.; *J. Am. Chem. Soc.* **1935**, *57*, 1007 - 1022.
- [40] Blodgett, K. A.; *Phys. Rev.* **1937**, *51*, 964 - 982.
- [41] Bigelow, W. C.; Pickett, D. L.; Zisman, W. A.; *J. Colloid Sci.* **1946**, *1*, 513 - 538.
- [42] Shafrin E. G.; Zisman, W. A.; *J. Colloid Sci.* **1949**, *4*, 571 - 590.
- [43] Schulman, F.; Zisman, W. A.; *J. Colloid Sci.* **1952**, *7*, 465 - 481.

- [44] Sagiv, J.; *J. Am. Chem. Soc.* **1980**, *102*, 92 - 98.
- [45] Bierbaum, K.; Kinzler, M.; Wöll, Ch.; Grunze, M.; Hähner, G.; Heid, S.; Effenberger, F.; *Langmuir* **1995**, *11*, 512 - 518.
- [46] Balachander, N.; Sukenik, C. N.; *Langmuir* **1990**, *6*, 1621 - 1627.
- [47] Chaudhury, M. K.; Whitesides, G.M.; *Science* **1992**, *255*, 1230 - 1232.
- [48] Lee Y. W.; Reed-Mundell, J.; Sukenik, C. N.; Zull, J. E.; *Langmuir* **1993**, *9*, 3009 - 3014.
- [49] Chupa, J. A.; Xu, S.; Fischetti, R. F.; Strongin, R. M.; McCauley, J.P.; Smith, A. B.; Blaise, J. K. J.; *J. Am. Chem. Soc.* **1993**, *115*, 4383 - 4384.
- [50] Paulson, S.; Morris, K.; Sullivan, B. P. J.; *J. Chem. Soc. Chem. Commun.* **1992**, 1615 - 1617.
- [51] Wassermann, S. R.; Biebuyck, H.; Whitesides, G. M.; *J. Mater. Res.* **1989**, *4*, 886 - 892.
- [52] Silberzan, P.; Léger, L.; Ausserré, D.; Benattar, J. J.; *Langmuir* **1991**, *7*, 1647 - 1651.
- [53] Wassermann, S. R.; Tao, Y.-T.; Whitesides, G. M.; *Langmuir* **1989**, *5*, 1074 - 1087.
- [54] Netzer, L.; Iscovichi, R.; Sagiv, J.; *Thin Solid Films* **1983**, *100*, 67 - 76.
- [55] Maoz, M.; Sagiv, J.; *Langmuir*, **1987**, *3*, 1034 - 1044.
- [56] Ogawa, K.; Mino, N.; Tamura, H.; Hatada, M.; *Langmuir* **1990**, *6*, 1807 - 1809.
- [57] Pomerantz, M.; Segmüller, A.; Netzer, L.; Sagiv, J.; *Thin Solid Films* **1985**, *132*, 153 - 162.
- [58] Tillmann, N.; Ulman, A.; Penner, T. L.; *Langmuir* **1989**, *5*, 1020 - 1026.
- [59] Li, D. Q.; Ratner, M. A.; Marks, T. J.; Zhang, C. H.; Yang, J.; Wong, G. K. J. ; *J. Am. Chem. Soc.* **1990**, *112*, 7389 - 7390.
- [60] Kakkar, A. K.; Yitzchaik, S.; Roscoe, S. B.; Kubota, F.; Allan, D. S.; Marks, T. J.; Lin, W.; Wong, G. K. J.; *Langmuir* **1993**, *9*, 388 - 390.
- [61] Yitzchaik, S.; Roscoe, S. B.; Kakkar, A. K.; Allan, D. S.; Marks, T. J.; Xu, Z.; Zhang, C. H.; Lin, W.; Wong, G. K. J.; *J. Phys. Chem.* **1993**, *97*, 6958 - 6960.

- [62] Tripp, C. P.; Hair, M. L.; *Langmuir* **1992**, *8*, 1120 - 1126.
- [63] Angst, D. L.; Simmons, G. W.; *Langmuir* **1991**, *7*, 2236 - 2242.
- [64] Le Grange, J. D.; Markham, J. L.; Kurjian, C. R.; *Langmuir* **1993**, *9*, 1749 - 1753.
- [65] Brandriss, S.; Margel, S.; *Langmuir* **1993**, *9*, 1232 - 1240.
- [66] Nuzzo, R. G.; Allara, D. L.; *J. Am. Chem. Soc.* **1983**, *105*, 4481 - 4483.
- [67] Dubois, L.H.; Nuzzo, R. G.; *Ann. Phys. Chem.* **1992**, *43*, 437 - 463.
- [68] Bain, C. D.; Whitesides, G. M.; *Adv. Mater.* **1989**, *1*, 110 - 116.
- [69] Lee, T. R.; Laibinis, P. E.; Folkers, J. P.; Whitesides, G. M.; *Pure Appl. Chem.* **1991**, *63*, 821 - 828.
- [70] Whitesides, G. M.; Ferguson, G. S.; *Chemtracts-Org. Chem.* **1988**, *1*, 171.
- [71] Sellers, H.; Ulman, A.; Schnidman, Y.; Eilers, J. E.; *J. Am. Chem. Soc.* **1993**, *115*, 9389 - 9401.
- [72] Ulman, A.; *J. Mat. Ed.* **1989**, *11*, 205 - 207.
- [73] Stewart, K.R.; Whitesides, G. M.; Godfried, H. P.; Silvera, I. F.; *Rev. of Sci. Instr.* **1986**, *57*, 1381 - 1383.
- [74] Blackman, J. C. F.; Dewar, M. J. S.; *J. Chem. Soc.* **1957**, 171 - 176.
- [75] Blackman, L. C. F.; Dewar, M. J. S.; Hampson, H.; *J. Appl. Chem.* **1957**, *7*, 160 - 171.
- [76] Love, J. C.; Wolfe, D. B.; Haasch, R.; Chabinyk, M. L.; Paul, K. E.; Whitesides, G. M.; Nuzzo, R. G.; *J. Am. Chem. Soc.* **2003**, *125*, 2597 - 2609.
- [77] Troughton, E. B.; Bain, C. D.; Whitesides, G. M.; Nuzzo, R. G.; Allara, D. L.; Porter, M. D.; *Langmuir* **1988**, *4*, 365 - 385.
- [78] Nuzzo, R. G.; Zegarski, B. R.; Dubois, L. H.; *J. Am. Chem. Soc.* **1987**, *109*, 733 - 740.
- [79] Katz, E.; Itzhsk, N.; Willner, I.; *J. Electroanal. Chem.* **1992**, *336*, 357 - 362.
- [80] Cooper, J. M.; Greenough, K. R.; McNeil, C. J.; *J. Electroanal. Chem.* **1993**, *347*, 267 - 275.
- [81] Uvdal, K.; Bodö, P.; Liedberg, B.; *J. Colloid Interf. Sci.* **1992**, *149*, 162 - 173.

- [82] Mielczarski, J. A.; Yoon, R. H.; *Langmuir* **1991**, *7*, 101 - 108.
- [83] Ihs, A.; Uvdal, K.; Liedberg, B.; *Langmuir* **1993**, *9*, 733 - 738.
- [84] Bain, C. D.; Evall, J.; Whitesides, G. M.; *J. Am. Chem. Soc.* **1989**, *111*, 7155 - 7164.
- [85] Fibbioli, M.; *New Types of Ion-selective electrodes: Hydrophilic Anions and Solid-Contacted Membranes*, Dissertation, ETH Zürich, **2000**.
- [86] Delamar, E.; Michel, B.; Biebuyck, H. A.; Gerber, C.; *Adv. Mater.* **1996**, *8*, 719 - 729.
- [87] Biebuyck, H. A.; Bain, C. D.; Whitesides, G. M.; *Langmuir* **1994**, *10*, 1825 - 1831.
- [88] Chadwick, J. E.; Myles, D. C.; Garrel, R. L.; *J. Am. Chem. Soc.* **1993**, *115*, 10365 - 10365.
- [89] Uvdal, K.; Persson, I.; Liedberg, B.; *Langmuir* **1995**, *11*, 1252 - 1256.
- [90] Fenter, P.; Eisenberger, P.; Li, J.; Camillone, N. I.; Bernasek, S.; Scoles, G.; Ramnanarayanan, T. A.; Liang, K. S.; *Langmuir* **1991**, *7*, 2013 - 2016.
- [91] Schlenhoff, J. B.; Li, M.; Ly, H.; *J. Am. Chem. Soc.* **1995**, *117*, 12528 - 12536.
- [92] Hickman, J. J.; Kaibinis, P. E.; Auerbach, D. I.; Zou, C.; Gardner, T. J.; Whitesides, G. M.; Wrighton, M. S.; *Langmuir* **1992**, *8*, 357 - 359.
- [93] Sheen, C. W.; Shi, J.-X.; Martensson, J.; Parikh, A. N.; Allara, D. L.; *J. Am. Chem. Soc.* **1992**, *114*, 1514 - 1515.
- [94] Gu, Y.; Lin, Z.; Butera, R. A.; Smentkowski, V. S.; Waldeck, D. H.; *Langmuir* **1995**, *11*, 1849 - 1851.
- [95] Wirth, M. J.; Fairbank, W. P.; Fatunmbi, H. O.; *Science* **1997**, *275*, 44 - 47.
- [96] Linford, M. R.; Chidsey, C. E. D.; *J. Am. Chem. Soc.* **1993**, *115*, 12631 - 12632.
- [97] Linford, M. R.; Fenter, P.; Eisenberger, P. M.; Chidsey, C. E. D.; *J. Am. Chem. Soc.* **1995**, *117*, 3145 - 3155.
- [98] Bansal, A.; Li, X.; Lauermann, I.; Lewis, N. S.; Yi, S. I.; Weinberg, W. H.; *J. Am. Chem. Soc.* **1996**, *118*, 7225 - 7226.
- [99] Bain, C. D.; Troughton, E. B.; Tao, Y.-T.; Evall, J.; Whitesides, G. M.; Nuzzo, R. G.; *J. Am. Chem. Soc.* **1989**, *111*, 321 - 335.

- [100] Ulman, A.; Tillman, N.; *Langmuir* **1989**, *5*, 1418 - 1420.
- [101] Somorjai, G. A.; *Chemistry in two dimensions-Surfaces*, **1982**, Cornell University Press, Ithaca.
- [102] Brust, M.; Walker, M.; Bethell, D.; Schiffrin, D. J.; Whyman, R.; *J. Chem. Soc., Chem. Commun.* **1994**, 801 - 802.
- [103] Thomas, R. C.; Sun, L.; Crooks, M.; *Langmuir* **1991**, *7*, 620 - 622.
- [104] Chailapakul, O.; Sun, L.; Xu, C.; Crooks, M.; *J. Am. Chem. Soc.* **1993**, *115*, 12459 - 12467.
- [105] Strong, L.; Whitesides, G. M.; *Langmuir* **1988**, *4*, 546 - 558.
- [106] Delamarche, E.; Michel, B.; Kang, H.; Gerber, Ch.; *Langmuir* **1994**, *10*, 4103 - 4108.
- [107] Li, Y.; Huang, J.; McIver, R. T.; Hemminger, J. C.; *J. Am. Chem. Soc.* **1992**, *114*, 2428 - 2432.
- [108] Folkers, J. P.; Zerkowski, J. A.; Laibinis, P. E.; Seto, C. T.; Whitesides, G. M.; *ACS Symp. Ser.* **1992**, *499*, 10 - 12.
- [109] Bain, C. D.; Whitesides, G. M.; *Langmuir* **1989**, *5*, 1370 - 1378.
- [110] Bain, C. D.; Whitesides, G. M.; *J. Am. Chem. Soc.* **1988**, *110*, 6560 - 6561.
- [111] Folkers, J. P.; Laibinis, P. E.; Whitesides, G. M.; Deutch, J.; *J. Phys. Chem.* **1994**, *98*, 563 - 571.
- [112] Stranick, S. J.; Attre, S. V.; Parikh, A. N.; Wood, M. C.; Allara, D. L.; Winograd, N.; Weiss, P. S.; *Nanotechnology* **1996**, *7*, 438 - 442.
- [113] Stranick, S. J.; Parikh, A. N.; Tao, Y.-T.; Allara, D. L.; Weiss, P. S.; *J. Phys. Chem.* **1994**, *98*, 7636 - 7646.
- [114] Hayes, W. A.; Kim, H.; Yue, X.; Perry, S. S.; Shannon, C.; *Langmuir* **1997**, *13*, 2511 - 2518.
- [115] Sagiv, J.; *Israel Journal of Chemistry* **1979**, *18*, 346 - 353.

## **4. Methods of surface characterization**

There are many surface sensitive techniques available to investigate thin films on surfaces. Each technique has only a very small focus and so it is always necessary to combine several methods to get a more or less complete picture of an ultrathin film.

In case of self assembled monolayer, especially those of alkanethiols on gold there have been a lot of studies exploiting the techniques listed in the table 4.1 below. In the following the most important methods used in this work for surface characterization are described in detail.

**TABLE 4.1.** *Common methods for surface characterization used for self assembled monolayers of thiols on gold.*

<b>Information</b>	<b>Technique</b>	<b>References</b>
Composition	X-ray photoelectron spectroscopy (XPS)	[1, 2]
	Time of flight secondary ion mass spectroscopy	[1, 3]
	Temperature programmed desorption (TPD)	[4]
Structure	Infrared spectroscopy	[5 - 7]
	Atomic force microscopy (AFM)	[8, 9]
	X-ray diffraction	[1]
	Electron diffraction	[1, 10]
	Surface raman scattering	[1]
	Sum frequency generation spectroscopy	[1]
	Low energy helium diffraction	[1]
Coverage	Quartz crystal microbalance (QCM)	[11]
	Surface acoustic wave device	[1, 12]
	Electrochemical methods	[12, 13]
Thickness	Ellipsometry	[14, 15]
	Surface plasmon resonance spectroscopy (SPR)	[1, 16]
Defects	Scanning probe microscopy (STM and AFM)	[3, 17]
	Wet etching	[18]
Wettability	Contact angle measurements	[1, 19]



## 4.1 Contact angle measurement

If a liquid is dropped on a surface two phenomena are well known (figure 4.1). The first is that the surface becomes wetted, the second can be described by formation of droplets which can be easily spilled off the surface.

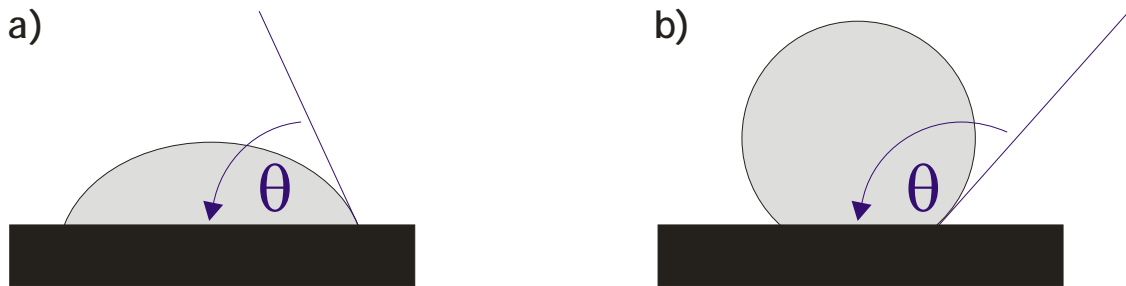


**FIGURE 4.1.** Contact angle  $\theta$  of water on a solid surface. The surface has hydrophilic properties (a) when  $\theta < 90^\circ$ . In the case of  $\theta > 90^\circ$  the surface is hydrophobic (b).

All liquids which do not completely wet a solid surface form droplets on the surface which can be characterized by a definite angle,  $\theta$ , given by the tangent to the surface at the three-phase boundary, the so called contact angle [1] (figure 4.1). On plane, homogenous surfaces the shape of the droplet, and therefore the contact angle is the result of the free energy of the drop in affection of the free energy of the surface. So the wetting properties of a liquid on a plane substrate give information about the homogeneity of the surface. The relationship between the free energy of the surface and the contact angle  $\theta$ , in equilibrium and under ideal conditions is given by YOUNG's equation (4.1) [20, 21].

$$\gamma_{LG} \cdot \cos \theta = \gamma_{SG} - \gamma_{SL} \quad (4.1)$$

with:

$\gamma_{SL}$	surface-free energy at the solid-liquid interface
$\gamma_{SG}$	surface-free energy at the solid-gas interface
$\gamma_{LG} \cdot \cos \theta$	surface-free energy at the liquid-gas interface
$\theta$	contact angle

In practice it is hardly to get thermodynamic equilibrium, and so the angle differs by measurements, when a droplet is advanced ( $\theta_{advancing}$ ) or receded ( $\theta_{receding}$ ). In general  $\theta_{receding} < \theta_{advancing}$  and the difference between this two angles, the hysteresis [22 - 24], is getting bigger the more heterogeneous the structure of the surface is. The hysteresis is also caused by contaminations of the surface or the liquid [1], surface roughness, or reorientation of the surface molecules due to interactions between the surface and the liquid.

For smooth surfaces of heterogeneous chemical composition, the contact angle can be described by the CASSIE Equation (4.2) [25]:

$$\cos \theta = \varepsilon_1 \cdot \cos \theta_1 + \varepsilon_2 \cdot \cos \theta_2 \quad (4.2)$$

with

- $\theta$  contact angle of a liquid on a heterogeneous surface
- $\varepsilon_i$  fraction of the compound  $i$ ;  $\varepsilon_1 + \varepsilon_2 = 1$
- $\theta_i$  contact angle of this liquid on a pure, homogeneous surface of  $i$ .

The CASSIE Equation takes the cohesion of the liquid to the surface into account. This work of cohesion,  $W$  is known as

$$W = \gamma_L(1 + \cos \theta) \quad (4.3)$$

with

- $\gamma_L$  free-surface energy of the liquid.

For a heterogeneous surface,  $W$  can be described by the sum of the fraction 1 multiplied by  $W_1$  and fraction 2 multiplied by  $W_2$ , where 1 and 2 stands for the two compounds of the mixed surface. This assumes that the surface is composed by well defined domains, which is not the truth in mixed monomolecular films. In case of SAMs VAN DER WAALS and electrostatic forces [26] suggest that the polarizability, surface charges and the dipole moment of the surfaces should be averaged and not the cohesion energy. This has been done by ISREALACHVILI and GEE. They took the arithmetic mean values of the polarizability and the dipole moment of each compound and calculated the VAN DER WAALS interaction. For a

monomolecular film of two compounds with domain of only molecular dimension they got an equation which is known as ISRAELACHVILI-GEE equation [27]:

$$(1 + \cos \theta)^2 = \varepsilon_1 \cdot (1 + \cos \theta_1)^2 + \varepsilon_2 \cdot (1 + \cos \theta_2)^2 \quad (4.4)$$

This equation is still a simplification, because all interactions among the surface functional groups are neglected.

By comparison of the ISRAELACHVILI-GEE equation (4.4) with the CASSIE equation (4.2) one can see that the values for the contact angle of the same surface are always larger if they were calculated by the CASSIE equation. In practice, this means if we are moving from the randomly mixed monomolecular film to a layer with an increase of the area of one domain, also an increase in the contact angle hysteresis should be found [27, 28]. Therefore the measurement of contact angle can provide useful information about the heterogeneity of a mixed SAM.

## **4.2 Electrochemistry of monomolecular surfaces**

Electrochemistry studies on electrodes covered by thin molecular films provide a lot of information, not only for characterization of the quality of the monomolecular layer; it is also a useful method for the investigation of the receptor properties of the spreader-bar coated electrodes. Two techniques are of special interest in this work: a) impedance measurements and b) cyclic voltammetry.

### **4.2.1 Electrochemical impedance spectroscopy**

The electrochemical impedance is a variable that represents the ability of an electric circuit to resist the flow of electrical charge. In alternating current circuits impedance has the same physical meaning as resistance in direct current circuits. In contrast to resistance, impedance usually depends on the frequency of the

voltage. Measurements of the impedance of an electrochemical cell are done by applying a sinusoidal AC potential with low amplitude at different frequencies and analysis of the current response through the cell. This response is an AC current signal with the same frequency but shifted in phase (figure 4.2).

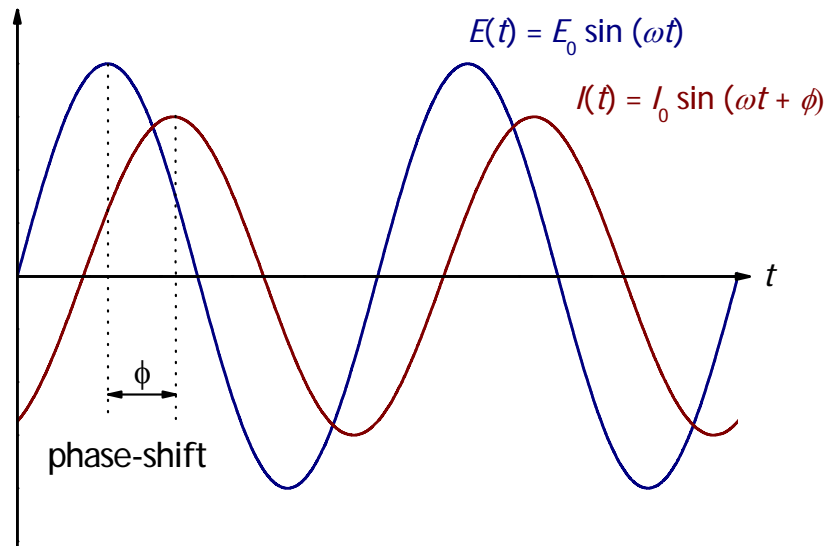


FIGURE 4.2. Typical responding current  $I(t)$  of a electrochemical cell by applying a voltage  $E(t)$ .

According to OHM's Law, the impedance  $Z(t)$  can be calculated from the excitation potential  $E(t)$  and the measured current  $I(t)$  as follows:

$$E(t) = E_0 \cdot \sin(\omega \cdot t) \quad (4.5)$$

$$I(t) = I_0 \cdot \sin(\omega \cdot t + \phi) \quad (4.6)$$

$$Z(t) = \frac{E(t)}{I(t)} = \frac{E_0 \cdot \sin(\omega \cdot t)}{I_0 \cdot \sin(\omega \cdot t + \phi)} = Z_0 \cdot \frac{\sin(\omega \cdot t)}{\sin(\omega \cdot t + \phi)} \quad (4.7)$$

with

$E(t)$  electrical potential, as a function of the time  $t$

$E_0$  amplitude of the excitation potential

$I(t)$  electrical current, as a function of the time  $t$

$I_0$  amplitude of the resulting current

$\omega = 2 \cdot \pi \cdot f$  angular frequency, ( $f$  is the frequency)

$\phi$  phase angle.

From expression (4.7) impedance can be described by  $Z_0$  and the phase angle  $\phi$ . This implies to use the complex plane for the illustration of the impedance (Figure 4.3).

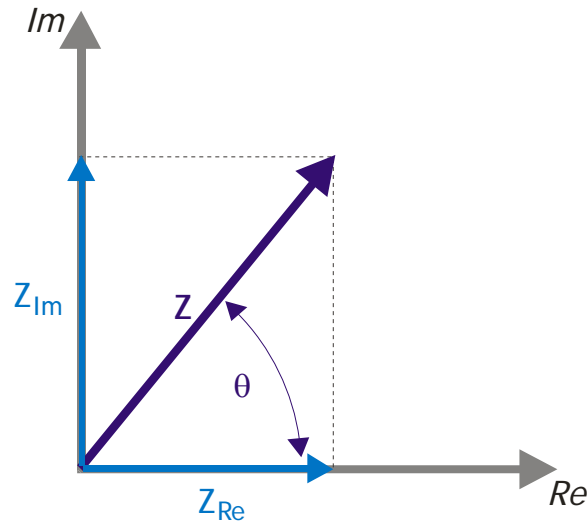


**FIGURE 4.3.** Illustration of the impedance  $Z(t)$  in the complex plane. The imaginary part represents the capacitance and the real part the conductivity of the system.

$$Z(t) = Z_{Re} + i \cdot Z_{Im} \quad (4.8)$$

with

$Z_{Re}$  real part of the impedance

$Z_{Im}$  imaginary part of the impedance

$i^2 = -1$ .

The absolute value of the impedance  $Z_0$  and the phase angle  $\phi$  are given by equations (4.9) and (4.10):

$$Z_0 = \sqrt{Z_{Re}^2 + Z_{Im}^2} \quad (4.9)$$

$$\tan \phi = \frac{Z_{Im}}{Z_{Re}} \quad (4.10)$$

For simple electronic circuits, of only a resistor, the phase angle  $\phi$  is 0, or of only a capacitor, the phase angle is  $-\frac{\pi}{2}$ . For electrochemical systems usually phase angles in between these two values are found.

Electrochemical impedance spectroscopy (EIS) studies the change of impedance as a function of the frequency. There are two common ways for data presentation, the so called BODE plot and the NYQUIST plot. In BODE plot the logarithm of the impedance,  $\log |Z|$  as well as the phase angle  $\phi$  is plotted against the logarithm of the angular frequency,  $\log \omega$ . A NYQUIST plot is characterized by presenting the imaginary part of impedance  $Z_{Im}$  versus the real part of impedance  $Z_{Re}$ . For each measured frequency, the obtained values are plotted in this coordinate system. For data analysis the spectra are fitted by theoretical data obtained from electrical equivalent circuits of consisting of common electrical elements as resistors, capacitors, and inductance, and elements like WARBURG impedance or the constant phase element (table 4.2).

TABLE 4.2. Elements for description of equivalent circuits of electrochemical systems.

Element	Current and voltage relationship	Impedance Z	Phase-shift $\phi$
Resistance, $R$	$E = I \cdot R$	$R$	$0$
Capacitance, $C$	$I = C \cdot \frac{dE}{dt}$	$\frac{1}{i \cdot \omega \cdot C}$	$-\frac{\pi}{2}$
Inductance, $L$	$E = L \cdot \frac{dI}{dt}$	$i \cdot \omega \cdot L$	$+\frac{\pi}{2}$
Constant phase element, CPE	-	$\frac{1}{(i \cdot \omega)^n \cdot C}$	$-n \cdot \frac{\pi}{2}$
Warburg Impedance, $\sigma$	-	$\frac{\sigma \cdot (1 - i)}{\sqrt{\omega}}$	$-\frac{\pi}{4}$

All these elements used for modeling of equivalent circuits in data analysis are related to electrode processes. A resistor can be used for describing the resistance of the solution. The effect of charging an electrical double layer as well as the coating of an electrode by an insulating layer is represented by the physical meaning of a capacitance. Electrochemical reactions can show similar behavior

like an inductor as common electrical element. The elements of WARBURG impedance and constant phase element (CPE) have been designed to simulate electrochemical phenomena that cannot be described by the known electrical elements. The WARBURG impedance for example is used to model the diffusion of the electroactive species to the electrode [29, 30]. For a planar diffusion with an infinite thickness of the diffusion layer, the WARBURG impedance  $Z_W$  is given by equation 4.11:

$$Z_W = \frac{\sigma \cdot (1-i)}{\sqrt{\omega}} \quad (4.11)$$

with the WARBURG coefficient  $\sigma$ , which is defined as:

$$\sigma = \frac{R \cdot T}{n^2 \cdot F^2 \cdot A \cdot \sqrt{2}} \cdot \left( \frac{1}{c_{ox}^0 \cdot \sqrt{D_{ox}}} + \frac{1}{c_{red}^0 \cdot \sqrt{D_{red}}} \right) \quad (4.12)$$

with

- $A$  surface of the electrode
- $D$  diffusion coefficient of oxidative (ox) and reductive (red) species
- $c^0$  bulk concentration of oxidative (ox) and reductive (red) species.

The characteristics of WARBURG impedance can be easily identified from the NYQUIST plot by its appearance as a straight line with a slope of 0.5, due to equal values for the imaginary part and the real part of the impedance.

The CPE helps to fit non ideal characteristics of the capacitance of the double layer. An electrochemical double layer is formed, when there is an excess of ions with opposite charge to that on the electrode surface at the phase boundary. For a capacitor the phase angle  $\phi$  is  $-90^\circ$ , but this shift is often at some other, non-ideal, values for double layer capacitance. For that case, the impedance of a CPE,  $Z_{CPE}$  differs from the capacitance by an exponent  $n$ :

$$Z_{CPE} = \frac{1}{(i \cdot \omega)^n \cdot C} \quad (4.13)$$

The value for  $n$  is between 0 and 1, and it is an empirical constant. For an ideal capacitor  $n = 1$ .

### 4.2.2 Cyclic voltammetry

In cyclic voltammetry the current flow of an electrochemical cell is measured during the application of a potential to the working electrode, which alters in triangular waveform with time (figure 4.4). This technique is widely used to study oxidative or reductive processes, their mechanism and kinetics, but it is also a valuable tool for the investigation of adsorption or desorption of some species to an electrode surface.

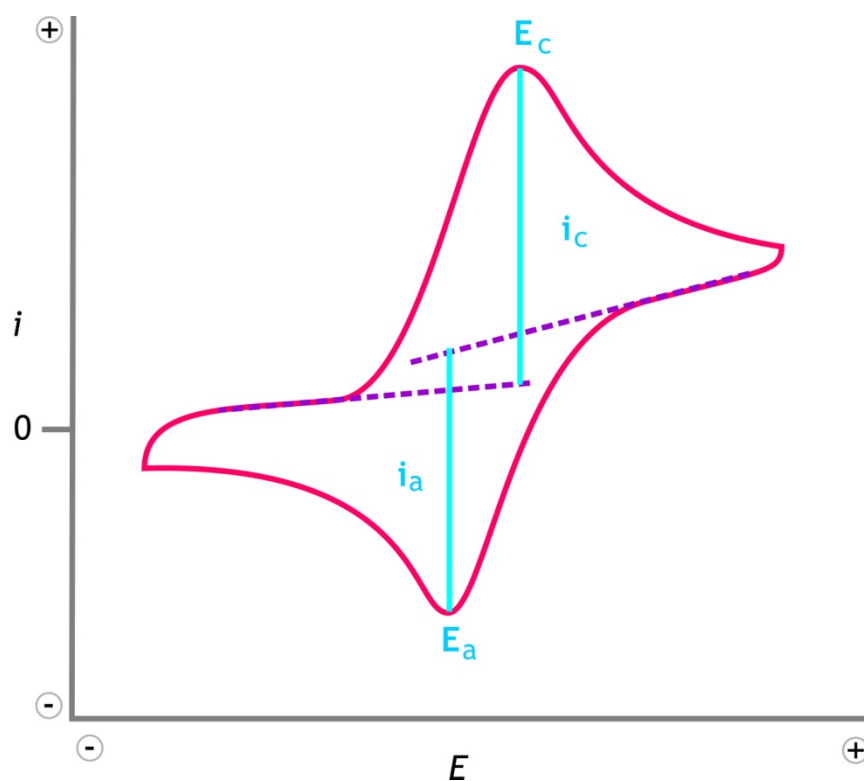


**FIGURE 4.4.** A typical cyclic voltammogram with oxidative and reductive species in solution. The potential is cycled forth and back between a starting potential and a reversal potential. The resulting current is measured.

The characteristic peaks in a cyclic voltammogram are caused by the mass transport of the reductive or oxidative species in solution, which is usually slower in contrast to the sweep rate of the potential. The process of oxidation and



reduction is diffusion controlled. For analytic purpose, it is interesting to notice that the peak current  $i_a$  and  $i_c$  are proportional to the concentration of electroactive species in solution.

For electrodes, covered by an insulating layer, cyclic voltammetry can be used to detect defects in the layer which form microelectrodes or ultramicroelectrodes. These types of electrodes are characterized by very small surface area in the micrometer or nanometer range and they show a different behavior in cyclic voltammogram. Due to diffusion controlled processes, the shape of the resulting curve is sigmoid. This can be described by different ways of diffusion. For planar electrodes the diffusion is linear, because of its relative large dimensions in contrast to that of the diffusion layer. For ultramicroelectrodes and not too fast sweep rates of the potential this is changed, the diffusion becomes spherical, and therefore the shape of the voltammogram becomes different [31].

### 4.3 X-ray photoelectron spectroscopy (XPS)

X-ray photoelectron spectroscopy (XPS) is a very sensitive analytical technique for investigation of the chemical composition of surfaces. The idea behind XPS goes back to the photoelectric effect, first proposed by ALBERT EINSTEIN in 1905. It describes the possibility to get information of the binding energy by studying the electrons emitted by irradiation with photons [16, 32, 33] (figure 4.5):

$$E_{binding} = h \cdot \nu_0 - E_{kin} - \phi \quad (4.14)$$

with

$E_{binding}$	binding energy of the electrons before photo ionization
$h \cdot \nu_0$	energy of the excited photons
$E_{kin}$	kinetic energy of the emitted photoelectron
$\phi$	work function of the material for the amount of energy which is necessary to exceed the potential barrier at the surface.

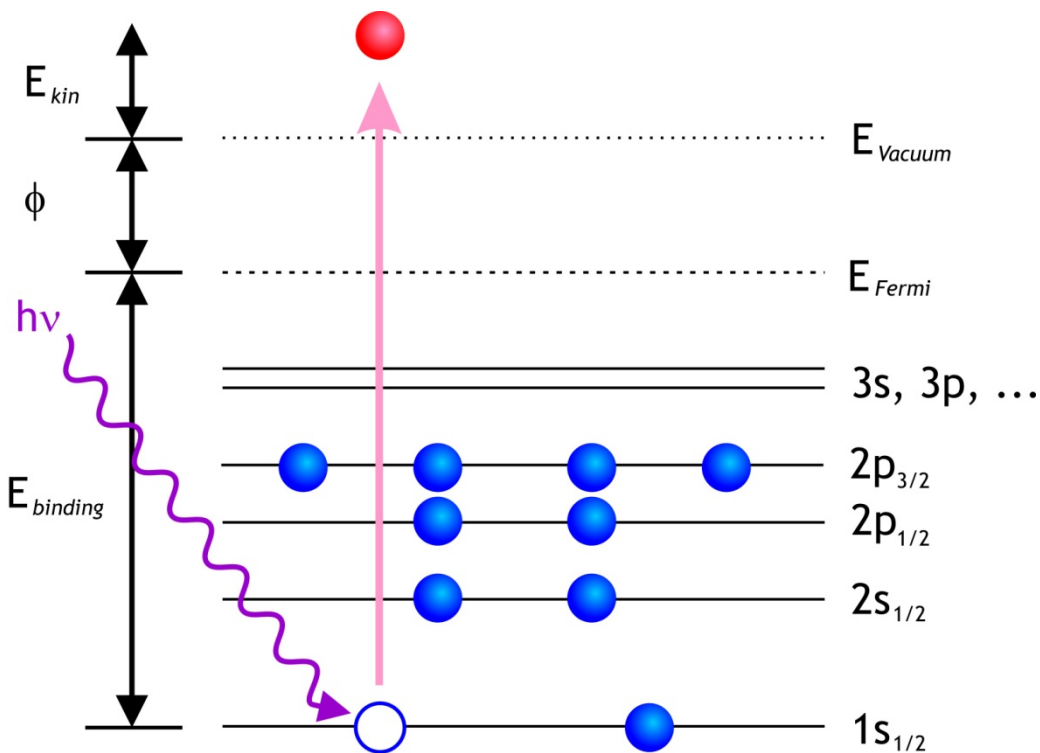


FIGURE 4.5. Scheme of the X-ray photoelectron emission process [34].

This emission of electrons is characteristic for each element due to its unique set of binding energies. By observing the number and the kinetic energy of the emitted photoelectrons it is possible to identify the elements in a surface and get information about their concentration in the surface.

An important parameter is the energy of the incident photon. This energy determines whether an electron from the valence or from the core will be emitted. With low photon energies ( $< 100$  eV) the valence electrons are emitted, this is used in ultraviolet photo electron spectroscopy (UPS) [32]. In classical XPS – this technique is also called electron spectroscopy for chemical analysis (ESCA) – high photon energies are used, and the emission of core electrons is detected. This detection has to be done in ultra high vacuum (UHV,  $\sim 10^{-9}$  mbar) to prevent collisions of the emitted electrons. Typical the photon energy of magnesium K (1253.6 eV) or aluminum K (1486.6 eV) X-ray irradiation is used.

The high surface sensitivity of the XPS technique is because of the fact that the emitted photoelectrons can only escape short distances in the material due to

inelastic collisions with other electrons. Therefore about 95% of all detected electrons come from a maximum distance of 10 nm in the surface [35]. The maximum deepness from which an electron can escape from a surface depend on its kinetic energy. The detection is done by an electron spectrometer, with tunable range for scanned energies. A variable electrostatic field in front of the analyzer allows visualizing different energies of the electrons.

Beside the identification of an element, XPS can also be used to estimate the concentration of an element in a surface. All elements except Hydrogen and Helium can be detected. For homogeneous surfaces the peak intensity for an element X is described by equation (4.15) [36]:

$$I_X = N_X \cdot \sigma_X^e(h\nu) \cdot L_X(\gamma) \cdot \lambda_S(E_{kin}) \cdot B \quad (4.15)$$

with

$I_X$	XPS intensity of atom X
$N_X$	atomic density of atom X
$\sigma_X^e(h\nu)$	cross section for electron e of atom X at photon energy $h\nu$
$L_X(\gamma)$	angular asymmetry factor
$\gamma$	angle between the X-ray beam and the electron beam to the spectrometer
$\lambda_S(E_{kin})$	mean free path length at $E_{kin}$ in the surface
$B$	instrumental constant.

With the estimation that  $L_X(\gamma)$  is equal for all atoms and  $\lambda_S(E_{kin})$  is independent of  $h\nu$ , the atomic concentration  $x_1$  of compound 1 of a mixed monomolecular layer of two compounds can be calculated as:

$$x_1 = \frac{I_1/I_1^\infty}{\sum_{i=1,2} I_i/I_i^\infty} \quad (4.16)$$

with

$I_i^\infty$  intensity from a pure monolayer of compound  $i$ .

X-ray photoelectron spectroscopy is a very helpful surface analytical technique for investigating monomolecular films of thiols on gold surfaces. In case of the spreader-bar systems, by using heteroaromatic molecules together with alkanethiols, the intensity of the nitrogen peak can be used to determine the surface concentration of the spreader-bar molecules in the surface.

#### 4.4 NEXAFS spectroscopy

The near edge X-ray absorption fine structure (NEXAFS) spectroscopy is a technique based on X-ray emission spectroscopy which was used for structural investigations since the 1920s. In contrast to XPS, which has its focus on the occupied part of the electronic state of the sample, NEXAFS spectroscopy is providing information about the unoccupied orbitals. Therefore the sample will be irradiated by photons with energy of that height that there occurs no complete cleavage of the electrons from the atom.

To give an idea of the emission of X-rays a simple model describes in a first step the elimination of an electron of the inner K-shell of the atom. In a second step refilling of this blank by an electron from the next shell (L-shell) seems to be most likely. This change in energy of the atom is accompanied by the emission of radiation. The most probably electron transfer comprise the line with the highest intensity in the K-spectrum, this is called the  $K_\alpha$ -line.

The absorbed energy of an atom in a molecule shows a fine structure which covers an energy range of several hundreds eV above the absorption edge. This fine

structures are caused by intramolecular electron migration from 1s electrons to the empty or partly occupied non binding molecule orbitals with  $\pi^*$ - and  $\sigma^*$ -symmetry. The typical resonances give information about bindings in the molecule. In case of adsorbed molecules to a surface it is possible to obtain information about the orientation of the molecules on the surface by analysis of resonance intensity as a function of the angle of incidence of the x-ray beam.

One of the experimental difficulties in NEXAFS-spectroscopy is the low content of atoms in the adsorbed film. If an X-ray absorption cross section for carbon is in the range of  $10^{-18}$  cm<sup>2</sup> per molecule is considered,  $10^3$  photons per each absorption is needed if there are  $10^{15}$  molecules per cm<sup>2</sup>. By estimation that every photoelectron for each absorption process can be detected by an efficiency of  $10^{-3}$ , it becomes clear that a high rate of photons of about  $10^9$  photons per second is required to get 1000 counts per second. This calculation clarifies that one requirement for studying NEXAFS is the need to have radiation from a synchrotron [37].

## 4.5 Infrared spectroscopy

Infrared spectroscopy is a well known technique to identify chemical bonds due to the fact that irradiation in the range between about 800 nm and 50  $\mu$ m stimulates molecular vibration and rotation. If this motion changes the dipole moment of the molecule energy will be adsorbed.

In the simplest model, when atoms are illustrated by balls and the binding between them behave like a perfect spring, HOOKE's law can be used to calculate the frequency  $f$  for the resulting vibration:

$$f = \frac{1}{2\pi} \sqrt{\frac{k}{\mu}} \quad (4.17)$$

with

$k$  spring constant

$\mu$  reduced mass.

To describe the vibrational energies with a quantum mechanical model the potential and kinetic energies of this harmonic oscillator have to be introduced into the HAMILTON operator. Equation (4.18) shows the Eigenvalues, or energy levels. The selection rules for the IR absorption process,  $\Delta v = \pm 1$ , results in discrete energy levels.

$$E_{vibr} = h \cdot f \cdot \left( v + \frac{1}{2} \right) \quad (4.18)$$

with

$h$  PLANCK's constant

$f$  frequency of the vibration

$v$  vibration quantum number ( $v = 0, 1, 2, \dots$ ).

The observed wavenumbers  $\bar{\nu}$  can be calculated from the absorbed energy by exciting the first harmonics ( $v=1$ ) from the vibrating ground state ( $v=0$ ),  $\Delta E = E_1 - E_0 = h \cdot c \cdot \bar{\nu}$  under consideration of the equations (4.17) and (4.18):

$$\bar{\nu} = \frac{1}{2\pi \cdot c} \sqrt{\frac{k}{\mu}} \quad (4.19)$$

with

$c$  velocity of light in vacuum.

Equation (4.19) shows that the wavenumbers depend on the mass of the atoms and the strength of the binding between them.

Until the 1980's infrared spectra were mainly measured by using classical dispersive spectrometers. With the development of computers fourier transform infrared (FTIR) spectrometers brought the advantages of more exact measurement,

higher signal-noise ratio and faster scans of the spectra. FTIR spectrometers use laser light for measuring the position of the moveable mirror, which allows simultaneous calibration of the wavelength. The higher signal-noise ratio is due to the fact that no entrance slits or monochromators are needed and therefore higher intensities of the light are possible. And the main advantage is that all wavelengths are measured at the same time [38 - 40].

A polychromatic IR beam is split and by passing an interferometer one part is sent to the sample. From a moveable mirror the beam is reflected in that way that it interferes and superimposes with the separated, initial beam. Depending on the position of the mirror the intensity of the beam is increased or decreased and an interferogram is obtained. The absorption by the sample alters the interferogram and this effect is recorded by a detector.

For investigating a thin film on a surface, FTIR has to be combined with the attenuated total reflection (ATR) technique. This method allows that the beam not only passes once the sample, which is due to the small dimensions of a monolayer not enough to detect any characteristic vibrations. As the name ATR implies, this can be realized by total reflection of the infrared beam at the interface between an infrared-transparent crystal with refractive index  $n_{\text{crystal}}$  and the sample with refractive index  $n_{\text{sample}}$ . If the crystal is optically denser than the sample ( $n_{\text{crystal}} > n_{\text{sample}}$ ), total reflection takes place for angles of incidence  $\theta_i$  which have to be greater than the so-called critical angle  $\theta_c$ . According to SNELL'S Law [41] the critical angle for total reflection is described by equation (4.20):

$$\theta_i \geq 90^\circ \Leftrightarrow \theta_i > \theta_c \quad \text{with} \quad \sin\theta_c = \frac{n_{\text{sample}}}{n_{\text{crystal}}} \quad (4.20)$$

At the reflecting interface, an evanescent field is generated by the interference of the incident and the reflected electromagnetic field. The evanescent field, as a standing wave, is aligned perpendicular to the surface with a sinusoidal shape. By passing the interface into the sample with lower refractive index, its amplitude decreases exponentially with the distance from the interface. Three variables have influence on the depth of penetration: (i) the angle of incidence  $\theta_i$ , (ii) the ratio of

$n_{\text{sample}}$  to  $n_{\text{crystal}}$ , and (iii) the depth is proportional to the wavelength of the light in the ATR crystal. When the polarization of the infrared radiation is parallel to the plane of incidence it causes a transverse magnetic wave (figure 4.6). Its amplitude  $E_{\parallel,0}$  is given by:

$$E_{\parallel,0} = \sqrt{|E_{z,0}|^2 + |E_{x,0}|^2} \quad (4.21)$$

with

$E_{z,0}, E_{x,0}$  spatial components of the amplitude of the electric field.

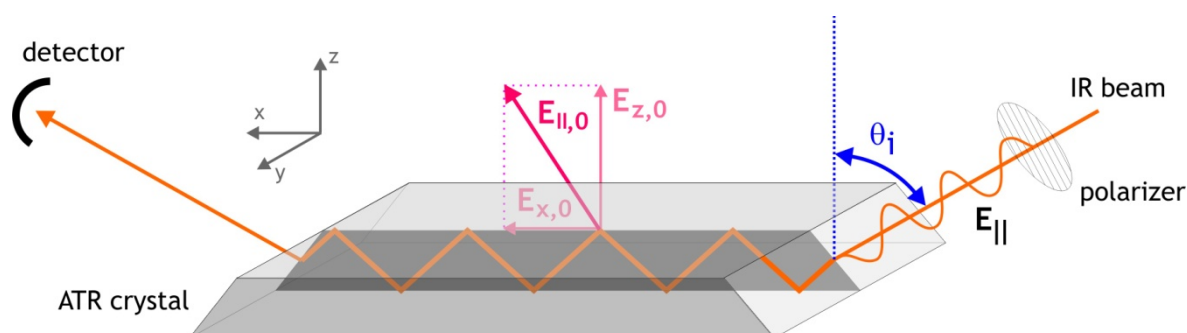


**FIGURE 4.6.** Scheme of a FTIR-ATR configuration with multiple reflections and parallel polarized infrared radiation (TM).

The transverse magnetic wave (TM) can interact with the dipole moments of molecules in  $x$ - and  $z$ -orientation. To excite dipole moments oriented in the  $y$ -axis, the polarization of the laser radiation has to be changed in perpendicular position to the plane of incidence and a transverse electric wave (TE) is generated.

By this way, one can get information on the chemical structure of a molecule and the orientation of the molecule can be estimated.

A further increase of the signal-noise ratio is done by measurement of many scans (usually about 500) in series. Practical problems are caused by atmospheric distortion because of interference of water or  $\text{CO}_2$ . This is overcome by measuring in vacuum, or inert gas atmosphere.



## 4.6 Surface plasmon resonance

Surface plasmon resonance (SPR) technique is a widely used method to study molecular interactions at thin metal films [42 - 44]. Changes in surface plasmon resonance can be detected with high precision and within very short time. These changes are caused by alterations in refractive index near a thin metal film. For typical SPR measurements a dielectric transparent substrate, usually a prism, which has been coated at one side with a suitable noble metal of a thickness of about 50 nm is used. This metal layer is further coated by a thin layer and adsorption processes on this film will be studied. When monochromatic  $p$ -polarized light passes through the substrate in a certain angle, it gets reflected at the metallic interface between substrate and the medium which should be investigated. The angle of the incident light has to be greater than the critical angle in order to obtain total reflection. For a certain wavelength, at this certain angle of incidence, surface plasmon waves along the metallic interface will be evoked and therefore the energy of the reflected light is diminished (figure 4.7).

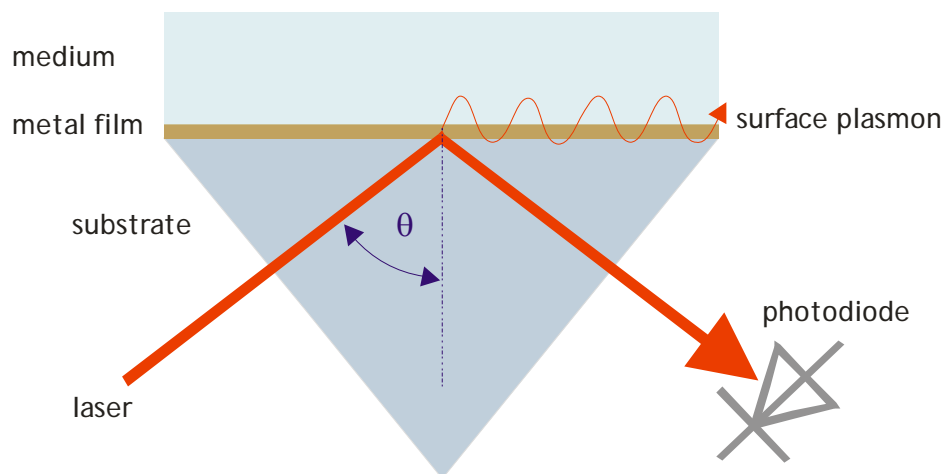


**FIGURE 4.7.** One possible scheme of a surface plasmon resonance transducer. If the refractive index of the substrate is higher than that of the medium, a laser beam at a certain angle of incidence is reflected at a thin metal layer between substrate and medium and surface plasmons are induced. The intensity of the reflected light is measured.

When the intensity of the reflected light is observed as a function of the angle of incidence at constant wavelength the surface plasmon resonance effect can be seen

as a sharp attenuation of the signal which passes a minimum. The angle of incidence which represents the minimum is the so called resonance angle. The position of the resonance angle is very sensitive to changes in the refractive index on top of the metal film. In case that the refractive index is not uniform due to mixed composition of this layer or because of partly adsorption of molecules, an average of the refractive index is measured [45]. As the evanescent field decays exponentially from the surface, the SPR technique is sensitive to refractive index variation within a few hundreds of nm from the surface [46].

## 4.7 Ellipsometry

Ellipsometry is an optical method for investigation of optical constants of a material or to measure the thickness of a thin homogeneous film adsorbed on a reflecting substrate [47]. For a substrate covered by an isotropic medium, FRESNEL found the principles for reflection ( $R$ ) and transmission ( $T$ ), and how they are related to the ellipsometric angles  $\Delta$  and  $\Psi$  that describe the change in the polarization of the light reflected at the surface.

Polarized light, reflected at a metallic surfaces changes amplitude and phase of both parallel,  $E_{\parallel}$  and perpendicular,  $E_{\perp}$  components. For example, linearly polarized, monochromatic light will become elliptically polarized after reflection on a surface. A typical setup for measuring ellipsometry is outlined in figure 4.8.

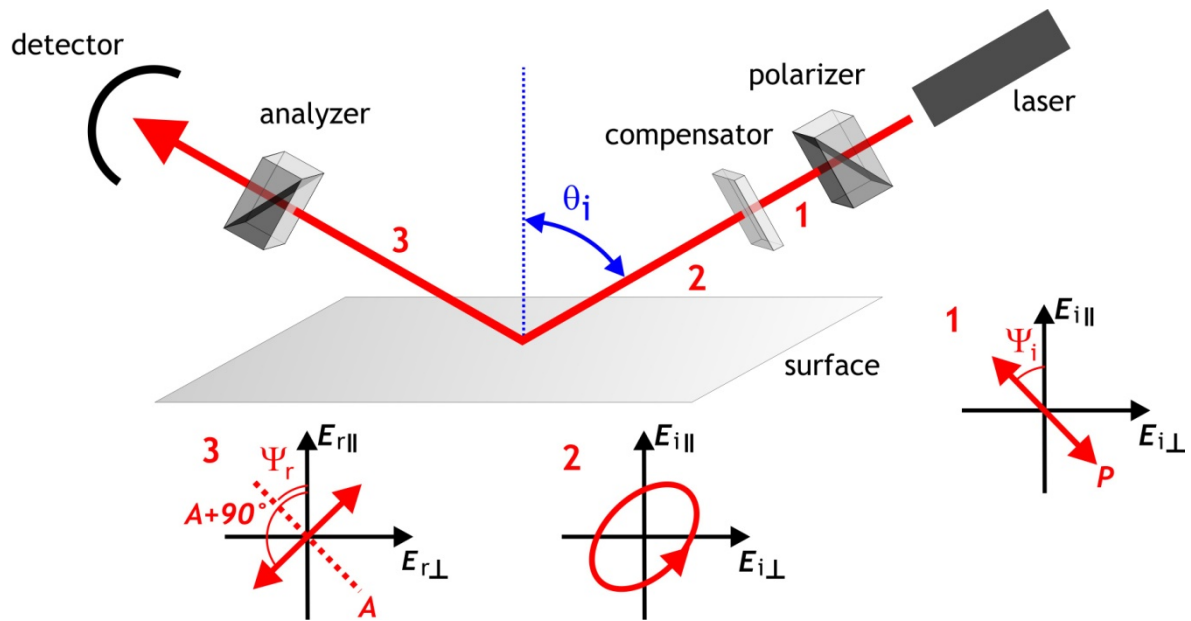


**FIGURE 4.8.** Experimental setup of a PCSA ellipsometer, consisting of polarizer, compensator, sample and analyzer. Initially linear polarized light becomes elliptically polarized by the compensator and after reflection the laser beam again is linear polarized. Analyzer and polarizer are rotatable. The analyzer is adjusted to give zero intensity at the detector [15].

The polarization of the reflected light is detected by the orientation of the analyzer. Its orientation is varied until no light passes through the analyzer. When the polarization of the incident light is known, the relative phase change  $\cos(\Delta)$  and the relative change in amplitude  $\tan(\Psi)$  can be calculated from the orientation.

The reflection properties of a sample change with the thickness of a layer on top of the sample. To study the thickness of a thin film, the change in the reflection properties are measured. To calculate the thickness, the refractive index of the film on the surface has to be known. For monolayers of alkanethiols on gold a refractive index of 1.45 is used [1]. The thickness of a layer can be estimated with ellipsometry with a precision of several ångströms.

## 4.8 Atomic force microscopy

Atomic force microscopy (AFM) is a surface analytical method providing information about the topography of a sample. The surface is scanned with a sharp tip mounted on the end of a cantilever (figure 4.9). The flexible cantilever bends in response to force between the tip and the sample. A laser beam is adjusted to the end of the cantilever and the reflected light is detected by a quadrant photodiode. When the force between the specimen and tip is changed, the cantilever got bend and therefore the position of the light hitting the photodiode is altered. As a result the electrical current produced by the photodiode changes.

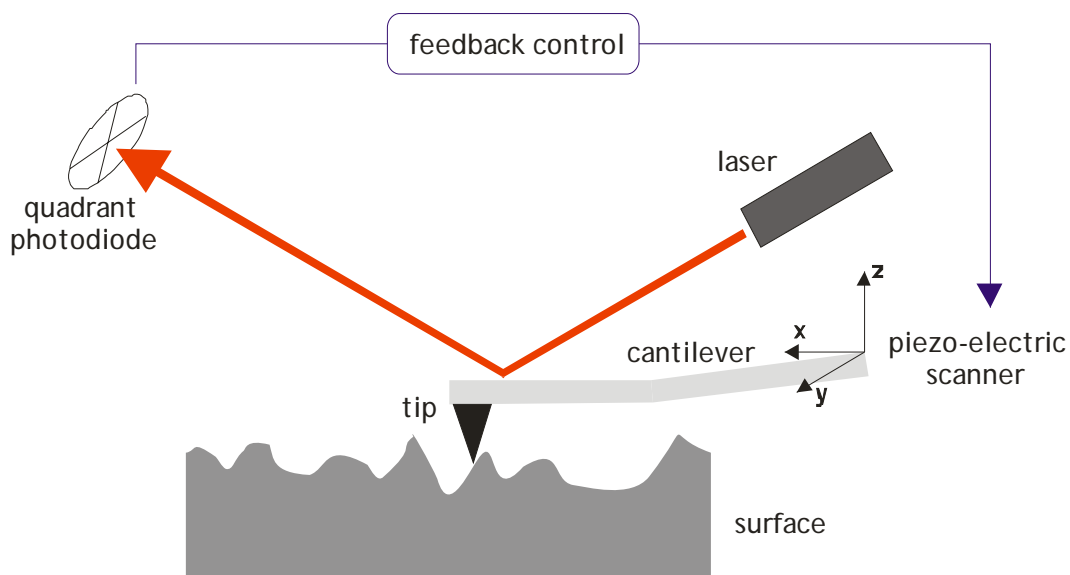


**FIGURE 4.9.** Scheme of the atomic force microscopy concept for surface sensitivity probing.

If the cantilever is lowered by a movement in  $z$ -direction, past the point where the tip touches the surface, the photodiode will measure the normal force between the tip and surface due to a bend upwards of the cantilever. Movements of the cantilever in  $x$ - or  $y$ -direction twist the cantilever and the resulting changes in the current of the photodiode include components due to lateral force between the tip and surface. By taking different combinations of the four parts of the photodiode

one can separate out the lateral and normal force components for a particular scan direction.

By recording the deviations in the force between the tip and the surface, which is the easiest way to scan a surface by AFM, there are two risks. First, if the surface is not very flat, scanning in  $x$ - and  $y$ -directions can result in large forces that will damage either the tip or specimen by scratching. And second, if the tip is not close enough to the surface, the forces between the tip and the surface will get to weak, or even lost.

Therefore a more elegant way to practice AFM is to scan the surface in  $x$ - and  $y$ -direction while maintaining a constant normal force. This is known as *contact mode* measurement. A negative feedback is used to adjust the tip height by controlling the voltage on the  $z$ -piezo positioning element as an answer to a deviation of the force on the tip from a user-determined set point. The voltage applied to the  $z$ -piezo is directly related to the level of the tip to the surface. Therefore it is possible to image the  $z$ -piezo voltage as topography of the scanned surface.

A different method is the so called *non-contact* or *tapping mode*: The cantilever oscillates at its resonant frequency during the surface scan. The variation in the amplitude of oscillation due to the attracting or repulsing forces between the tip and the sample is measured. A feedback control system overcomes systematical errors due to a constant decrease in the amplitude of oscillation relative to the amplitude, which is the case when the tip gets too far from the surface. The advantage of this method is that there is no permanent contact with the surface and thereby a damage of the sample or the tip is avoided. In contrast to measurements in contact mode lateral forces are much lower in tapping mode. Difficulties in getting images representing the real surface in non-contact mode occur when there is a purely attractive force between the tip and the surface. Then it is requires to operate the AFM in ultra-high vacuum. Although it has to be taken into account that in case of measurements in ambient conditions a water layer can

be formed on top of the surface which would result in interference or causes the tip to jump into intermittent contact.

Many artifacts in AFM images are caused by tip shape and imperfections in the feedback control system not recognized by untrained personal. In perfect conditions, the tip should be infinitely sharp in order to be sensitive enough to recognize as much of the surface as possible. And the feedback algorithm should give an infinitely sharp impulse response to instantly adjust the level of the tip by scanning over the surface. In reality, the tip has a pyramidal or conical shape with some definite end radius so it is durable enough to withstand the surface interaction forces. The effects of the tip shape cannot be avoided and these result in characteristic tip-dilation artifacts.

## **4.9 Scanning electron microscopy**

A scanning electron microscope (SEM) investigates a sample by irradiation with a sharply focused high energy beam of electrons and detects the resulting electrons that scatter out of the sample (figure 4.10).

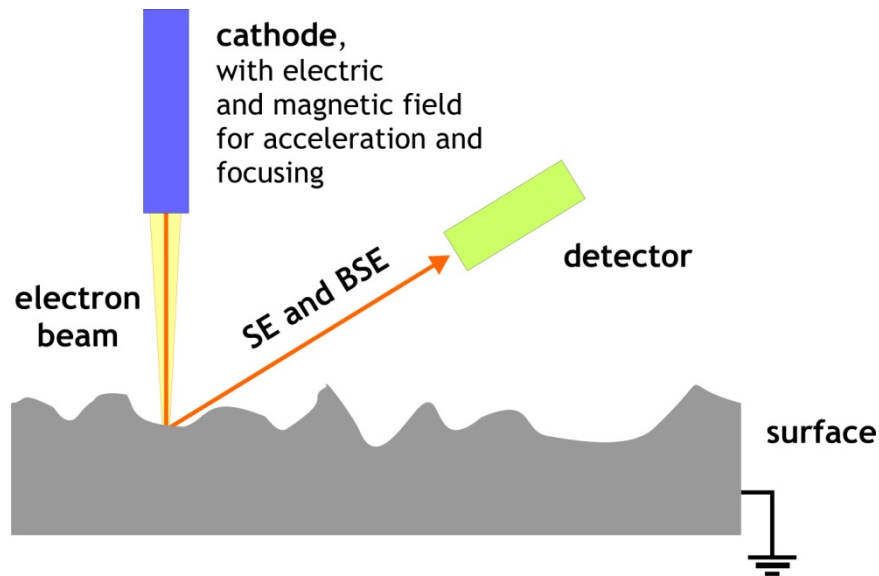


**FIGURE 4.10.** Basic principle of an scanning electron microscope. The sample is irradiated by a high energy electron beam. The deflected back scattered electrons (BSE) and the secondary electrons (SE), kicked out of the sample are detected.

The electron beam is focused from an initial diameter of about ten micrometers to a very small spot of only several nanometers in diameter by magnetic lenses. By electromagnetic deflection, similar to the beam in a cathode ray tube, this spot is directed over the surface in order to create an image of sample. The signal produced by scattered electrons from the sample is recorded by an appropriate detector and displayed as image on a screen. The electron beam direction determines the projection of the image. Its deflection is typically about one centimeter above the sample. Because of the great distance between deflection point which is the effective center of projection, in contrast to the diameter of several nanometers of the electron beam at the surface, the direction of the electron beam will be almost constant and therefore, the resulting projection can be considered as nearly orthographic.

The electrons, emitted from a cathode, accelerated by the electric field, hit the surface of the sample and interact due to their energy with the atoms of the sample. There are different ways of interactions possible. First, the electron can hit another electron which belongs to the atom of the sample. By this inelastic interaction some energy is transferred from one electron to the other. And second,

the electron can hit the heavy nucleus of the atom, and it will be deflected with almost no loss of energy by elastic interaction.

When a high energy electron is penetrating the surface its velocity is decreased by numerous inelastic interactions on its way into the sample. The inelastic interactions with the nucleus occur much less often, but they are more responsible for the change of direction of the electron. Electrons deflected from the sample are known as a back-scattered electron (BSE). The electrons that are kicked out from the atoms of the sample by inelastic interactions are the so called secondary electrons (SE). The origin of scattered electrons cannot be measured directly; therefore, they are characterized by their energy. Typically the electron gun is at a potential of -1000 volts relative to the sample, so each electron hits the surface with 1 keV. One electron penetrating the surface generates multiple secondary electrons with much lower energy of below 50 eV. Because of their low energy secondary electrons cannot overcome big distances and they get stopped by collisions with atoms in the sample. So the only secondary electrons which can leave the sample are those, generated within a very thin layer of several nanometers thickness near the surface of the sample. To distinguish if an electron is from the type of a SE or of the type of BSE, the energy they have is the determining factor. The energy of back scattered electrons is about 0.8 to 0.9 times of the energy of the incident electron beam [48], and the secondary electrons typically reaches energies in the range of 3 - 5 eV, but by convention all detected electrons of energies below 50 eV are classified as SE, all with energies higher 50 eV as BSE. Such a classification, given typical SE and BSE energy distributions, attempts to minimize the probability that an electron will be misclassified as SE or BSE.

If the sample which is scanned by SEM has some regions where the roughness is significant higher than on other regions, the rough parts will appear brighter than the smooth parts. Surface roughness means that the total area of surface is increased, and therefore the volume of the thin layer from which electrons can escape will be higher and of course the number of these electrons reaching the detector will be increased, and the image becomes brighter. The same phenomenon occurs near sharp edges where electrons scattering within the



specimen effectively have more opportunities to escape the specimen and reach the detector, the image gets brighter too.

Figure 4.11 shows a comparison of the artifacts of AFM and SEM for the same sample. In AFM, due to the finite size of the dip, the resulting output cannot image the sharp borders, and in SEM the borders will get brighter due to the bigger amount of electrons that can leave the surface.

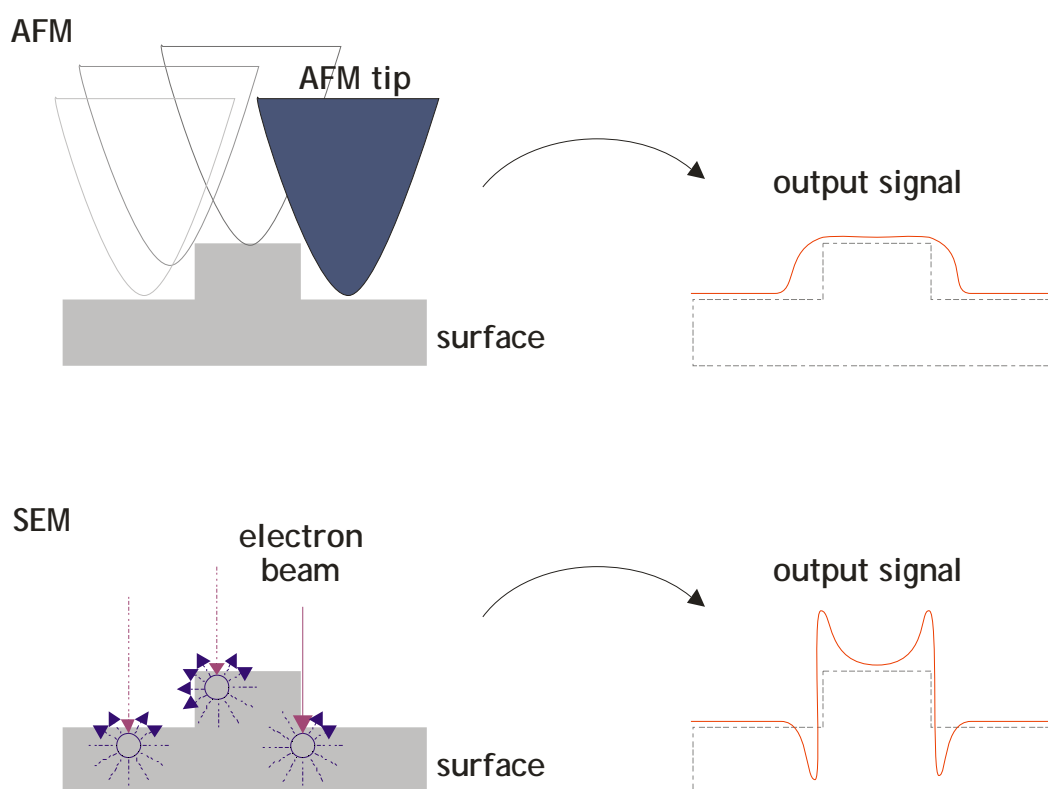


**FIGURE 4.11.** Simplified scheme of the output signals for a surface at an elevation with sharp edge, for AFM and SEM.

## 4.10 References

- [1] Ulman, A.; *An Introduction to Ultrathin Organic Films*, **1991**, Academic Press, Boston.
- [2] Folkers, J. P.; Laibinis, P. E.; Whitesides, G. M.; *Langmuir*, **1992**, 8, 1330 - 1341.
- [3] Tarlov, M. J.; Newman, J. G.; *Langmuir*, **1992**, 8, 1398 - 1405.

- [4] Dubois, L. H.; Zegarski, B. R.; Nuzzo, R. G.; *J. Am. Chem. Soc.*, **1990**, 112, 570 - 579.
- [5] Colthup, N. B.; Daly, L. H.; Wiberly, S. E.; *Introduction to Infrared and Raman Spectroscopy*, **1990**, Academix Press, San Diego.
- [6] Dubois, L. H.; Nuzzo, R. G.; *Annu. Rev. Phys. Chem.* **1992**, 43, 437 - 463.
- [7] Anderson, M. R.; Evaniak, M. N.; Zhang, M.; *Langmuir* **1996**, 12, 2327 - 2331.
- [8] Binnig, G.; Rohrer, H.; *Rev. Mod. Phys.* **1987**, 59, 615 - 625.
- [9] Delamarche, E.; Michel, B.; Biebuyk, H. A.; Gerber, C.; *Adv. Mater.* **1996**, 8, 719 - 729.
- [10] Strong, L.; Whitesides, G. M.; *Langmuir* **1988**, 4, 546 - 558.
- [11] Buttry, D. A.; Ward, M. D.; *Chem. Rev.* **1992**, 92, 1355 - 1379.
- [11] Buttry, D. A.; Ward, M. D.; *Science* **1990**, 249, 1000 - 1007.
- [12] Li, S.; Crooks, M.; *Langmuir* **1993**, 9, 1951 - 1954.
- [13] Badia, A.; Back, R.; Lennox, R. B.; *Angew. Chem. Int. Ed. Engl.* **1994**, 33, 2332 - 2335.
- [14] Bain, C. D.; Troughton, E. B.; Tao, Y.-T.; Evall, J.; Whitesides, G. M.; Nuzzo, R. G.; *J. Am. Chem. Soc.* **1989**, 111, 321 - 335.
- [15] Tengvall, P.; Lundström, I.; Liedberg, B.; *Biomaterials*, **1998**; 19; 407 - 422.
- [16] Chapman, R. G.; Ostuni, E.; Yan, L.; Whitesides, G. M.; *Langmuir* **2000**, 16, 6927 - 6936.
- [17] Poirer, G. E.; *Chem. Rev.* **1997**, 97, 1117 - 1127.
- [18] Zhao, X.-M.; Wilbur, J. L.; Whitesides, G. M.; *Langmuir* **1996**, 12, 3257 - 3264.
- [19] Bain, C. D.; Whitesides, G. M.; *J. Am. Chem. Soc.* **1988**, 110, 3665 - 3666.
- [20] Young, T.; *Miscellaneous works*, **1855**, Peacock, G.; Ed.; Murray, London.
- [21] Bikerman, J. J.; *Physical Surfaces*, **1970**, Academic Press, New York.
- [22] Zisman, W. A.; *Adv. Chem. Ser.* **1964**, 43, 1 - 51.
- [23] Adamson, A. W.; *Physical Chemistry of Surfaces*, **1990**, John Wiley & Sons, New York.

- [24] de Gennes, P. G.; *Rev. Mod. Phys.* **1985**, 57, 827 - 863.
- [25] Cassie, A. B. D.; *Discuss. Faraday Soc.* **1948**, 3, 11 - 16.
- [26] Israelachvili, J. N.; *Intermolecular and Surface Forces*, **1990**, Academic Press; London, New York.
- [27] Schwartz, L. W.; Garoff, S. J.; *Langmuir* **1985**, 1, 219 - 230.
- [28] Schwartz, L.W.; Garoff, S. J.; *J. Colloid Interface Sci.* **1985**, 106, 422 - 437.
- [29] Macdonald, J. R.; *Impedance Spectroscopy*, **1987**, John Wiley & Sons, New York.
- [30] Bard, A. J.; Faulkner, L. R.; *Electrochemical Methods: Fundamentals and Applications*; Second ed. **2001**; John Wiley & Sons, New York.
- [31] Hamann, C. H.; Vielstich, W.; *Elektrochemie*, **1998**, Wiley-VCH, Weinheim.
- [32] Moulder, J. F.; Stickle, W. F.; Sobol, P. E.; Bomben, K. D.; *Handbook of X-Ray Photoelectron Spectroscopy*, **1995**, Chastain, J., Ed.; Perkin-Elmer Corporation, Minesota
- [33] Siegbahn, K.; *Science* **1982**, 217, 111 - 121.
- [34] Persson, H.; *Tailoring MixedSelf-Assembled Monolayers (SAMs) for Adhesion Studies*, Dissertation, ETH Zürich, **2000**.
- [35] Ebel, M. F.; *Angewandte Oberflächenanalyse*, **1986**, Grassbauer, M; Dudek, H. J.; Ebel, M. F.; Eds.; Springer, Berlin.
- [36] Briggs, D.; Sheah, M. P.; *Practical Surface Analysis, Vol. 1*, **1990**, John Wiley and Sons; Chichester.
- [37] Stöhr, J.; *NEXAFS Spectroscopy, Springer Series in Surface Science*; Vol. 25, **1992**, Springer, New York.
- [38] Perkins, W. D.; *J. Chem. Edu.* **1986**, 63(1), A5 - A10.
- [39] Perkins, W. D.; *J. Chem. Edu.* **1987**, 64(11), A269 - A271.
- [40] Perkins, W. D.; *J. Chem. Edu.* **1987**, 64(12), A297 - A305.
- [41] Bergmann – Schäfer; *Lehrbuch der Experimentalphysik, Band 3 – Optik*; Niedrig, H., ed.; 9th edition, Walter de Gruyter, Berlin **1993**.

- [42] Knoll, W.; *Annu. Rev. Phys. Chem.* **1998**; 49; 569 - 638.
- [43] Lukosz, W.; *Biosens. Bioelectron.* **1997**; 12; 175 - 184.
- [44] Melendez, J.; Carr, R.; Bartholomew, D. U.; Kukanskis, K.; Elkind, J.; Yee, S.; Furlong, C.; Woodbury, R.; *Sens. Actuators, B* **1996**; 35; 212 - 216.
- [45] Jung, L. S.; Campbell, C. T.; Chinowsky, T. M.; Mar, M. N.; Yee, S. S.; *Langmuir* **1998**, 14, 5636 - 5648.
- [46] Chinowsky, T. M.; Quinn, J. G.; Bartholomew, D. U.; Kaiser, R.; Elkind, J. L.; *Sens. Actuators B Chem.* **2003**, 91, 266 - 274.
- [47] Drude, P.; *Ann. Phys. Chem.*, **1889**; 36; 865 - 897.
- [48] Goldstein, J. I.; Yakowitz, H.; *Practical Scanning Electron Microscopy and Ion Microprobe Analysis*, **1975**, Plenum, New York.

## **5. Results and discussion**

A method for formation of a new type of nanostructured monomolecular films, with high reproducibility and affordable effort was an important feature of this work. This was one of the reasons to decide that the fabrication of the nanostructured films should be done completely by self assembly in one experimental step, from solution onto polycrystalline gold surfaces. In this case there are only a few parameters, like concentration of the molecules used, the solvent, and the time and temperature for the self assembly process which have influence on the resulting layer. All these parameter can be easy adjusted and they warrant a reproducibility of the nanostructured films obtained. Furthermore there is no need of expensive devices or material to perform the formation of molecularly structured ultrathin films. As main criterion for optimization of the

conditions for self-assembly, the receptor properties of the resulting spreader-bar systems were taken into account.

Of course, there are a lot of other techniques to get structured self assembled monolayer, like soft lithography [1 - 8], irradiation techniques [9 - 12], electron beam writing [13, 14] or by using scanning probes [15 - 20], but all of these techniques are limited either the resolution of the structures or by its high experimental complexity compared to self assembly. In view of these considerations, self assembly in one step should be the best way to obtain the desired spreader-bar systems.

Freshly cleaned gold surfaces were kept for certain time in solutions of the two types of molecules: one of them was an alkanethiol (matrix molecule) the other one a spreader-bar molecule.

The spreader-bar molecule has to be rigid in its conformation, and it should exhibit a thiol group for anchoring it to the gold surface. Additionally it was favored if the spreader bar molecule was from aromatic or heteroaromatic type. In this case additional interaction of the  $\pi$ -electron-system with the gold [21 - 24] could be expected. This may stabilize the flat position of the spreader-bar, lying on the gold surface.

Alkylthiol monolayers with the following spreader-bars were investigated: 2-thiobarbituric acid (TBA), thiocyanuric acid (TCA), thiouric acid (TUA), thiol derivatives of the bases adenine (ASH), guanine (GSH), cytosine (CSH), thymine (TSH) and uracil (USH), stereoisomers of a conjugate of 1,1'-binaphthyl-2,2'-diamine with DL-6,8-thioctic acid (BNTA), a thiol modified 5,10,15,20-tetrakis(4-sulfonatophenyl)-porphyrine (TMPP), and aluminum naphthophthalocyanine chloride (Al-PC). The last molecule, Al-PC is without any thiol moiety, it was used to proof the idea that the  $\pi$ -interaction of an aromatic system could be strong enough to keep such a big molecule adsorbed on the gold surface in the presence of alkanethiols. All spreader-bars used in this work are depicted in figure 5.1.

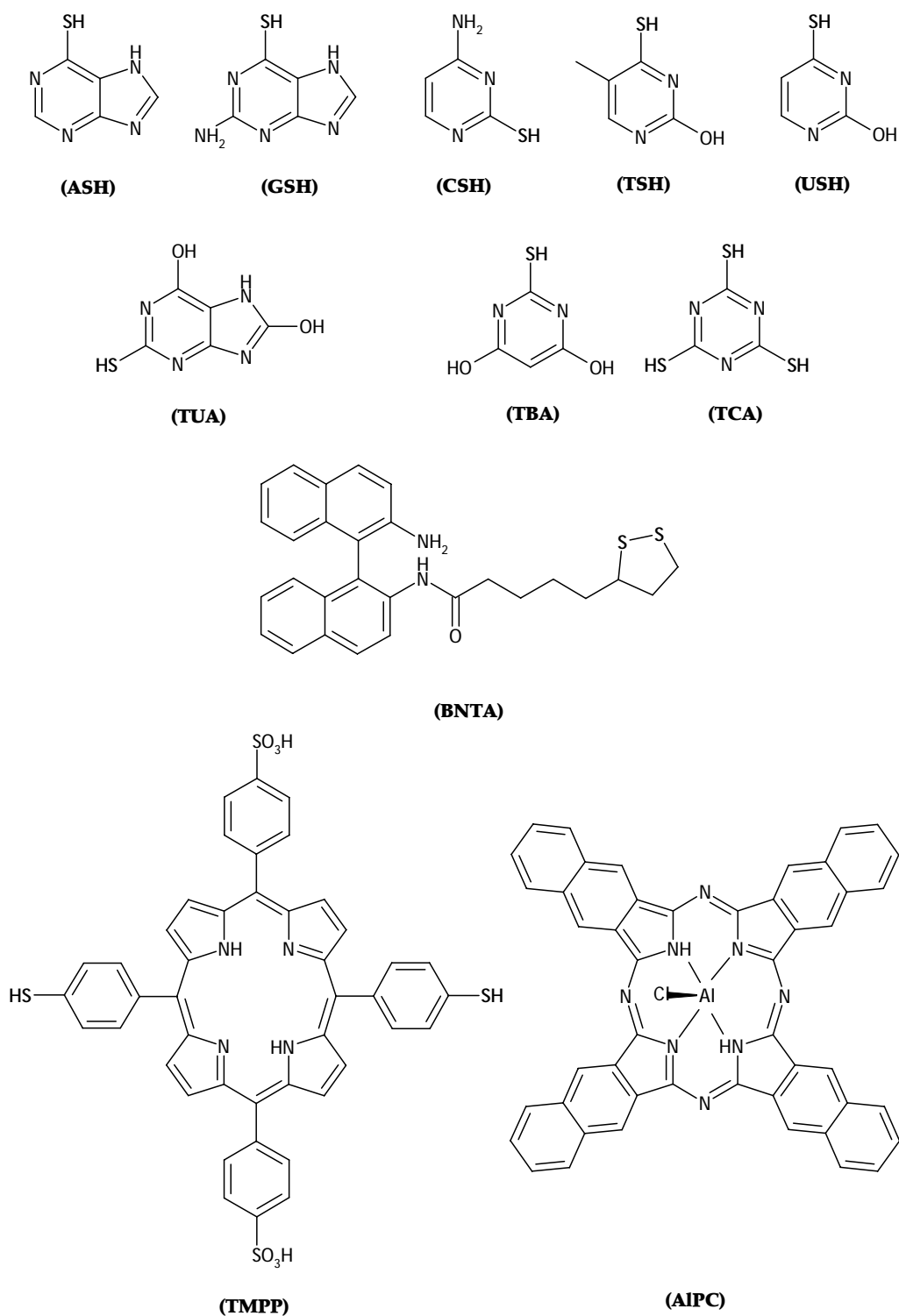


**FIGURE 5.1.** Chemical structures of the template molecules : 6-mercaptapurine (ASH), 2-amino-6-purinethiol (GSH), 4-amino-2-mercapto-pyrimidine (CSH), 4-hydroxy-5-methyl-2-mercaptopyrimidine (TSH), 4-hydroxy-2-mercaptopyrimidin (USH), 2-mercaptopuric acid (TUA), 2-thiobarbituric acid (TBA), trithiocyanuric acid (TCA), stereoisomers of a conjugate of 1,1' binaphthyl-2,2'-diamin with DL-6,8-thioctic acid (BNTA), 5,10,15,20-Tetrakis-(4-sulfonatophenyl)-porphyrin (TMPP) with partly reduced sulfonato-groups to thiol-groups, and aluminum 2,3-naphthalocyanine chloride (Al-PC).

All matrix molecules were generally from the type: HS-(CH)<sub>*n*</sub>-CH<sub>3</sub>, with *n* from 3 to 17, except tert.-butanethiol, 16-mercaptohexadecanoic acid, and DL-6,8-thioctic acid. An overview is given in table 5.1.

**TABLE 5.1.** Overview of the used matrix molecules for creation of nanostructured spreader-bar systems.

<b>Matrix molecule</b>	<b>Used in combination with these templates</b>
tert.-butanethiol	TBA
1-butanethiol (C4)	TBA
1-hexanethiol (C6)	TBA, ASH
1-octanethiol (C8)	TBA, ASH
1-dodecanethiol (C12)	TBA, ASH, CSH, GSH, TSH, USH, TUA, TCA, TMPP, AIPC
1-tetradecanethiol (C14)	TBA, ASH
1-hexadecanethiol (C16)	TBA, ASH, TMPP, BNTA, AIPC
1-octadecanethiol (C18)	TBA
16-mercaptohexadecanoic acid	BNTA
DL-6,8-thioctic acid	BNTA



## **5.1 Characterization of mixed monolayers formed by the spreader-bar technique**

### **5.1.1 Formation of mixed monolayers**

The spreader-bar technique enables the formation of mixed monolayers consisting of two types of molecules by immersion of a gold substrate into one solution containing both constituents. One type of molecules is responsible for the receptive properties of the resulting monomolecular film. It has to have a more or less rigid structure, similar to the shape of the desired analyte. We started the work with heteroaromatic systems like purines and pyrimidines. They are available in great number of variations, and most of them dissolve in a wide concentration range in solvents like ethanol, methanol or mixtures of ethanol and water. A lot of organic solvents have successfully been used for self assembly of pure thiols on gold. Important influence on the quality of the resulting layer was not found. For the preparation of mixed monolayer the situation becomes more difficult. It was demonstrated that the molar ratio of two different thiols within the monolayer can be controlled by the molar ratio of the two molecules in the deposition solution, but surface composition is determined neither by thermodynamics nor by kinetics [25 - 27]. In that case the choice of the solvent can be very important for the formation of mixed monolayer. In this work, only ethanol, methanol and mixtures of ethanol with water were used. There was no need to test other ones due to the success in the assembly of the spreader-bar system.

One difficulty is to find out the ratio of the matrix molecule and the spreader-bar molecule in the solution used for self assembly and the right time for immersion of the substrate into this solution. By studying the contact angles of several mixtures of purines and pyrimidines with 1-dodecanethiol it was found that the mixing ratio of alkanethiol and spreader-bar molecule has to be in the range of 1:100 and

1:10, in order to obtain monomolecular films with deviations in the contact angles from that of pure monomolecular films (figure 5.2).

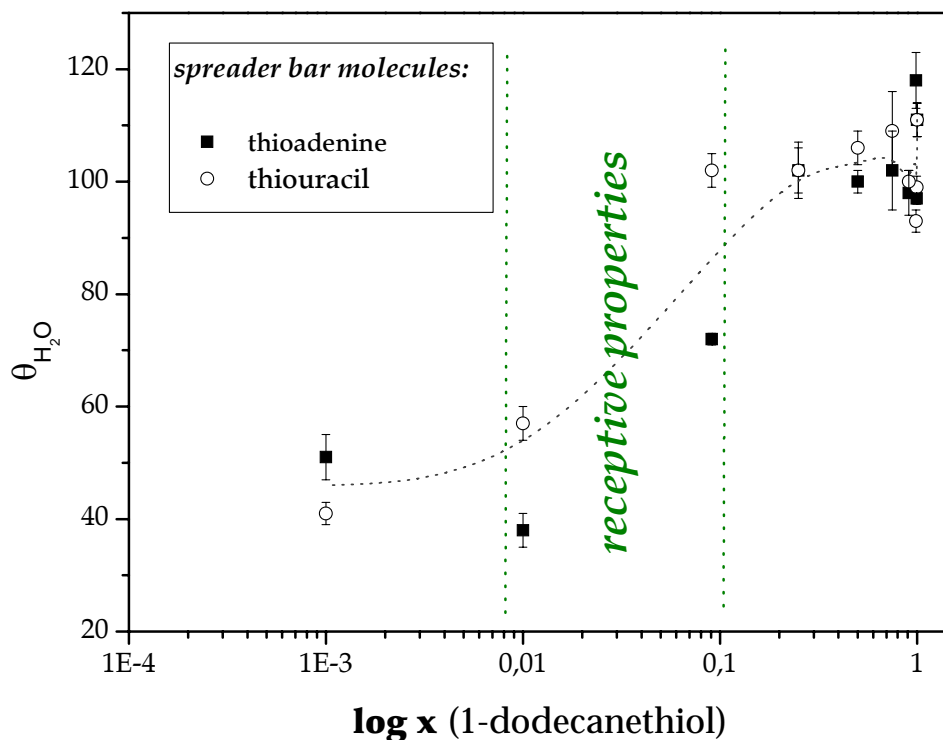


**FIGURE 5.2.** Advancing contact angle of water on different mixtures of a purine (ASH) and a pyrimidine (USH) with 1-dodecanethiol on gold.  $x$  represents the molar fraction of the spreader-bar molecule in the solution used for self assembly. Immersion from ethanolic solutions for 70 hours. The dotted line indicates a guideline for the eye.

For solutions with mixing ratios outside this range the measured contact angle are nearly the same as that of pure alkanethiol monolayer or that of pure spreader-bar monolayer.

The immersion time for the characterization of the spreader-bar coated gold surfaces by contact angle was 70 hours. Self assembled monolayers are usually formed within some minutes. In order to get a well packed ordered layer the immersion time is increased to several hours. In case of mixed monolayer consisting of molecules of different types with different affinity to the gold surface it is necessary to wait such long time to get equilibrium with no further change in

orientation or composition of the resulted monomolecular film. Only in this case one can obtain nanostructured surfaces with high reproducibility.

The receptive properties of the spreader-bar systems for purines and pyrimidines were monitored by electrical capacitance measurements. It was found that only systems immersed for at least about 70 hours for the self-assembly process exhibit receptive properties. Longer immersion time did not influence the performance of these modified surfaces as receptors. The influence of immersion time for creation of spreader-bar systems was evaluated by FTIR-spectroscopy (figure 5.3).

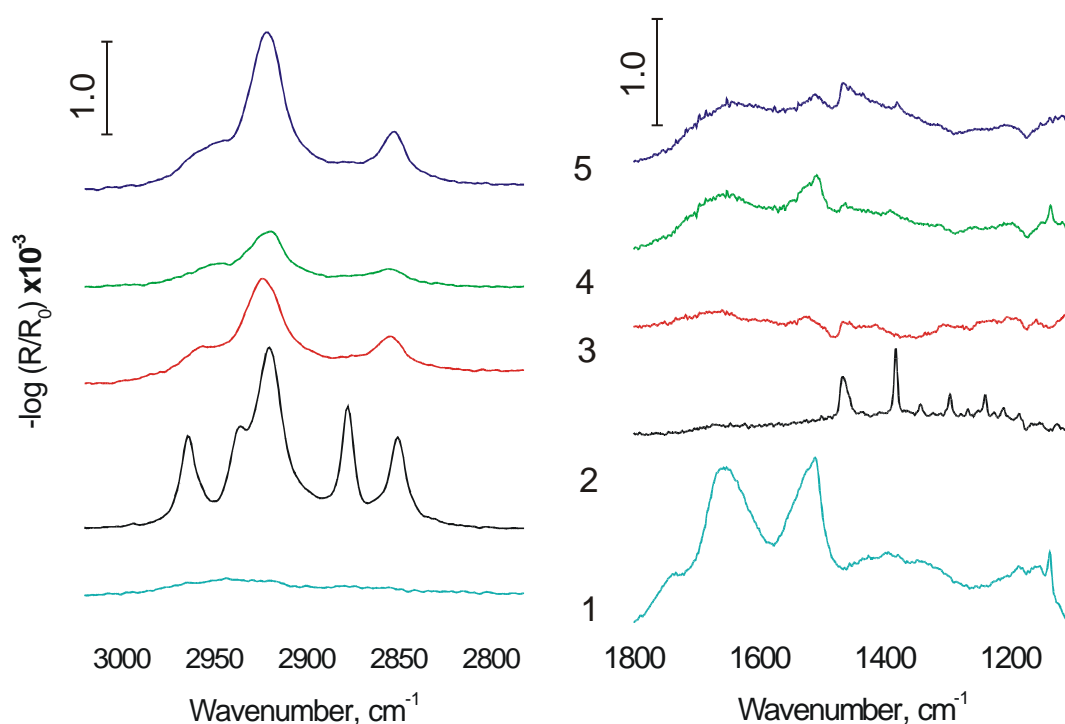


**FIGURE 5.3.** FTIR-spectra of 2-thiobarbituric acid (TBA) (1), 1-dodecanethiol (C12) (2) and a mixture of both (mixing ratio 1:100 C12:TBA) after immersion for one (3) and for three (4) days. (5) shows the spectra of (4) after additional immersion in pure 1-dodecanethiol for additional 1.5 hours.

The spreader-bar surface shows after long time immersion for three days the typical C-H vibrations of the alkanethiols as well as the specific bands of the spreader-bar molecule.

An analysis of the structure of the C-H vibrations point to a so called “spaghetti structure”: There are no sharp peaks as expected from well ordered pure alkanethiol monolayer caused by an upright  $-\text{CH}_3$  moiety at the top of the surface. So the structure is more likely described by spreader-bar molecules surrounded by very narrow band of alkanethiol molecules, which do not form a own domain detectable by infrared spectroscopy.

The mixed monolayer from the spreader-bar type were formed on the gold substrate by coadsorption of 1-dodecanethiol (C12) together with a large planar rigid molecule with a developed  $\pi$ -electron system, a thiolated derivate of 5,10,15,20-tetrakis-(4-sulfonatophenyl)-porphyrin (TMPP). The relative fractions of C12 and TMPP in the solution were varied. The deposition time was 72 hours, which is far beyond of a kinetic limit for surface/solution exchange of thiolated compounds on gold surface [28]. Therefore one can expect a quasi-equilibrium ratio of the template and matrix molecules in the film.

The large planar molecule aluminum phthalocyanine chloride was also tested as spreader-bar. The presence of 12 conjugated aromatic rings in the molecule and a suggestion on a strong  $\pi$ -electrons interaction with metal, caused us to expect that planar adsorption of these molecules occurs, even without exploiting of gold-thiol binding [29].

XPS spectra of the pure AIPC films and the films prepared from the mixed AIPC/C16 solutions are presented in figure 5.4. In the spectra of the pure AIPC films (bottom curves), characteristic emissions of all the elements comprising the AIPC molecule, including those related to nitrogen, chlorine, and aluminum could be found. The C 1s XPS spectrum of these films can be decomposed into two components, related to the aromatic core (the main peak) and C-N groups (the high BE shoulder), in accordance with the chemical composition of the AIPC molecule.

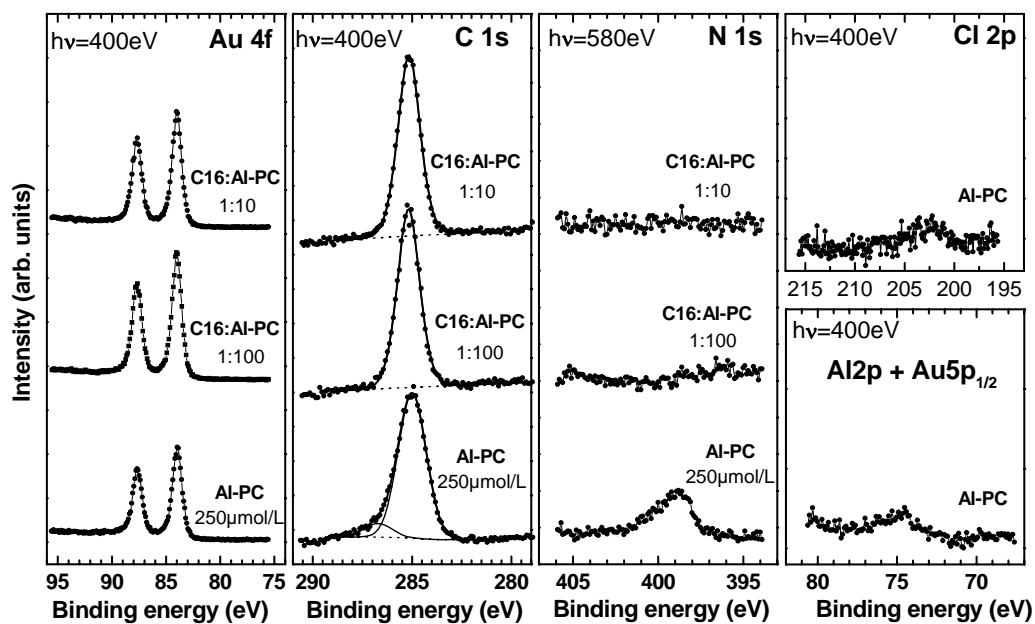


**FIGURE 5.4.** *Au 4f, C 1s, and N 1s XPS spectra of the SAMs formed from the AlPC and mixed C16/AlPC solutions, along with the Cl 2p and Al 2p spectra of the SAMs formed from the AlPC solution. The relative concentrations of C16 and AlPC in the primary solutions are given at the respective curves.*

The C and N K-edge NEXAFS spectra of the pure AlPC film are presented in figures 5.5 and 5.6, respectively (bottom lines). These spectra exhibit characteristic absorption resonances of naphthalenes ( $\approx 285$  eV) and pyridine-like moieties ( $\approx 400$  eV and  $\approx 410$  eV) [30]. In addition to these characteristic resonances and broader  $\sigma$ -resonances at higher photon energies, a low intense  $\pi$ -resonance related to the C=O moiety (288.7 eV) is observed in the C K-edge NEXAFS spectrum, suggesting that the AlPC film is slightly contaminated. This contamination stemmed, presumably, from the sample, which was exposed to ambient during its transfer from the evaporation chamber to immersion solution. Presumably, contamination was not completely removed upon the absorption of the AlPC molecules.

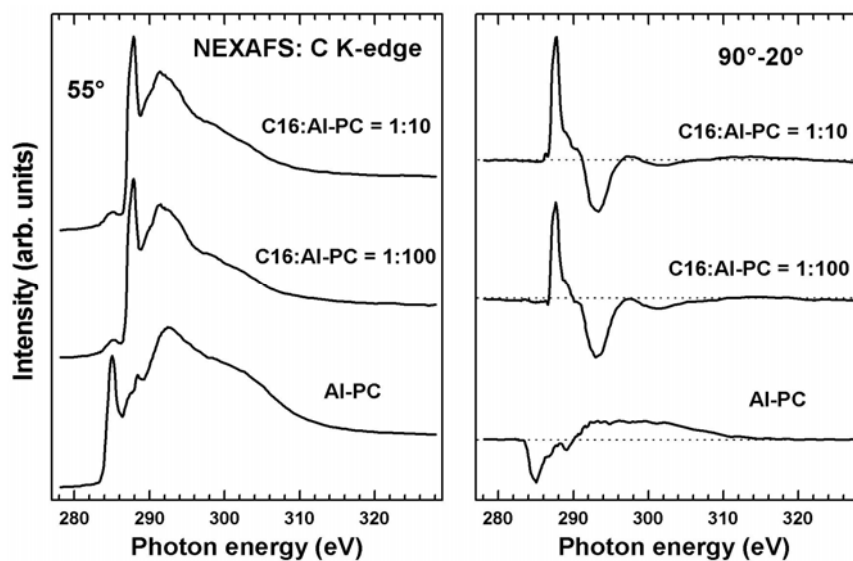


**FIGURE 5.5.** C K-edge NEXAFS spectra of the films formed from the AIPC and mixed C16/AIPC solutions; the relative concentrations of C16 and AIPC in the primary solutions are given at the respective curves. Left panel: The spectra acquired at a magic X-ray incidence angle of  $55^\circ$ . Right panel: the differences between the spectra acquired at X-ray incidence angles of  $90^\circ$  and  $20^\circ$ .

The spectra presented in the left panel of figure 5.5 and figure 5.6 were acquired at so called magic angle of X-ray incidence,  $55^\circ$ . At this particular orientation, NEXAFS spectra are not affected by molecular orientation of the AIPC film [30]. The information on the molecular orientation can, however, be derived from the entire set of the NEXAFS spectra acquired at different angles of X-ray incidence, since the cross-section of the resonant photoexcitation process depends on the orientation of the electric field vector of the linearly polarized synchrotron light with respect to the molecular orbital of interest (so called linear dichroism in X-ray absorption) [30]. Generally, a high intensity is observed if the direction of the  $E$ -vector coincides with the direction of the transition dipole moment of the molecular orbital under consideration. A fingerprint of the molecular orientation is the difference between the spectra acquired at the normal ( $90^\circ$ ,  $E$ -vector is parallel to the sample surface) and grazing ( $20^\circ$ ,  $E$ -vector is almost perpendicular to the sample surface) incidence of X-rays. Such a difference spectrum for AIPC/Au is presented in the right panel of figure 5.5 (bottom curve). In this spectrum, the difference peaks related to the  $\pi^*$ - and  $\sigma^*$ -resonances of the AIPC molecule have the negative and positive signs, respectively. Taking into account

that the  $\pi^*$ - and  $\sigma^*$ -orbitals are perpendicular to and coplanar with the molecular plane of the AlPC molecule, respectively, it can be concluded that these molecules are predominantly oriented parallel to the substrate surface. The average angle between Al-PC molecules and surface was estimated to be about  $40^\circ$ .

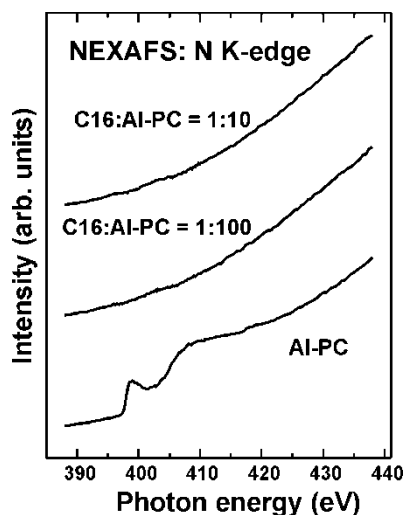


**FIGURE 5.6.** N K-edge NEXAFS spectra of the films formed from the AlPC and mixed C16/AlPC solutions; the relative concentrations of C16 and AlPC in the primary solutions are given at the respective curves. The spectra were acquired at a magic X-ray incidence angle of  $55^\circ$ .

On the basis of the XPS data (the C 1s and Au 4f intensities) and assuming an exponential attenuation of the photoemission signals and the attenuation lengths reported in ref. 31, the effective thickness of the AlPC film was estimated at about 2 nm. This value correlates with the size of the AlPC molecule, suggesting that this film represents mainly a monolayer. Taking into account the obtained average tilt angle of the AlPC molecules in the film ( $40^\circ$  with respect to the substrate surface), it can be suggested that the molecules are mostly adsorbed in a diagonal orientation, so that one bond of the naphthalene substituent is placed parallel to the metal surface. The inclined orientation of the APC molecules can be caused by a relatively strong contribution of the intermolecular interaction (stacking) of Al-PC as compared to the interaction with the substrate. Under definite circumstances (see below), the energy gain associated with a dense, SAM-like molecular packing of the AlPC moieties (inclined geometry) can prevail over the energy gain obtained at the optimal interaction of the molecules with the substrate, which

occurs at their in-plane orientation, since the latter geometry involves a loose molecular packing. Note that an inclined stacking has been observed previously for similar molecules, e.g. on the (001) surface of alkali halide [32] on stepped sapphire surface [33], and on silicon dioxide surface [34]. Additionally, the deviation from the parallel-to-the-substrate orientation, which is often observed in the case of organic molecular beam deposition of naphthalocyanines in ultra high vacuum (UHV) [35], can be caused by interaction of chlorine atom, standing out of the phtalocyanine plane [36], with gold by a similar way as in ref. 37.

An important factor, which can contribute to the formation of the inclined phase, hindering the optimal interaction of the Al-PC molecules with the substrate, is surface contamination. Whereas, under UHV conditions, the substrate is usually completely cleaned from contamination before the molecular deposition, it is slightly contaminated in the case of deposition from solution (see above), since it was exposed to ambient, even though for a short time, before the immersion. In the case of chemisorption of dissolved molecules, so-called self-cleaning, i.e. complete removal of contamination upon the adsorption occurs, as it, e.g., happens for alkanethiols [38]. In contrast and presumably, contamination persists to some extent in the case of the comparably weak ( $\pi$ -d) bonding, characteristic of the adsorption of phtalocyanines.

The situation changed crucially as soon as the Au substrates were immersed into the mixed AlPC/C16 solutions. In spite of the strong AlPC excess (by factors of 10 and 100), the respective XPS and NEXAFS spectra in figures 5.4 to 5.6 are characteristic of a one-component C16 SAM and do not exhibit any features related to the AlPC molecules. In particular, the C 1s XPS spectra of both C16/AlPC films in Figure 5.4 exhibit a relatively sharp emission at about 285.0 eV, which is characteristic of the intact alkanethiolate SAMs [39, 40] whereas no emissions were observed in the N 1s, O 1s, Cl 2p, and Al 2p ranges. In the S 2p XPS spectra (not shown), a characteristic doublet at 162.0 eV (S2p<sub>3/2</sub>) [40] related to the thiolate headgroup of C16 appeared. The effective thickness of both films prepared from the mixed AlPC/C16 solutions was estimated at about 18.9 Å, which is the expected value for the C16 SAM on Au [40].



The C K-edge NEXAFS spectra of both C16/AIPC films in Figure 5.4 also exhibit characteristic absorption resonances of well-ordered aliphatic SAMs: a mixed C-H\*/Rydberg resonance at 287.7 eV and C-C and C-C'  $\sigma^*$  resonances at  $\approx$  293.4 eV and  $\approx$  301.6 eV. These resonances show pronounced linear dichroism (see the right panel of figure 5.5), which is characteristic of well-ordered aliphatic SAMs. The average tilt angle of the aliphatic chains in both C16/AIPC films was estimated at 32° with respect to the substrate normal, which is the typical value for alkanethiolate SAMs on Au. Most important, no characteristic resonances of the AIPC molecule was observed in both C and N K-edge NEXAFS spectra of the C16/AIPC films, as shown in Figures 5.5 and 5.6, respectively. A low-intense feature at a photon energy of 285 eV in the C K-edge spectra is frequently observed for alkanethiolate SAMs and is alternatively assigned to a contamination or an excitation into alkane-metal orbitals. The N K-edge NEXAFS spectra for both C16/AIPC films represent identical smooth and structure-less curves, without any features related to the excitation from the N1s core level to nitrogen-derived unoccupied molecular orbitals.

Thus, it can be concluded that both C16/AIPC films represent well-ordered and densely packed C16 SAMs, which do not contain any AIPC molecules within the detection limit of XPS and NEXAFS spectroscopy (several % of the monolayer surface). It should be stressed out once more that the molar ratio of AIPC and C16 in the mixed solutions used for the substrate coating was as high as 10:1 or even 100:1. The deposition time was 72 h, which is above the characteristic time required for the formation of a well-ordered molecular monolayer. This result implies that even for large planar molecules with developed  $\pi$ -electron systems special anchor groups (e.g. thiol) are important.

Such molecules were synthesized by partial reduction of sulfonated tetraphenyl porphyrines, the XPS spectra imply that the average amount of the sulfone and thiol groups is approximately equal. The resulted thiolated tetraphenylporphyrine (TMPP) were used as spreader-bar in the mixture with alkanethiol as matrix and result in formation of mixed monolayer with the ratio dependent on the TMPP/alkanethiol ratio (figure 5.7).

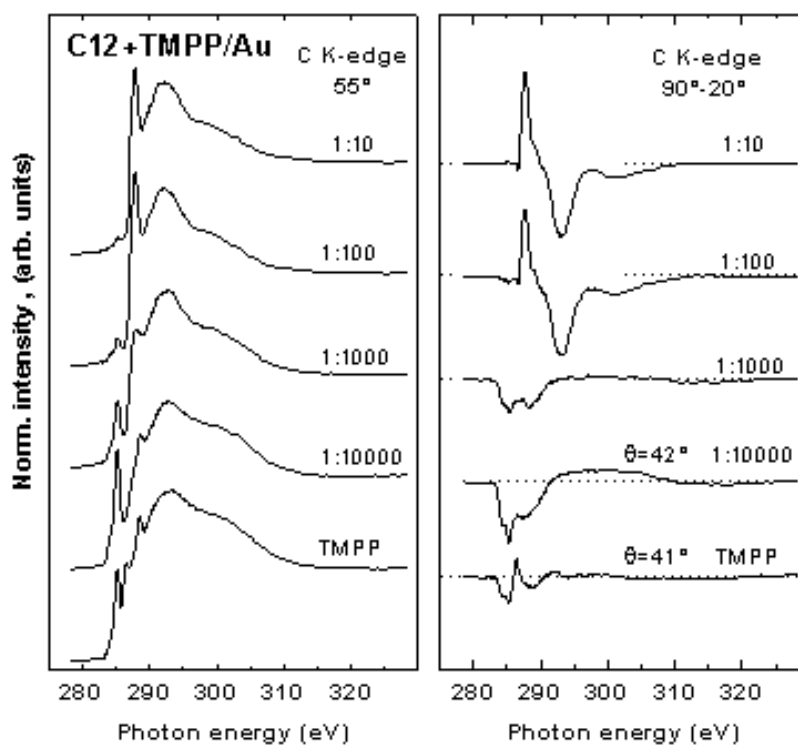


**FIGURE 5.4.** Left panel: C K-edge NEXAFS spectra of SAMs formed from one-component and mixed solutions of TMPP and 1-dodecanethiol (C12). Right panel: Difference between the spectra acquired at X-ray incidence angles of  $90^\circ$  and  $20^\circ$ . A continuous variation of the spectra and difference curves with the solution composition (C12:TMPP) is observed, which assumes the formation of a mixed film of variable composition depending on the relative portions of TMPP and C12 in the solution.

According to the spectra and the XPS data (see e.g. S 2p spectra in figure 5.8), the film formed from the 1:10000 (1-dodecanethiol:TMPP) solution contains only TMPP moieties, the "1:1000" film is mostly TMPP with some percentage of 1-dodecanethiol, the "1:100" film contains a minor amount of TMPP, and the spectra for the "1:10" film exhibit only 1-dodecanethiol features. Thus, the amount of the TMPP species in the mixed film can be precisely adjusted. According to the NEXAFS difference curves (left panel in figure 5.7), the TMPP molecules both in the one-component and mixed films has an in-plane (strongly inclined) geometry.

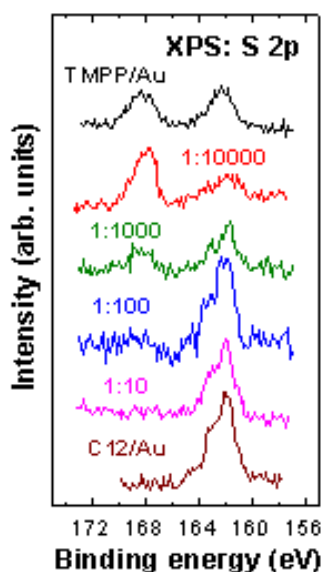


**FIGURE 5.8.** *S 2p XPS spectra of SAMs formed from one component and mixed solutions of TMPP and 1-dodecanethiol (C12). In the film formed from the one-component TMPP solution, two doublets related to the thiolate (a binding energy for  $S 2p_{3/2}$  of 162.0 eV) and sulfonate (a binding energy for  $S 2p_{3/2}$  of 168.5 eV) are observed. The occurrence of the thiolate-related doublet means a chemical anchoring of the TMPP species to the gold substrate. As C12 films do not contain the sulfonates species (see the bottom spectrum), the sulfonate-related peak can be considered as a fingerprint of the TMPP molecule and used to monitor the composition of the mixed TMPP/C12 films.*

The analysis of the structure and composition of the mixed C12/TMPP monolayers was performed by Near Edge X-ray Absorption Fine Structure (NEXAFS) spectroscopy, X-ray Photoemission Spectroscopy (XPS). According to the XPS and NEXAFS data (see e.g. the NEXAFS carbon K-edge spectra in the left panel of Figure 5.7 and S 2p XPS spectra in Figure 5.8), the monolayer formed from the 1:10000 (C12:TMPP) solution contains only TMPP moieties, the "1:1000" film is mostly TMPP with some percentage of C12, the "1:100" film contains a minor amount of TMPP, and the "1:10" film consists exclusively of C12 moieties. Thus, the amount of the TMPP species in the mixed film can be precisely adjusted. According to the NEXAFS difference curves (right panel in Figure 5.7), the TMPP molecules both in the one-component and mixed films have an in-plane (strongly inclined) orientation.

### 5.1.2 Distribution of molecules in the mixed monolayer

An indication of the content of spreader-bar molecules incorporated in the SAM of alkanethiol can be obtained by studying the thickness of the resulting layers by ellipsometry. If the thickness of a monolayer is not homogenous because of it consists of two molecules with different size, it can be expected that the measured thickness should be higher than the thickness of a monolayer from the smaller molecule and lower than value for the larger molecule. In the case of a self-assembled monolayer from 1-dodecanethiol a thickness of 16.9 Å was measured. The monomolecular film of 2-thiobarbituric acid has a thickness of 7.6 Å. For a mixed monolayer, obtained by immersion of the gold substrate to a mixture of 2-thiobarbituric acid and 1-dodecanethiol (100:1) under the same conditions like the pure monolayer, dissolved in 90% methanol and an immersion time of 70 hours, a thickness of 10.8 Å was measured. By assumption of a linear dependence of the resulted thickness as a function of the content of spreader-bar molecules in the surface, coverage of about 34% is found.

A similar estimation was done by measurement of the electrical capacitance and coverage of 48% was calculated. The difference of both values is due to different contribution of the single molecules to the sum of the resulted thickness. This may be taken into account especially for ellipsometry. The investigated structures are smaller than the wavelength of the light used. Therefore both values are rough estimations, but they are in the same range and show that both molecules cover the surface. For preparation of the spreader-bar monolayer of 2-thiobarbituric acid together with 1-dodecanethiol in such condition optimized to the receptive properties of this layer, the content of matrix molecules is slightly higher than that of 2-thiobarbituric acid. This is according to the model of the spreader-bar systems.

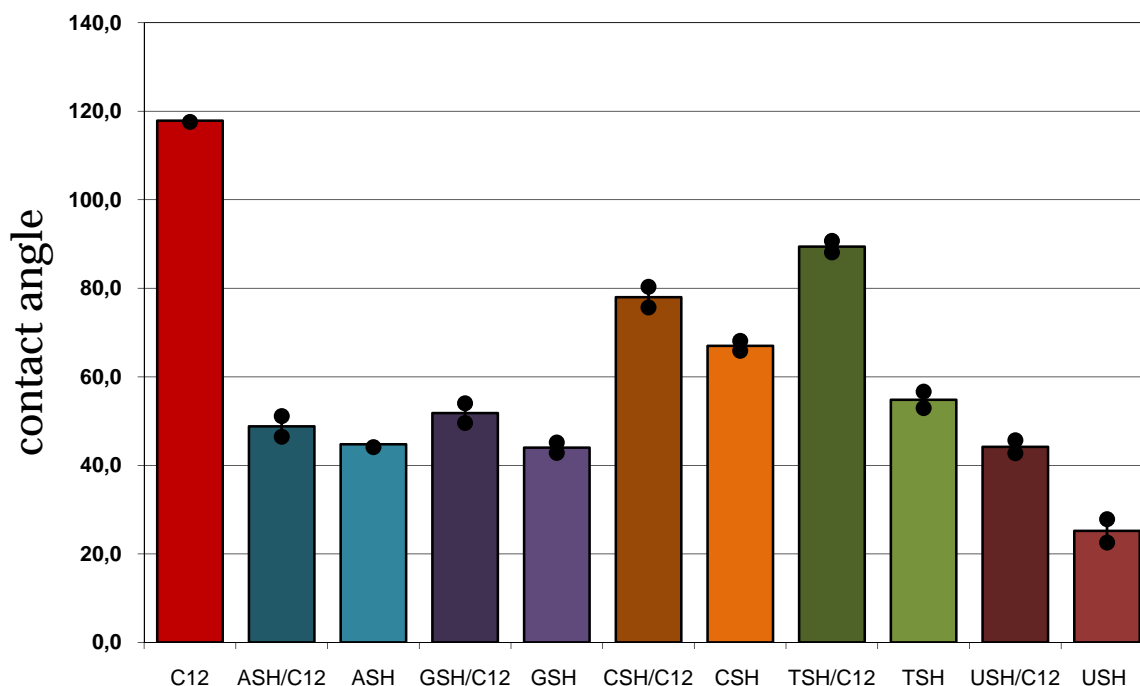


*FIGURE 5.9.* Contact angles of water on different self assembled monolayer and spreader-bar systems on gold. The contact angle on the mixed layers are always in between the angles measured for the two pure monolayers of the mixture.

Studies in contact angles of spreader bar systems show the same results (figure 5.9, table 5.2). Contact angles of mixed monolayers give values in between the contact angles of monolayers of their single compounds. The main information from this study is that there really is a mixture of the two components with random distribution of both molecules and without formation of any domains or regions which could be identified as a distinct phase.

**TABLE 5.2.** Advancing and receding contact angles of self assembled monolayer of 1-dodecanethiol (C12), 2-thiobarbituric acid (TBA) and the spreader bar system of a 1:100 mixture of C12:TBA on gold surfaces.

	water		hexadecane	
	advancing	receding	advancing	receding
TBA/C12	44°	15°	7°	5°
C12	104°	97°	43°	39°
TBA	36°	9°	7°	5°

The distinct hysteresis ( $\Delta\theta = \theta_{advancing} - \theta_{receding}$ ) of 29° for the contact angles of water in case of the spreader-bar system in contrast to a value of 7° for pure 1-dodecanethiol monolayer indicates the heterogeneity of the surface composition. But this is no evidence, because also the hysteresis of a pure monolayer of 2-thiobarbituric acid is nearly the same as for the mixture. An explanation of this result could be the rigid structure of 2-thiobarbituric acid. Because of that, a monolayer of pure spreader-bar molecules will be not able to result in a homogeneous film of such high order like for alkanethiols.

All spreader-bar systems assembled from alkanethiols together with purines or pyrimidines with thiol moieties were characterized by cyclic voltammetry. The modified gold electrodes show the typical redox activity of ruthenium(III)-hexammin and ferro cyanide (figure 5.10). The shape of the cyclovoltammograms exhibits the characteristics of macro electrodes with linear diffusion of the redox molecules to the electro active surface. This result indicates that the surface could not be characterized by a monolayer of alkanethiol with defects in molecular dimensions caused by incorporation of the spreader-bar molecules. In that case the cyclovoltammogram should have a shape with sharp peaks which are typical for spherical diffusion.

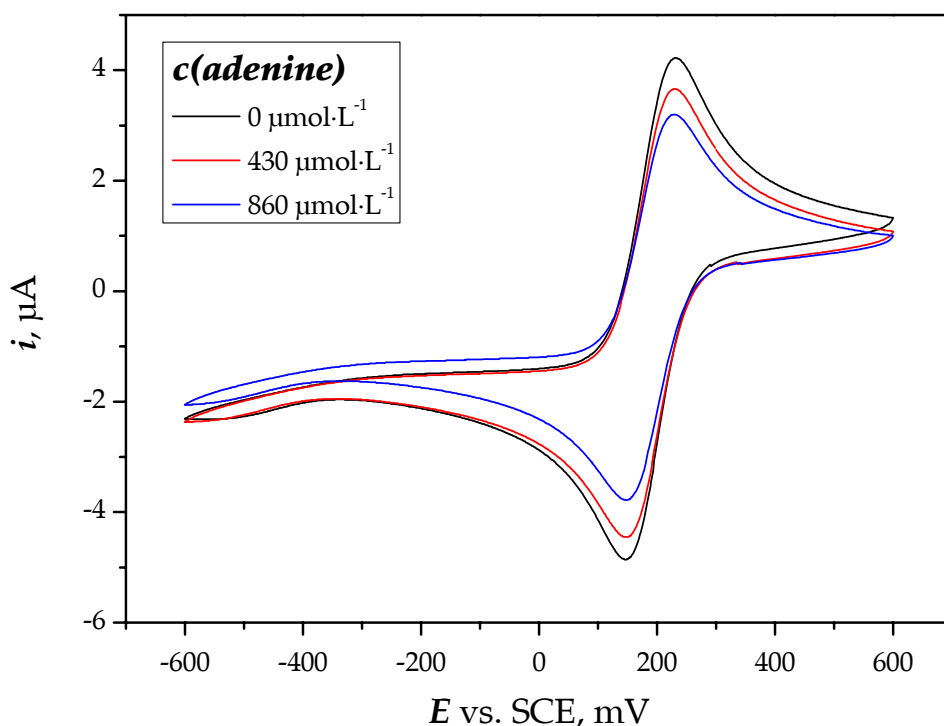


**Figure 5.10.** Cyclic voltammogram of a gold electrode covered by a monolayer of ASH and C12 measured in the presence of different concentrations of adenine. As electrolyte 10 mmol·L<sup>-1</sup> phosphate, 100 mmol·L<sup>-1</sup> potassium chloride and 5 mmol·L<sup>-1</sup> K<sub>3</sub>[Fe(CN)<sub>6</sub>] was used at pH 7.2 was used.

Gold electrodes covered by a pure monolayer of 1-dodecanethiol do not show the peaks of redox active substances like ferrocyanide and ruthenium(III)-hexammin at all. The redox processes are successfully blocked by the dense monolayer, which protect the gold surface from any contact to the Fe<sup>3+</sup>- and the Ru<sup>3+</sup>-ions in solution.

It was confirmed by impedance spectroscopy that the receptive properties of spreader-bar systems can be monitored by measurement of electrical capacitance, if, at the adjusted electrochemical potential, no compound in the solution shows redox activity.

From the BODE-plot (figure 5.11) one can see that for frequencies in the range from 10 to 100 Hz the phase angle of spreader-bar coated gold surfaces is near 80°. For an ideal capacitor a value of 90° is calculated. So this result allows in a first approximation to characterize the electrical properties of spreader-bar systems by

binding an analyte at the given frequencies as an increase of the dielectric thickness of the layer. The binding is straight proportional to the change in electrical capacitance.

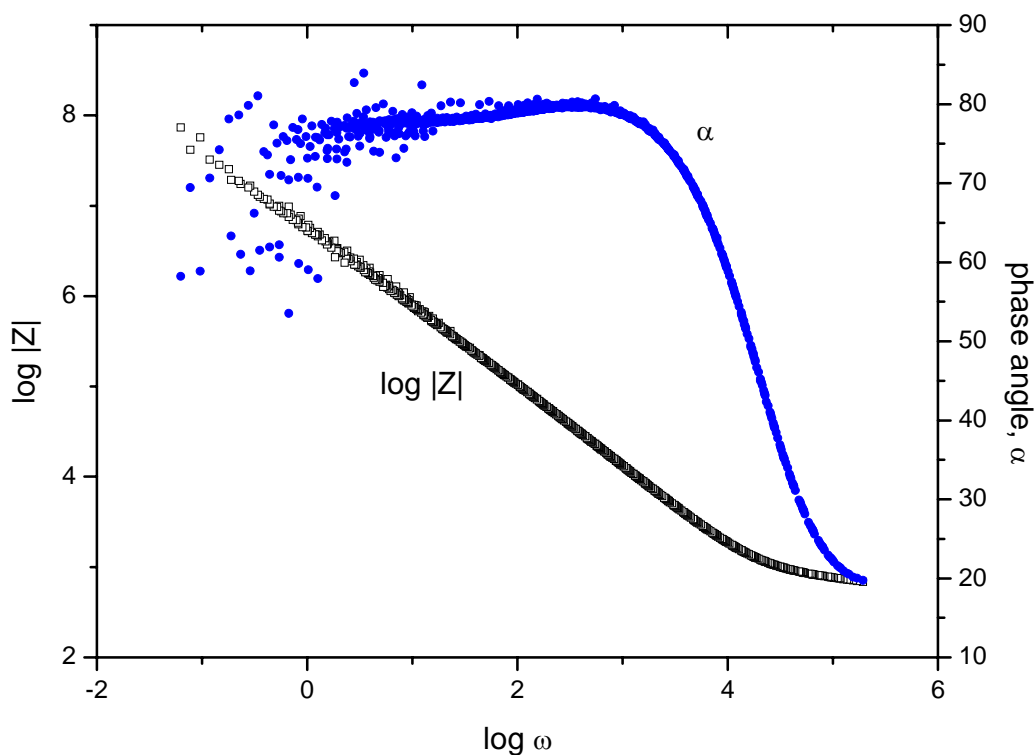


**FIGURE 5.11.** BODE-Plot of an impedance measurement of a gold electrode covered by a spreader-bar system consisting of ASH and C12.

At a more detailed view it gets clear that the simplest circuit of a capacitor in parallel to a resistor does not prove satisfactory the real situation. In the NYQUIST diagram (figure 5.12) this can be visualized easy. For the ideal system the values should describe a semicircle, but for low frequencies it was found that there is a linear increase. This can be described by WARBURG impedance. For an exact simulation of spreader-bar systems of alkanethiols and thiol modified purines and pyrimidines more complicated equivalent circuits consisting of capacitors and resistors in parallel together with WARBURG impedance in serial are necessary.



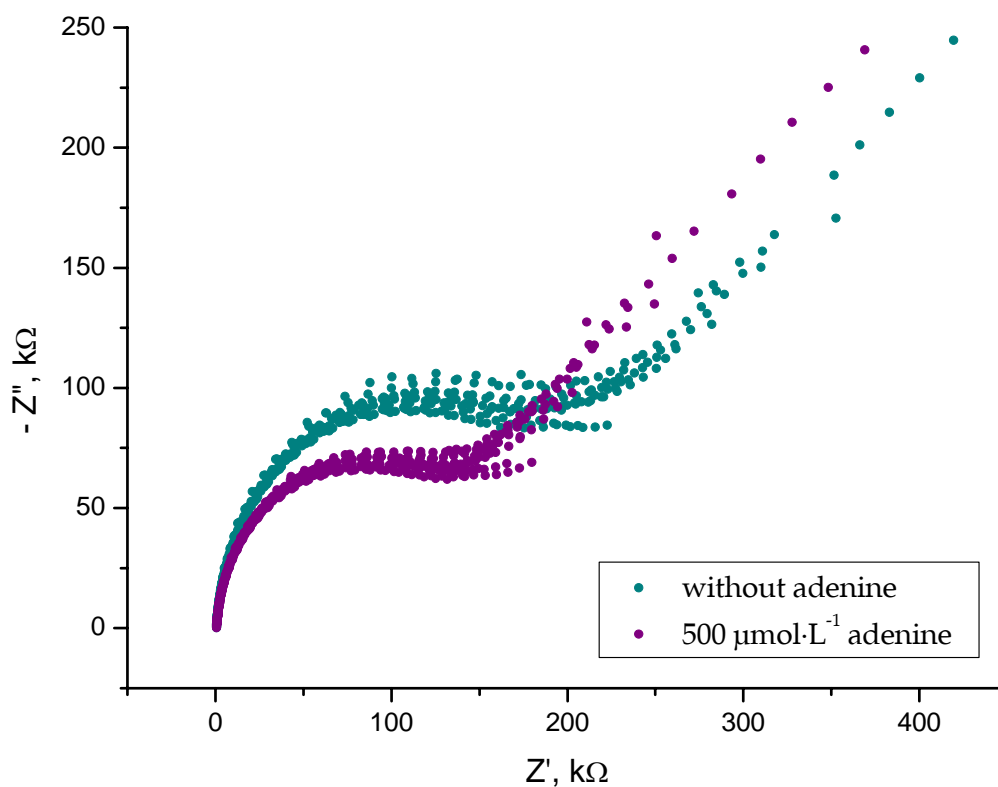


**FIGURE 5.9.** Nyquist diagram of a gold electrode covered by a spreader-bar system consisting of GSH and C12, without and in presence ( $500 \text{ mmol}\cdot\text{L}^{-1}$ ) of the analyte adenine..

Monolayer assembled from a solution consisting of 6-mercaptapurine and 1-dodecanethiol (6-mercaptapurine : 1-dodecanethiol = 100:1), the both species formed a mixed SAM on the gold surface. The analysis of the NEXAFS (figure 5.13) and XPS data suggest that there are about 74% of 6-mercaptapurine molecules in the mixed film. The orientation of the 6-mercaptapurine molecules in the mixed film ( $23^\circ$ ) differed from that in the one-component SAM while the orientation of the 1-dodecanethiol species ( $32^\circ$ ) was identical with the orientation in one-component 1-dodecanethiol film. It is interesting that the effect of alkanethiol on the orientation of 6-mercaptapurine was observed even at very low alkanethiol concentration in the coating solution where the concentration of alkanethiol in monolayers was less than the FTIR-detection limit. This confirms the initial suggestion and interpretation of FTIR spectra. XAM images taken with a resolution of 50 nm did not exhibit any domain structure.

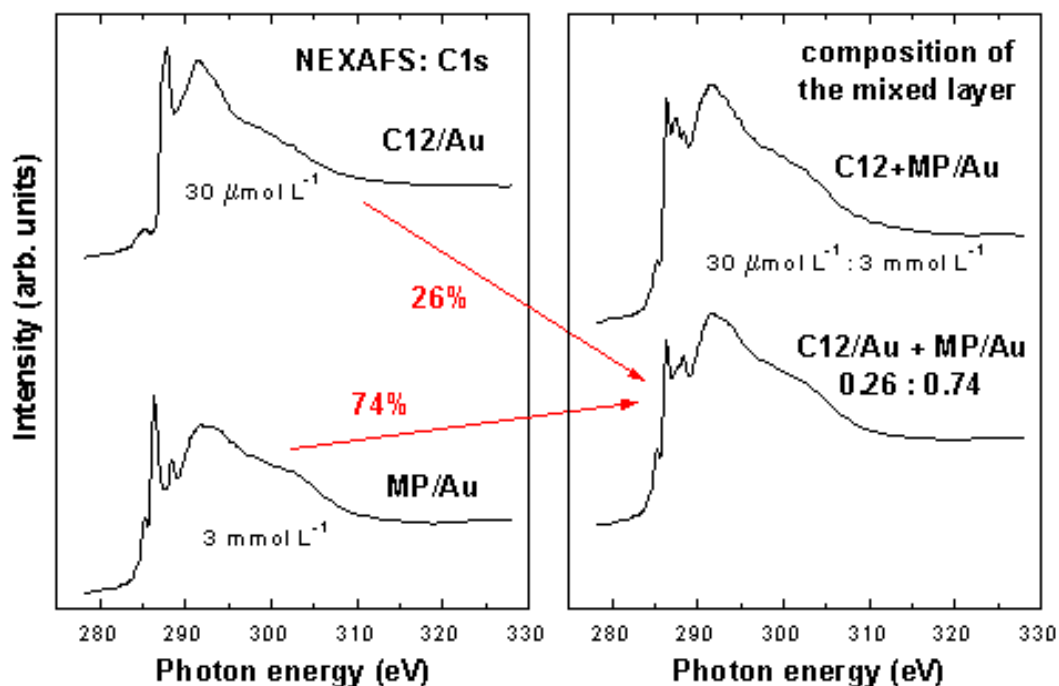


**FIGURE 5.13.** Left panel: C K-edge NEXAFS spectra of SAMs formed from 1-dodecanethiol (C12) and 6-mercaptopurine (6-MP) solutions. Right panel: a linear combination of the left panel spectra (bottom curve) in comparison to the spectrum of the film formed from a mixed C12/6-MP solution. As the spectrum of the mixed film is fully reproduced by the linear combination of the left-panel spectra, the content of the 6-MP molecules in the mixed film can be estimated as 74%.

### 5.1.3 Stability of mixed monolayer

For demonstration of the stability of spreader-bar coated gold surfaces, NEXAFS and XPS data were collected over time and compared. The behavior shown in figure 5.14 is in accordance with the C K-edge NEXAFS spectra and XPS data. In particular, no oxidation of the pristine thiolate groups occurred after the 4.5 months storage.

The one-component 6-mercaptopurine film and the mixed SAMs consisting of 6-mercaptopurine and 1-dodecanethiol reveal a good stability over the time, which is at least comparable with the stability of alkanethiol monolayer. According to the results from NEXAFS (figure 5.14) and XPS data, the chemical identity and the orientation order of the 6-mercaptopurine and the mixed SAMs was not destroyed during months-long storage.

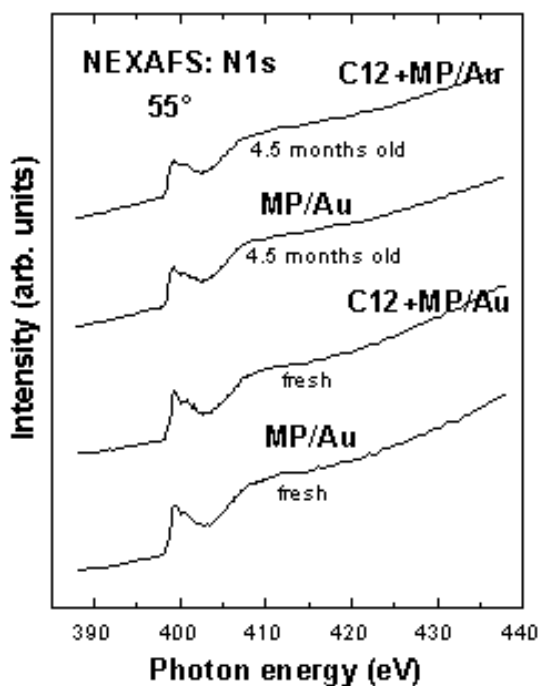


**FIGURE 5.14.** N K-edge NEXAFS spectra of SAMs formed from single components and from mixed 6-MP and C12 solutions. The spectra for the freshly assembled and 4.5 months old samples are compared. The characteristic absorption structure is preserved upon the sample storage, even though a small intensity reduction can be observed.

Electrochemical investigations also confirmed high stability of the spreader-bar structured monolayers. The results of four-month experiment are presented in the figure 5.15. While storage in ethanol led to some small desorption (the observed effect corresponds to desorption of  $\sim 1\%$  compounds), only minor changes of electrical capacitance were observed for the samples stored in the phosphate buffer, or in air. The cyclic voltammetry and impedance spectroscopy of these probes performed after 30 and 80 days storage, demonstrated also functional nativity of the spreader-bar structures. 6-mercaptopurine structured monolayers displayed binding of adenine.

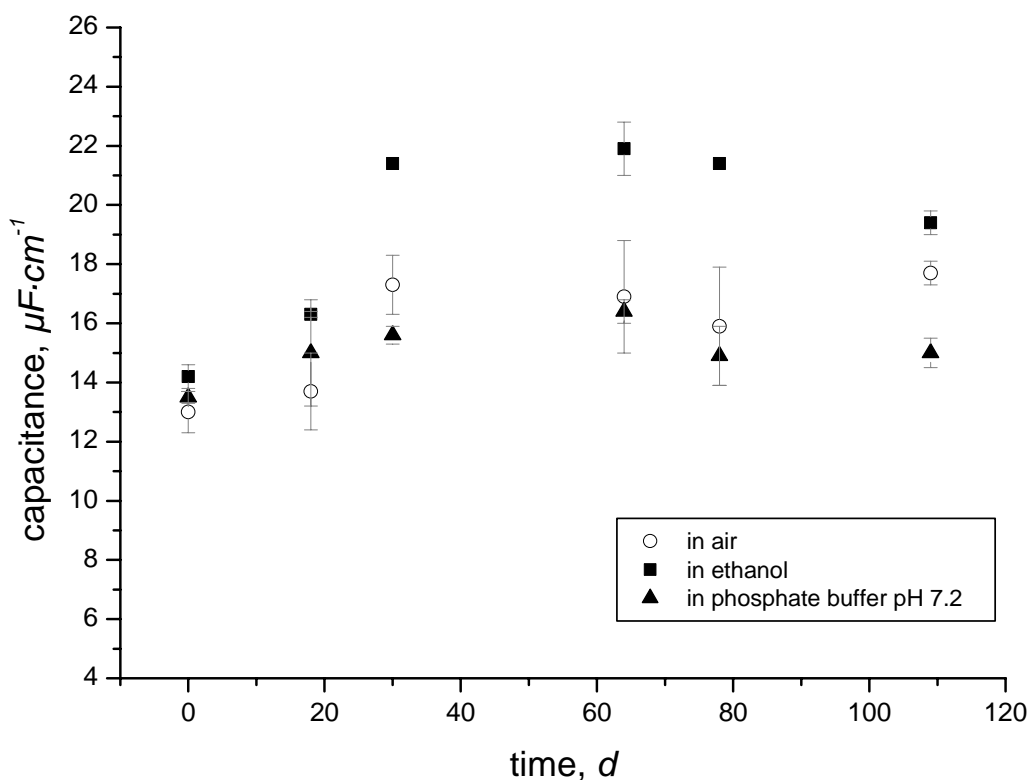


**FIGURE 5.15.** Changes of electrical capacitance of gold electrodes coated by dodecanethiol with 6-mercaptopurine spreader-bars during the long time storage in phosphate buffer ( $\blacktriangle$ ), in ethanol ( $\blacksquare$ ) and in air ( $\circ$ ), at usual laboratory conditions (room temperature, day light).

#### 5.1.4 Kinetics of the analyte binding in spreader-bar systems

The kinetics of the binding of analytes to spreader-bar systems consisting of 2-thiobarbituric acid and 1-dodecanethiol was studied. It was found that for concentrations of the analyte up to  $100 \mu\text{mol}\cdot\text{L}^{-1}$  the binding can be described by monoexponential kinetics (figure 5.16). For higher concentrations this model does not fit to the experimental data, the kinetics could only be described by two exponential functions (figure 5.17).

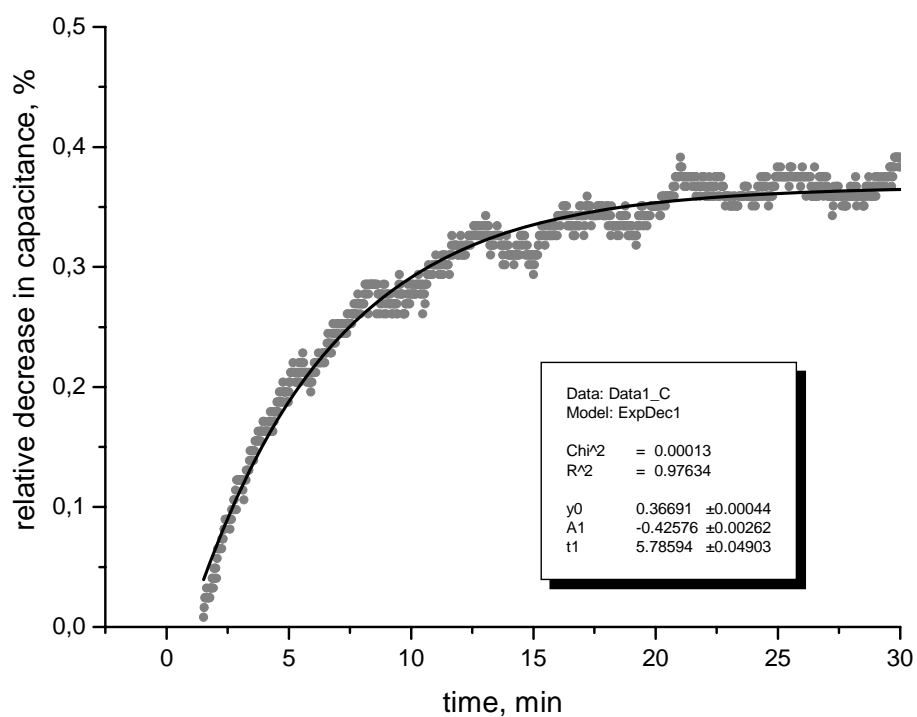


**FIGURE 5.16.** Kinetics of the binding of barbituric acid ( $100 \mu\text{mol}\cdot\text{L}^{-1}$ ) to a spreader-bar system formed by 2-thiobarbituric acid and 1-dodecanethiol.

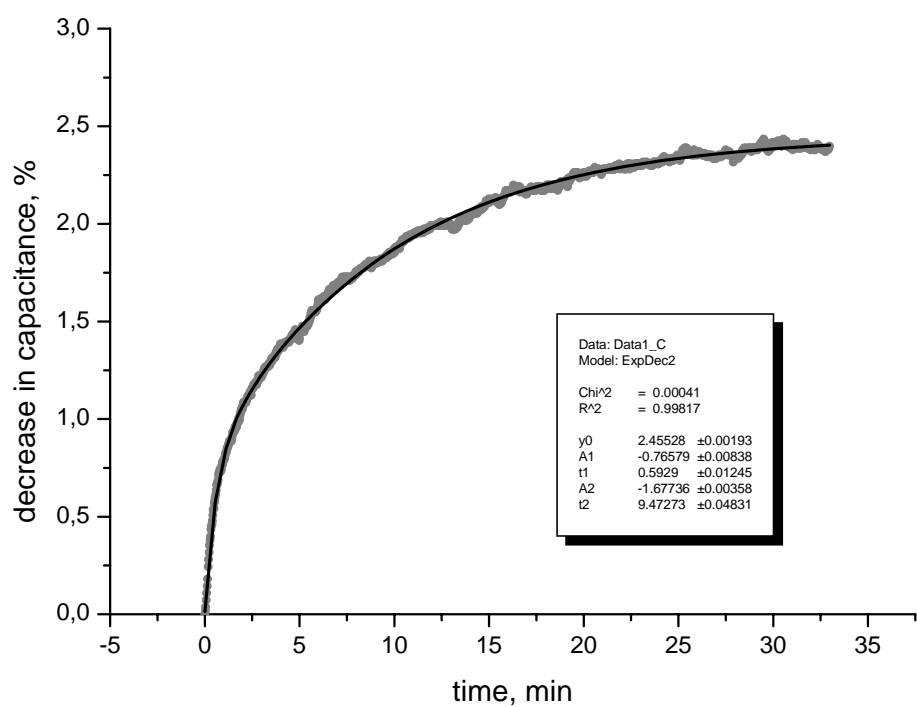


**Figure 5.17.** Kinetics of the binding of barbituric acid ( $470 \mu\text{mol}\cdot\text{L}^{-1}$ ) to a spreader-bar system formed by 2-thiobarbituric acid and 1-dodecanethiol.

The binding kinetics of barbituric acid and pyrimidine were measured at 30 °C for five different concentrations of each analyte. An analysis of the fitting parameters for the time constant shows a dependence on the analyte concentration for the faster process (figures 5.18 and 5.19).

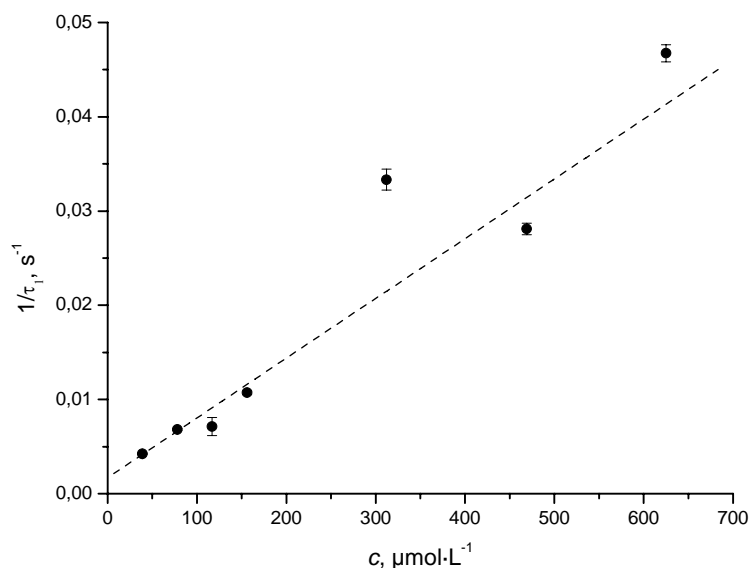


**FIGURE 5.18.** Concentration dependence of the time constant of the faster process for the binding of barbituric acid to spreader-bar systems of 2-thiobarbituric acid and 1-dodecanethiol.

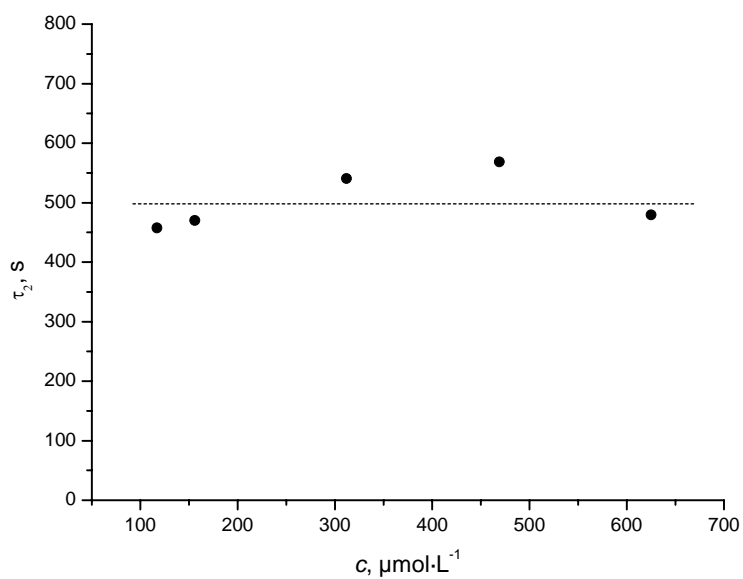


**FIGURE 5.19.** Concentration dependence of the time constant of the faster process for the binding of barbituric acid to spreader-bar systems of 2-thiobarbituric acid and 1-dodecanethiol.

Bi-exponential kinetics requires at best a three-state model to explain. A number of models was analyzed<sup>1</sup>. The simplest model describing these results the binding site performs a change in its conformation during the adsorption of the analyte. Therefore, after desorption of the analyte a relaxation process must take place in order to rebind another analyte molecule. By studying the adsorption and desorption by electrochemical measurement of the electrode capacitance for the concentration dependent kinetics  $k_b$  can be estimated to  $70 \text{ s}^{-1}\cdot\text{mol}^{-1}$ . For the desorption, from the concentration independent step  $k_{des}$  was estimated to  $4.5 \text{ s}^{-1}$ . For the relaxation process, which has no influence to the electrochemical capacitance,  $k_{rel}$  is according to this model about  $2\cdot 10^{-3} \text{ s}^{-1}$  (figure 5.20).

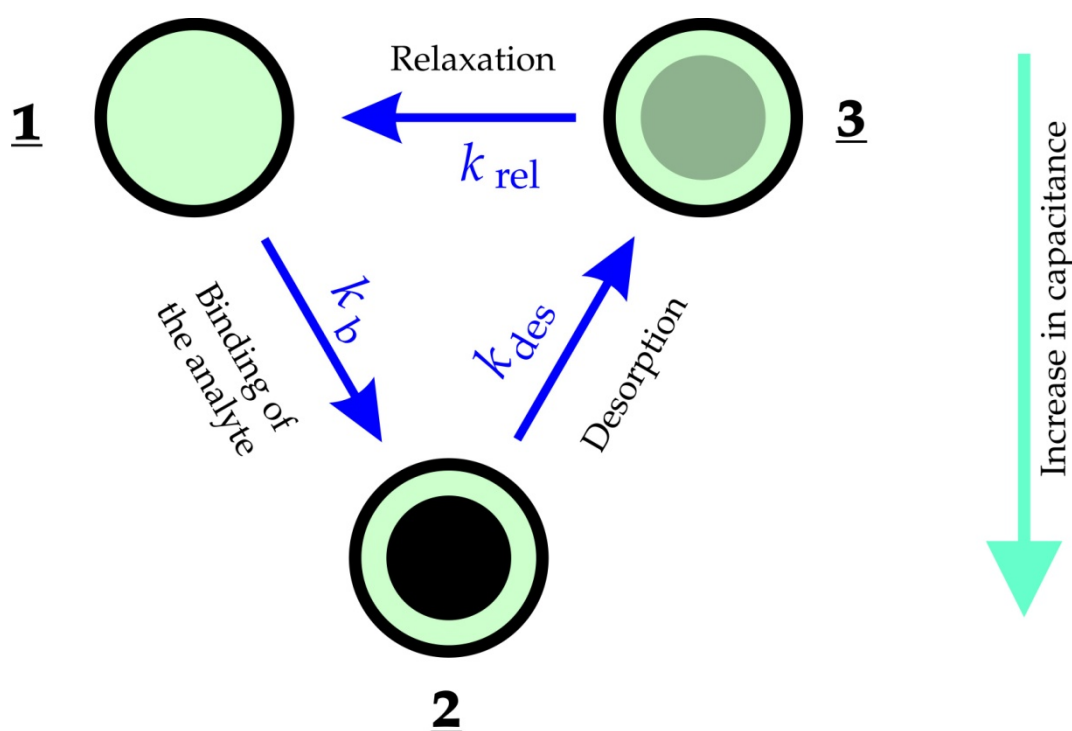


**FIGURE 5.20.** Model of the binding kinetics of the receptor sites in spreader-bar systems with the following states: (1) unoccupied, (2) after binding of the analyte, (3) after desorption of the analyte.

<sup>1</sup> in collaboration with V. I. Portnov, paper in preparation.

## 5.2 Applications

### 5.2.1 Spreader-bar systems as molecular receptors

The spreader-bar approach provides a simple method for producing a huge number of receptors with different selectivities, so as a first application a sensor-array of five receptors is introduced, which offers the possibility to detect different purines and pyrimidines by pattern recognition was tested. The pattern recognition technique, based on principal component analysis or neuronal nets, was used because it allows one to reach a very high selectivity of chemical analysis, but requires a pre-formation of an array of chemical sensors with essentially distinguished properties of single sensors.

With an array of electrodes, modified with mixed monolayers based on thiolated bases of nucleic acids as spreader-bars adenine, cytosine, thymine, uracil, caffeine and uric acid were used as analytes. The analyte binding was detected as changes of peak amplitude in cyclic voltammetry or modification of electrochemical impedance, the binding modifies reaction resistance and electrode capacitance while the Warburg impedance does not change. A monitoring of a capacitive current was used as the main detection method.

For gold electrodes covered by monolayer of a single component, either of matrix or spreader-bar molecules, no recognition abilities were found. For example, the changes of capacitive current at 80 Hz due to adsorption of purines and pyrimidines from a solution of  $300 \mu\text{mol}\cdot\text{L}^{-1}$  on 1-dodecanethiol coated electrodes were 0.7% for adenine or even less for every other substance.

A behavior of mixed monolayers consisting of dodecanethiol and one of thiolated purines or pyrimidines was quite different: an adsorption of adenine, cytosine, thymine, uracil, caffeine or uric acid resulted in over 25% changes of the capacitive current (figure 5.16).



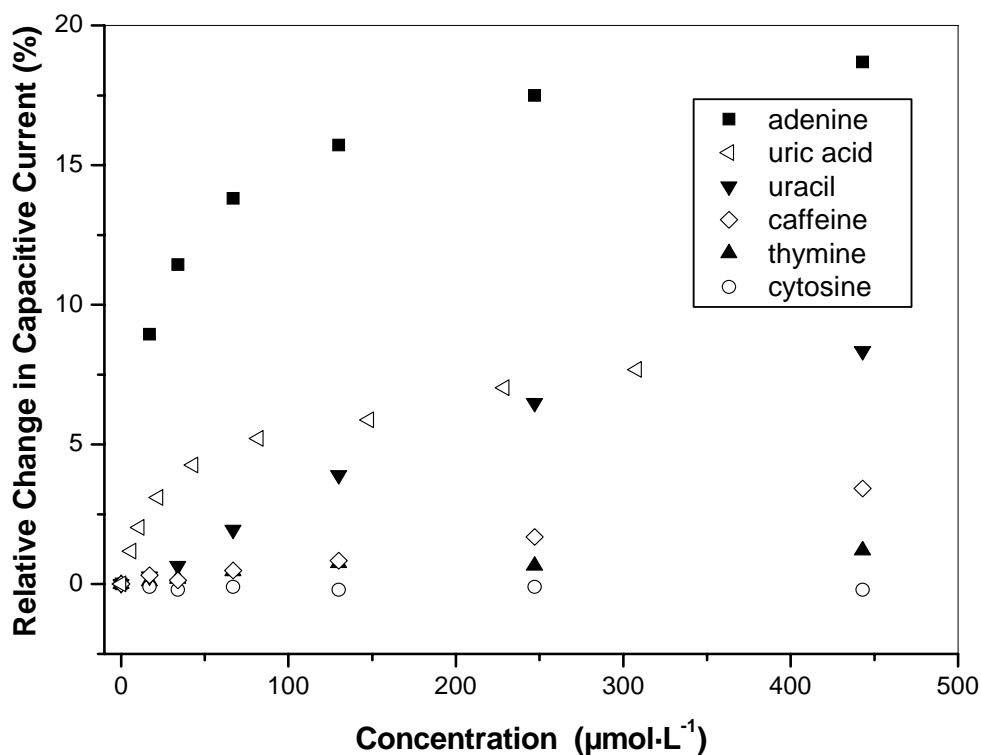


**FIGURE 5.16.** Concentration dependence of the relative changes in the capacitive current of gold electrode coated by mixed monolayer from dodecanethiol and ASH on addition of different analytes.

To obtain systems displaying such properties, the mixed monolayers have to be formed at definite concentration range of spreader-bar and matrix molecules in the coating solutions. An investigation of the obtained monolayers by IR reflection absorption spectroscopy (figure 5.3) and contact angle measurements (figures 5.2 and 5.9) has shown that namely this range of coating conditions corresponds to the formation of mixed monolayers with comparable surface concentrations of both components. An increase of the spreader-bar/matrix ratio in the coating solutions, or the reduction in deposition time result in formation of monolayers displaying only weak adsorption of analytes, which do not differ from the property of pure monolayers.

Concentration dependences of an electrode array consisting of 1-dodecanethiol and one of 6-mercaptopurine (ASH), 2-amino-6-purinethiol (GSH), 4-amino-2-mercapto-pyrimidine (CSH), 4-hydroxy-5-methyl-2-mercaptopyrimidine (TSH) or

4-hydroxy-2-mercaptopyrimidine (USH) on additions of adenine are shown in figure 5.17.

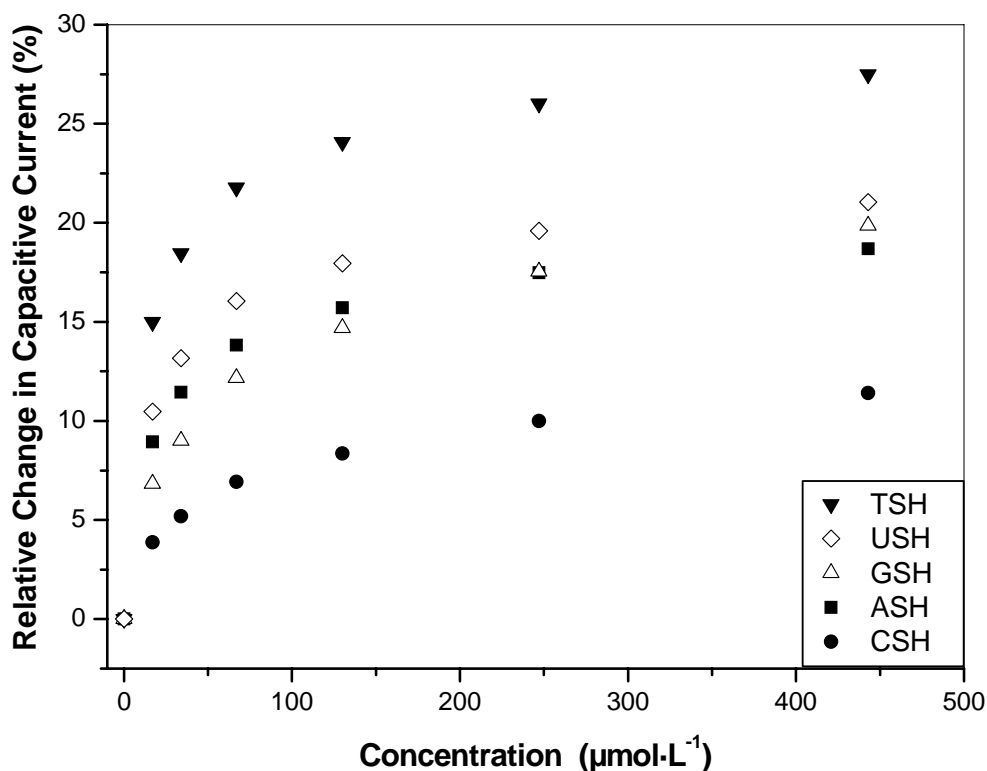


**FIGURE 5.17.** Concentration dependence of the relative changes in the capacitive current for an array of five different mixed monolayers on addition of adenine.

The response depends on a specific combination of spreader-bar and adsorbate. The electrode coated by a mixture of TSH and dodecanethiol exhibit the highest change of the signal on adenine addition; for electrodes with other spreader-bars, the signal decreased according to the order: USH > GSH > ASH > CSH. This order can be explained by interactions between the template and analytes. It is well known that adenine binds its complementary bases thymine or uracil; most probably it is valid also for thiolated derivatives of the latter compounds. GSH and ASH have the same shape like the analyte thus providing conditions for adsorption of these molecules into cavities formed by the template molecules and for  $\pi$ -stacking interaction with these molecules. Due to the minor energetic stabilization by  $\pi$ -stacking in contrast to the hydrogen binding [41], the binding of

adenine to GSH and ASH spreader bar systems is less effective. In case of the CSH spreader bar, no hydrogen binding can occur, and due to the smaller size of CSH, the surrounding dodecanethiol molecules hinder the analyte to come close enough to the template thus preventing a stacking interaction.

The observed interaction of adenine with mixed monolayers consisting ASH was a reason to test this system as an artificial receptor for ATP. The experiment confirmed this suggestion: an ATP addition resulted in a concentration dependent decrease of the capacitive current through the mixed monolayer with saturation at 2.2% and binding constant of about  $2 \cdot 10^4 \text{ L} \cdot \text{mol}^{-1}$  (figure 5.18).

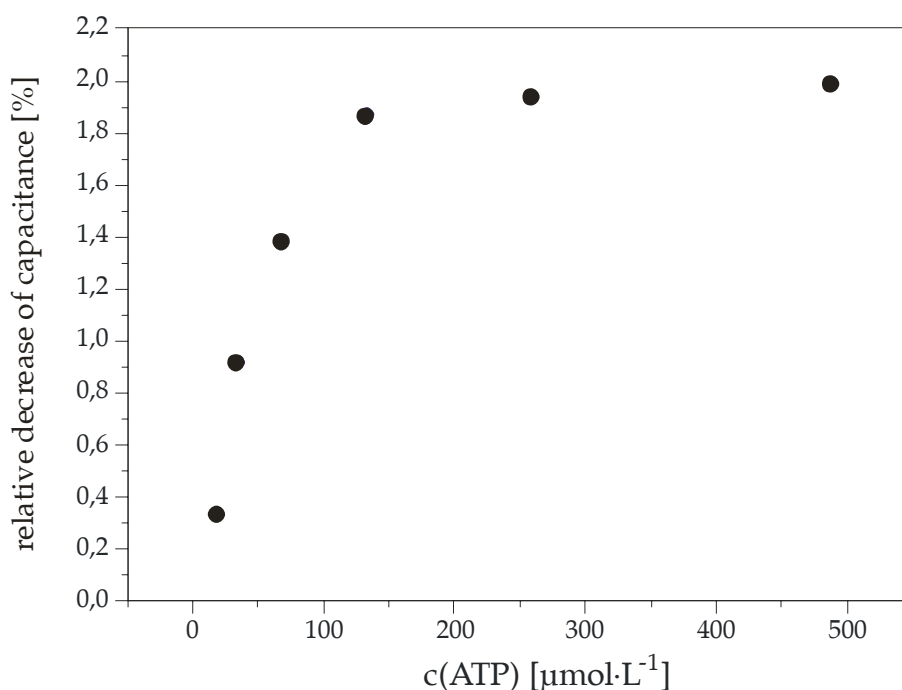


**FIGURE 5.18.** Change of electrochemical capacitance of an electrode covered by a mixed monolayer of 6-mercaptopurinethiol and 1-dodecanethiol in the presence of various concentrations of ATP.

Variations of spreader-bars lead to essential modifications in sensor behavior. A study of relative signal changes on adsorption of the same concentrations of different purines and pyrimidines onto mixed monolayers formed with either ASH, GSH, TSH, USH or CSH, results in signal patterns which are typical for every specific analyte used (table 5.1).

**TABLE 5.3.** Pattern of the effectiveness of spreader-bars for the recognition of different analytes.

<b>analyte</b>	<b>signal pattern<sup>a)</sup></b>
adenine	T > U > A > G > C
cytosine	U > G > A > t > c
thymine	g > a > t > u > C
uracil	T > U > C > A > G
caffeine	A > C T > U > g
uric acid	U > G > A > T > C

a) The spreader-bar molecules are named by the first letter (A represents ASH) and ordered by decreasing response. A small letter indicates signal changes lower than 0.3 %.

The sequences are valid for the whole concentration range (20 to 470  $\mu\text{mol}\cdot\text{L}^{-1}$ ) studied. This set of five artificial receptors based on these mixed monolayers allows one to identify every of the six different analytes tested (table 5.4) For cytosine and uric acid the patterns are the same, however the magnitude of the signal changes for uric acid was 5 to 17 times higher.

**TABLE 5.4.** Relative decrease (%) of the capacitive current on addition of analytes (250  $\mu\text{mol}\cdot\text{L}^{-1}$ ) for different spreader bar systems.

<b>spreader-bar</b>	<b>adenine</b>	<b>cytosine</b>	<b>thymine</b>	<b>uracil</b>	<b>caffeine</b>	<b>uric acid</b>
<b>ASH</b>	17.5	0.7	-0.1	6.5	1.7	7.0
<b>CSH</b>	10.0	-0.4	-2.0	10.4	1.0	5.5
<b>GSH</b>	16.2	1.2	0.0	4.6	0.7	8.0
<b>TSH</b>	26.0	0.4	-0.2	15.0	1.0	6.7
<b>USH</b>	19.6	1.8	-0.5	14.1	0.8	9.0

An analysis of principal components of the data array has shown that the first two components contain about 75 % of the data variation. The data obtained at different concentration for different analytes, being plotted in the virtual plane of the first and second principal components, add up by an arrangement in groups corresponding to individual substances (figure 5.19).

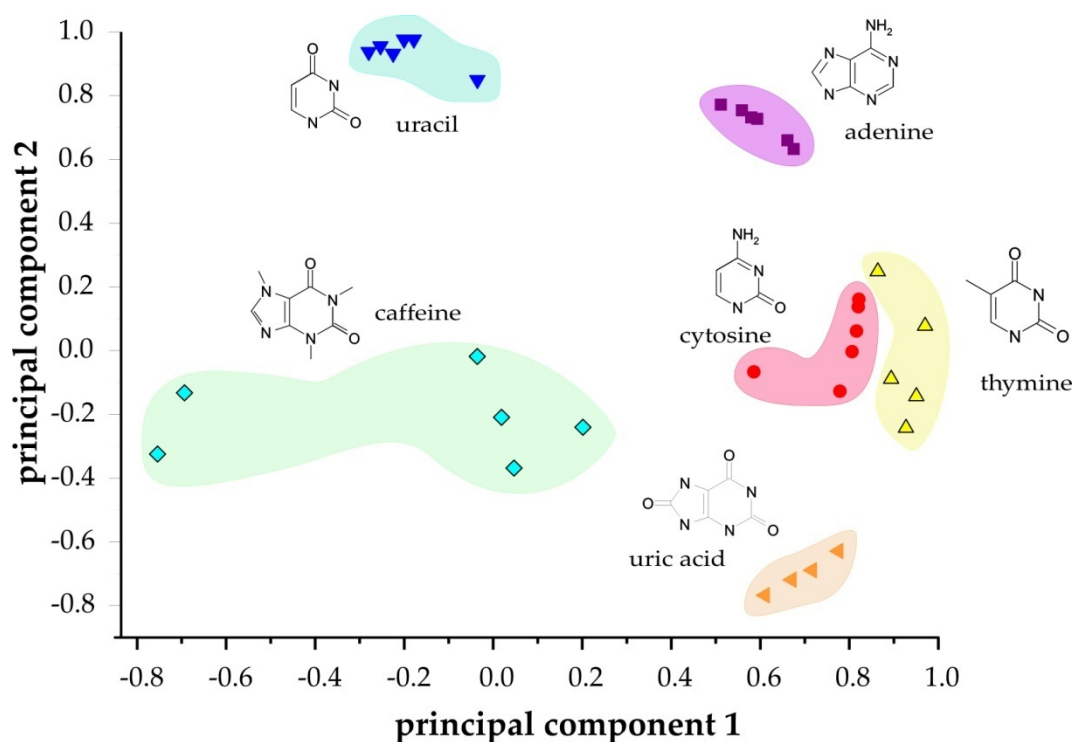


**FIGURE 5.19.** Patterns of different concentrations of caffeine, uracil, adenine, cytosine, thymine and uric acid on an array of artificial receptors formed by thiolated derivatives of purines (ASH, GSH) and pyrimidines (CSH, TSH, USH) presented in the plot of principal components. Capacitive transducing was used.

The results show that in spite of limited selectivity of every single sensor element, the sensor array can be used for recognition of bases of nucleic acids as well as caffeine and uric acid. This first application of the spreader-bar technology in sensor arrays illustrates its high potential in creation of large variety of chemoreceptors with different selectivity, thus fitting the main requirement in the development of modern analytical systems based on pattern recognition [42]. The spreader-bar technique provides a simple way to manufacture almost a non-limited number of such receptors: practically every thiol derivative can be used. Here an application of this approach to form an array of only five sensors is

demonstrated, but there is no technical limit to prepare such array with hundreds of sensing elements.

### 5.2.2 Spreader-bar systems as chiral selectors

The spreader bar systems were tested as a new method to form chirally sensitive artificial chemoreceptors on a solid support. Optical as well as electrical techniques were used for detection.

**TABLE 5.5.** Relative capacitive changes (in %) of gold electrodes coated by different self-assembled monolayers to racemic mixtures of phenylalanine (Phe) and 1,1-binaphthyl-2,2-diol. The molar concentration ratios of the spreader-bar and matrix molecules in the coating solution are given in parenthesis; the concentration of matrix molecule was always  $0.1 \text{ mmol}\cdot\text{L}^{-1}$ .

Electrode Coating	Effects to addition of racemic mixtures of		
	$1.25 \text{ mmol}\cdot\text{L}^{-1}$ Phe	$25 \text{ }\mu\text{mol}\cdot\text{L}^{-1}$ BNOH	$50 \text{ }\mu\text{mol}\cdot\text{L}^{-1}$ BNOH
1-Hexadecanethiol	0	0	0
Thioctic acid	-1.2	0.2	0.22
S-Conjugate	0	11.9	17.6
R-Conjugate	0	6.6	9.2
S-Conjugate / 16-Mercaptohexadecanoic acid (1/33)	-3.5	3.6	4.8
R-Conjugate / 16-Mercaptohexadecanoic acid (1/33)	-3.5	3.9	5.1
S-Conjugate / 1-Hexadecanethiol (1/33)	0	1.8	3.2
R-Conjugate / 1-Hexadecanethiol (1/33)	0	8.6	12.8

Table 5.5 presents changes in the capacitance of gold electrodes coated by various self-assembled monolayers on addition of racemic mixtures of phenylalanine and model target compound BNOH. It is notable that the electrodes coated by the conjugates of racemic thioctic acid with different enantiomers of 1,1'-binaphthyl-2,2'-diamine (R- and S-conjugates correspondingly), being used alone or in a mixture with matrix molecules, displayed no capacitance increase on addition of phenylalanine, even in millimolar concentrations. However, they are very sensitive to the addition of even micromolar concentrations of racemic R/S-BNOH solution. Deviations of the recognition properties of the receptors formed by the R- and S-conjugates from ideal symmetric behavior are most probably caused by preferable binding of definite optical isomers of thioctic acid during the conjugation, thereby leading to the formation of molecules with two chiral centers and loss of the mirror symmetry. The binding of a model analyte to the conjugate may be explained by  $\pi$ -electron interactions. The affinity of the model analytes to the conjugates allows their use as spreader-bars for the selective recognition of the individual enantiomers.

The ability of such surfaces to discriminate enantiomers was studied by measuring the change in the electrode capacitance on addition of R- or S-enantiomers of the analyte. The concentration range of BNOH was varied from 6.25 to 50  $\mu\text{M}$ . Capacity changes for a number of electrodes coated by different organic monolayers are presented in Table 5.6.

**TABLE 5.6.** Relative capacitive changes (in %) of electrodes with different coating on addition of  $50 \mu\text{mol}\cdot\text{L}^{-1}$  of chiral analytes. The molar concentration ratios of the spreader-bar and matrix molecules in the coating solution are given in parenthesis; the concentration of matrix molecule was always  $0.1 \text{ mmol}\cdot\text{L}^{-1}$ .

<b>Electrode coating</b>	<b>Response to S-BNOH</b>	<b>Response to R-BNOH</b>	<b>Enantio-selectivity</b>
1-hexadecanethiol	0	0	-
Thioctic acid	0.2	0.2	1.00
S-Conjugate	17.6	17.6	1.00
R-Conjugate	9.5	8.7	1.09
S-Conjugate/ 1-Hexadecanethiol (1/33)	3.3	3.6	0.92
R-Conjugate/ 1-Hexadecanethiol (1/33)	13	9.7	1.34
S-Conjugate/ 1-Hexadecanethiol (1/3.5)	9.3	2.9	3.21
R-Conjugate/ 1-Hexadecanethiol (1/3.5)	12.8	6.9	1.86
S-Conjugate/ 1-Hexadecanethiol (1/2)	32.4	6.8	4.76
R-Conjugate/ 1-Hexadecanethiol (1/2)	35	10.23	3.42
S-Conjugate/ 1-Hexadecanethiol (1/1)	60	43	1.39
R-Conjugate/ 1-Hexadecanethiol (1/1)	62	49	1.26
S-Conjugate/ 1-Dodecanethiol (1/3.5)	41	38	1.08
R-Conjugate/ 1-Dodecanethiol (1/3.5)	23	19	1.21



The ratio of the apparent capacitance changes assumed to be proportional to the adsorbed amount [43] and therefore to the enantioselectivity, was taken as a criterion for the chiral recognition properties of each of the tested coatings. The results showed that the concentration ratio between the matrix and the template molecules is the key parameter determining the chiral recognition properties of the modified surfaces.

As revealed from the results of Table 5.6, the sensitivity of the sensors to the target analyte increases on increasing the template concentration in the mixture with the matrix molecule. This is additional evidence for the important role of the template to create cavities of a specific size that act as a mould for the target analyte. The highest enantioselectivities were obtained for the gold electrodes coated by template/matrix mixtures with molar ratios of 1:3.5 and 1:2. The effectivity of artificial receptors was compared for two types of matrices, namely the long chain alkanethiols (1,16-mercaptohexadecanoic acid, 1-hexadecanethiol) and the shorter one (1-dodecanethiol). A decrease of the matrix thickness, realized by the substitution of 1-hexadecanethiol by 1-dodecanethiol, led to the loss of enantioselectivity.

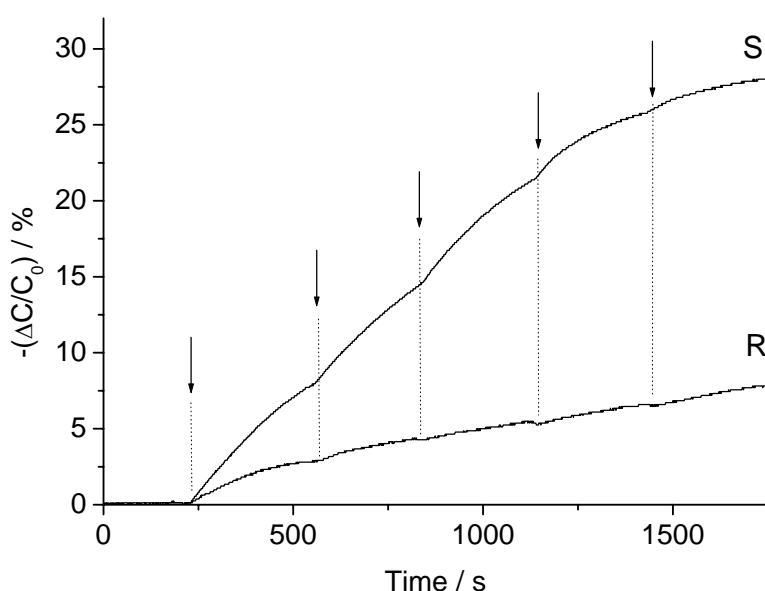


**FIGURE 5.20.** Capacitance changes on five successive additions of  $10 \mu\text{M}$  of R-BNOH (R) and S-BNOH (S). The gold electrodes were modified with a mixture of 1-hexadecanethiol ( $0.1 \text{ mmol L}^{-1}$ ) and S-conjugate ( $0.03 \text{ mmol L}^{-1}$ ) in ethanol/dioxane (9/1 v/v).

The kinetics of the decrease in capacitance on additions of analytes is shown in figure 5.20. The impedance spectra (figure 5.21) of gold electrodes modified by the same template with different matrices reveal the dependence on the length of alkyl chain of the matrix molecules.

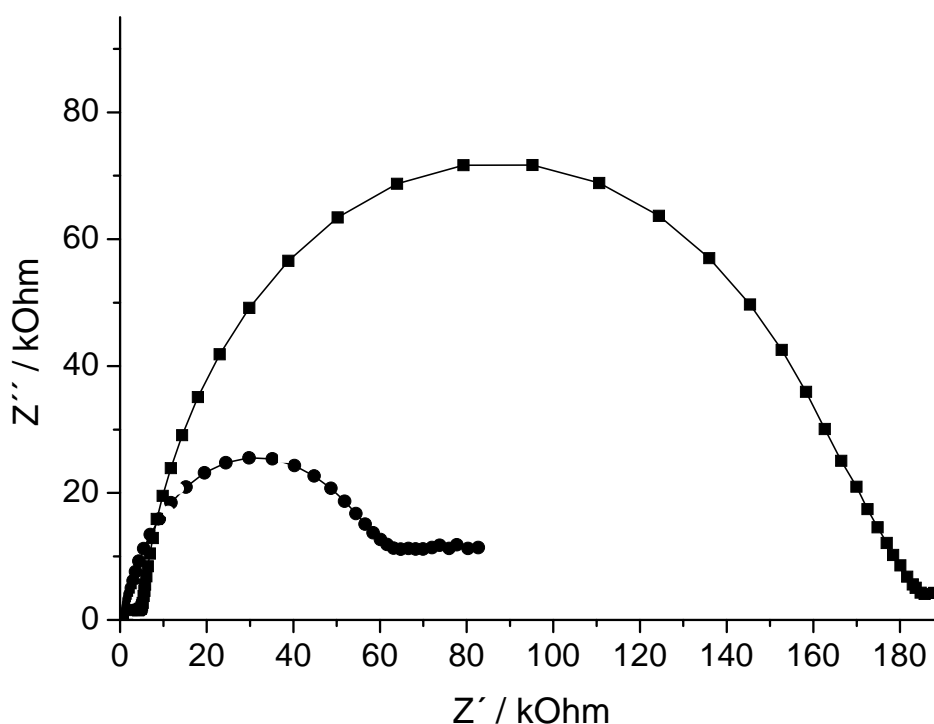


**FIGURE 5.21.** Impedance spectra of gold electrodes coated by a mixture of 1-hexadecanethiol ( $0.1 \text{ mmol}\cdot\text{L}^{-1}$ ) and S-conjugate ( $0.03 \text{ mmol}\cdot\text{L}^{-1}$ ) in ethanol/dioxane (9/1) (■) or by a mixture of 1-dodecanethiol ( $0.1 \text{ mmol}\cdot\text{L}^{-1}$ ) and S-conjugate ( $0.03 \text{ mmol}\cdot\text{L}^{-1}$ ) in ethanol/dioxane (9/1) (●). Measurement conditions are described in the experimental section.

The electrodes were coated with a mixture of 1-hexadecanethiol ( $0.1 \text{ mmol}\cdot\text{L}^{-1}$ ) and S-conjugate ( $0.03 \text{ mmol}\cdot\text{L}^{-1}$ ) in ethanol/dioxane (9/1, v/v) and a mixture of 1-dodecanethiol ( $0.1 \text{ mmol}\cdot\text{L}^{-1}$ ) and S-conjugate ( $0.03 \text{ mmol}\cdot\text{L}^{-1}$ ) in the same solvent. Impedance spectroscopy was performed in the presence of hexacyanoferrate. The results demonstrate that spreader-bar monolayers with larger matrix molecules possess an about four fold higher reaction resistance (Figure 5.21). These values are in between of that for bare gold electrodes and for the electrodes coated by pure matrix without spreader-bars.

The chiroselectivity of the spreader-bar structures with S-conjugate as the template was further examined by means of surface plasmon resonance measurements. The ratio of the template and matrix concentrations that had provided the highest enantioselectivity in the capacitive study (table 5.6) was used for coating the gold surface. As can be seen in figure 5.22, the signal changes upon addition of the S- and R-BNOH is higher in the case of S-BNOH. The enantioselectivity was calculated as a ratio of stationary SPR shifts on addition of corresponding enantiomers; a value of 2.55 was obtained. The unusual kinetics of the SPR signal may reflect some conformational changes in the receptor layer.

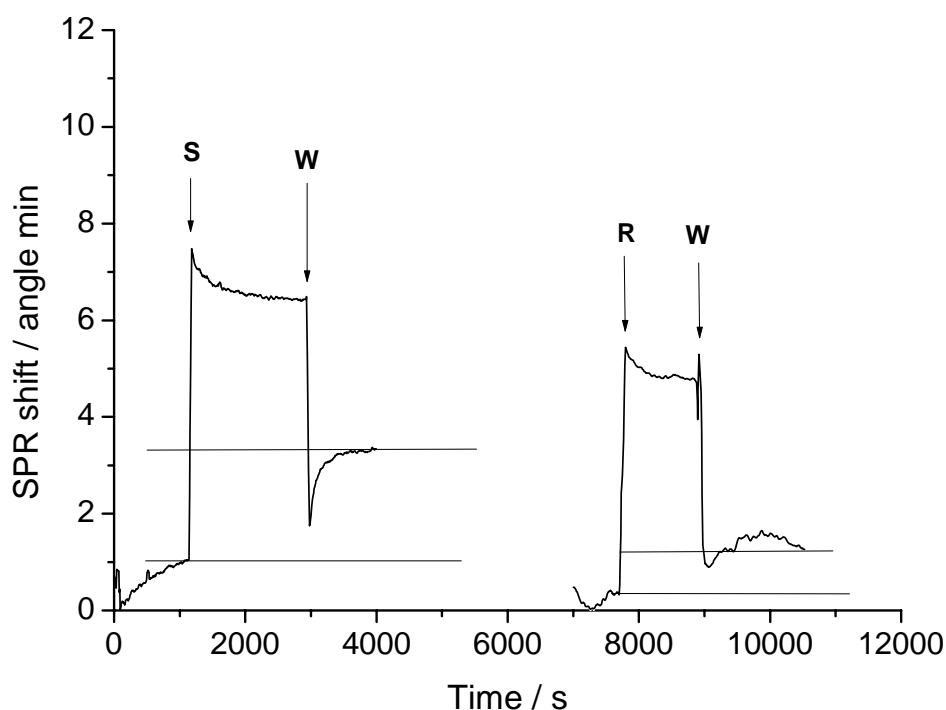


**FIGURE 5.22.** Shift of the surface plasmon resonance angle on addition of  $50 \mu\text{mol}\cdot\text{L}^{-1}$  S-BNOH (S) and  $50 \mu\text{mol}\cdot\text{L}^{-1}$  R-BNOH (R). Arrows (W) indicate washing by of the buffer solution. The gold coated glass slide was modified with a mixture of 1-hexadecanethiol ( $0.1 \text{ mmol}\cdot\text{L}^{-1}$ ) and S-conjugate ( $0.03 \text{ mmol}\cdot\text{L}^{-1}$ ) in ethanol/dioxane (9/1 v/v).

The proposed methodology is wide-applicable and can be used to form chirally selective receptors for a large variety of species. One can expect further increase of the chiral sensitivity by conjugating chiral spreader bar to a non-chiral thiolinker.

Such sensors may be used for analysis of chiral compounds in complex mixtures, for quality control of chiral drugs and food additives, and in related applications.

### **5.2.3 Spreader-bar systems as templates for metallic nanoparticles**

All spreader-bar-stabilized nanostructures were investigated by impedance spectroscopy and by cyclic voltammetry. The results demonstrated high electrochemical stability (except for the aluminum phthalocyanine chloride based systems) of the monolayers in the wide potential range; the shape of voltammograms indicated on homogeneous distribution of the spreader-bar molecules through the monolayer (no influence of nanostructures on the diffusion profile of ferro/ferri-cyanide ions). From these results it was considered to test the spreader-bar systems as templates for the generation of metallic nanoparticles by selective reduction of platinum into the nanopores formed by spreader-bar molecules.

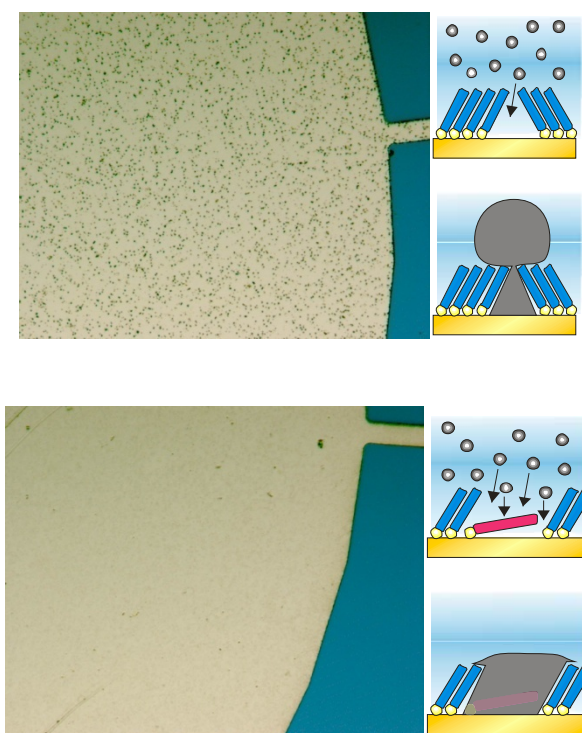


**FIGURE 5.23.** Optical microscopy of gold electrodes coated by 1-dodecanethiol (top) or TMPP together with 1-dodecanethiol (bottom) after reduction of platinum from  $\text{H}_2\text{PtCl}_6$  into defects and nanostructures of these monolayers. The reduction charge was  $63 \text{ C}\cdot\text{m}^{-2}$ . Magnification: 250.

First, a formation of such metallic particles for indirect provement through optical microscopy was performed. On the gold electrodes coated by pure alkanethiols, the reduction of platinum from  $\text{H}_2\text{PtCl}_6$  until the reduction charge reaches a value of  $63 \text{ C}\cdot\text{m}^{-2}$  leads to the formation of visible platinum islands (figure 5.23, top). The same experiment with gold electrodes coated by mixed monolayers of 6-mercaptopurine and 1-dodecanethiol and of TMPP and 1-dodecanethiol were tested. It was found, monolayers with nanostructures do not lead to the formation of optically visible defects (Figure 5.23, bottom). Therefore, the total area of electrochemically available gold area (obviously planar spreader-bars molecules with developed  $\pi$ -electron systems posses much higher electrical conductivity than alkanethiol molecules) is much higher in the nanostructured monolayers. This experiment also gives a new perspective to the high application potential of the spreader-bar structured monolayers in selective electrocatalysis: after showing

of the receptive properties, now here the electrical transfer through bottoms of these pores is demonstrated.

Systematic changes of the surface roughness in nanometer scale due to formation of spreader-bar stabilized nanostructures and platinum reduction within this nanostructure, were confirmed by experiments with atomic force microscopy. For example (figure 5.24), platinum (reduced until  $0.5 \text{ C}\cdot\text{m}^{-2}$ ) does not change the smooth surface of gold on mica (a); a formation of alkylthiol monolayer leads to characteristic relief (b), these inhomogeneities are larger for the spreader-bar structured monolayer (c) and are further increased after platinum reduction (d) according to the model (figure 5.23, bottom).

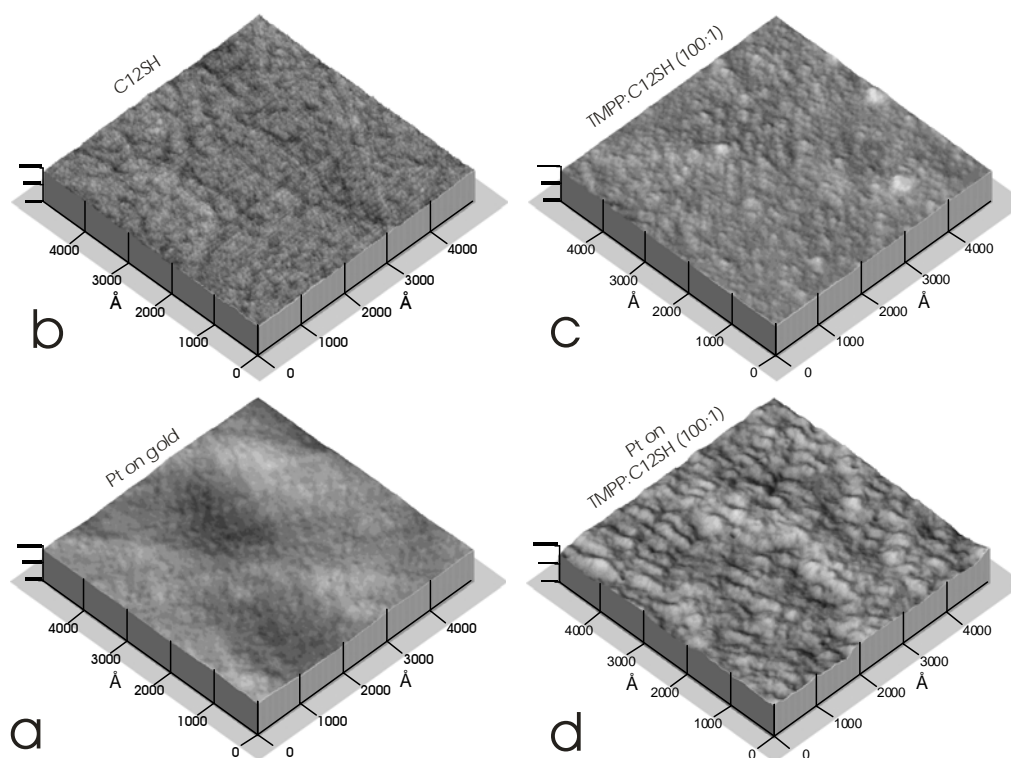


**FIGURE 5.24.** Atomic force microscopy (non-contact mode) of bare gold electrode (a), alkylthiol coated gold electrodes (b), gold electrodes coated by the nanostructured monolayer consisting of TMPP and 1-dodecanethiol before (c) and after (d) electrochemical platinum deposition. The deposition charge was  $0.5 \text{ C}\cdot\text{m}^{-2}$ .

A direct visualization of nanoparticles by electron microscopy was performed successfully. The nanoparticles were formed by reduction of copper or platinum (Figure 5.25). There should be no physical or chemical limitations for preparation

of nanoparticles from many other noble and transition metals according to this method. The particles are relatively homogeneous. Depending on the deposition charge, the size of nanoparticles can be controlled in the range between 20 nm and 1000 nm.

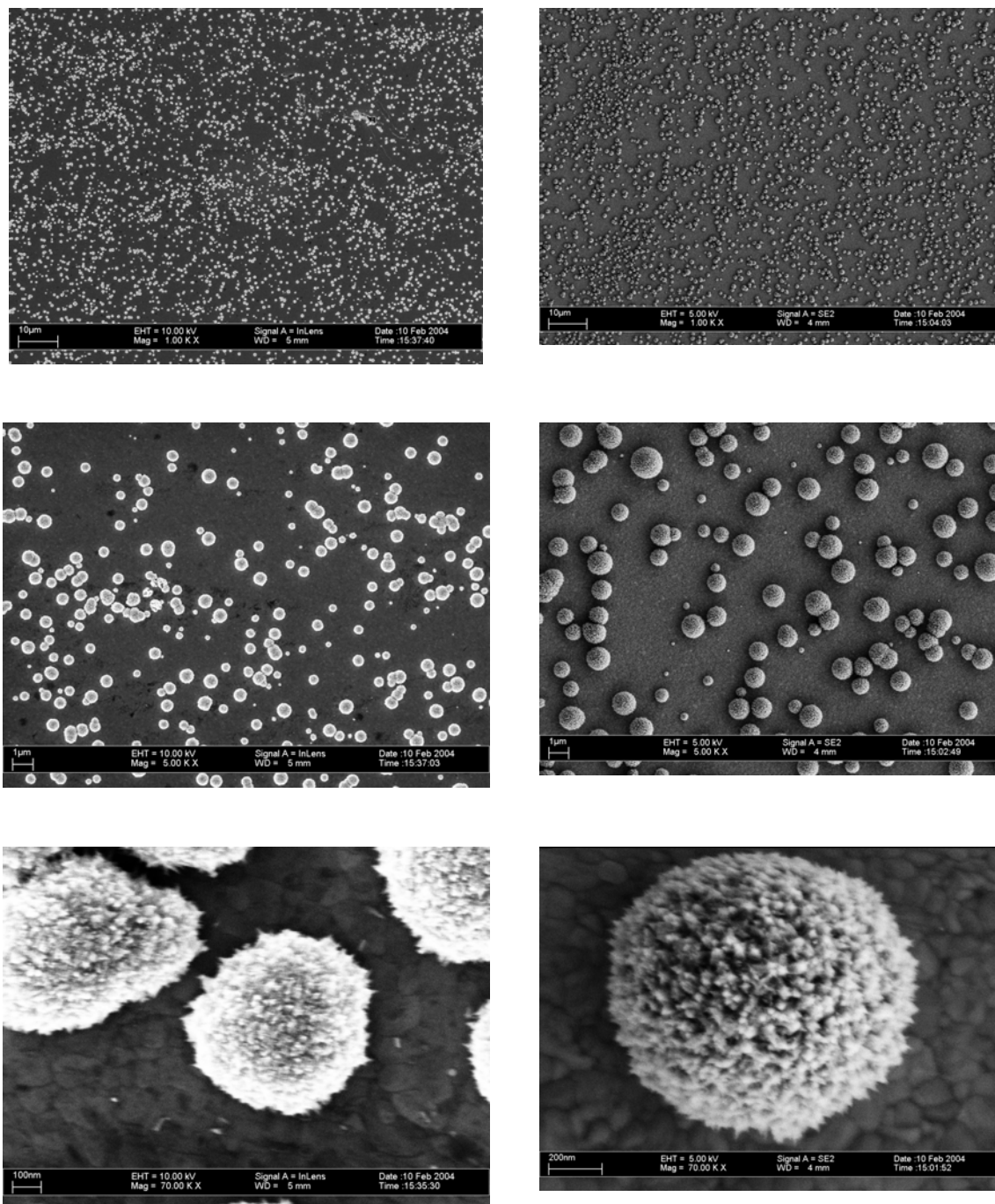


**FIGURE 5.25.** Scanning electron microscopy of gold electrodes coated by the nanostructured monolayer consisting of TMPP and 1-dodecanethiol after electrochemical platinum deposition. The deposition charge is 41 C·m<sup>-2</sup> (left column) and 160 C·m<sup>-2</sup> (right column).

It should be possible to form also smaller nanoparticles (the size is probably limited only by the size of the spreader-bar used, i.e. about 2 nm for TMPP), but by means of the electron microscopy it was not able to visualize the nanoparticles smaller than 20 nm (figure 5.26). The total area of the formed platinum nanoelectrodes, estimated from the investigation of underpotential deposition of copper, is about 1.5 times higher than geometrical electrode area. For smooth nanoparticles, it corresponds to the ratio of the nanoparticles radius to the mean distance between particles as about 0.35; this is similar to that value obtained from the digital analysis of electron microscopy images (0.22).

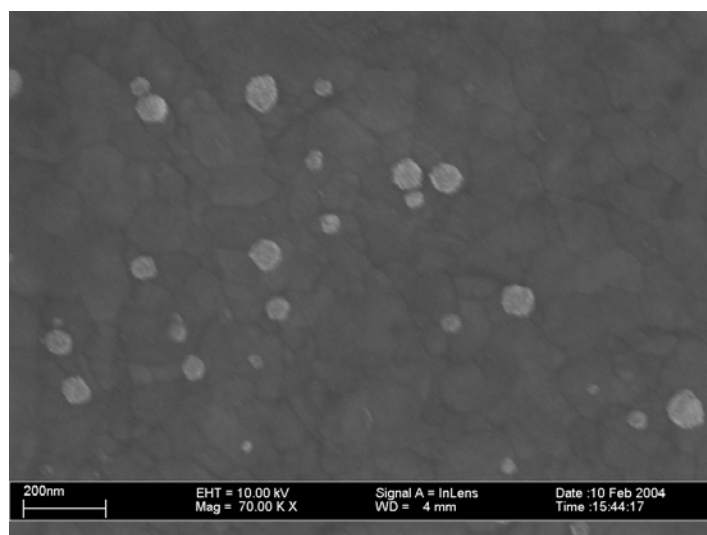


*FIGURE 5.26. Scanning electron microscopy of gold electrodes coated by the nanostructured monolayer consisting of TMPP and 1-dodecanethiol after electrochemical platinum deposition. The deposition charge is  $6.5 \text{ C}\cdot\text{m}^{-2}$ . The resolution of the used microscope did not allow to visualize smaller nanoparticles.*

## **5.2.4 Spreader-bar systems used as support for studying ionic pumps**

The first investigated nanostructured monolayers were tested as a support for functional reconstitution of Na,K-ATPase. Adsorption of membrane fragments with Na,K-ATPase, detected as decrease of electrical capacitance, on different



surfaces was studied; it was shown that the adsorption is similar to the surfaces coated by hydrophobic alkanethiols without nanostructures and to the nanostructured surfaces formed by 1-dodecanethiol and 6-mercaptopurine. To check functional activity of the Na,K-ATPase, impedance spectroscopy in the presence and without ATP in the electrolyte without potassium was compared. The absence of potassium blocks the turnover of the enzyme providing high concentration of the dephosphorylated Na-bound enzyme state. An addition of ATP in such conditions leads to the opening of the sodium channel and sodium transfer. An application of alternative current induces movement of sodium ions in the channel which should lead to the frequency dependent modifications of impedance spectra. The impedance spectroscopy confirmed this suggestion: the subtraction of admittance measured in the presence and in the absence of ATP evaluated frequency dependent changes of capacitance and conductance (Figure 5.27, curves 1-2) related to the activity of Na,K-ATPase.

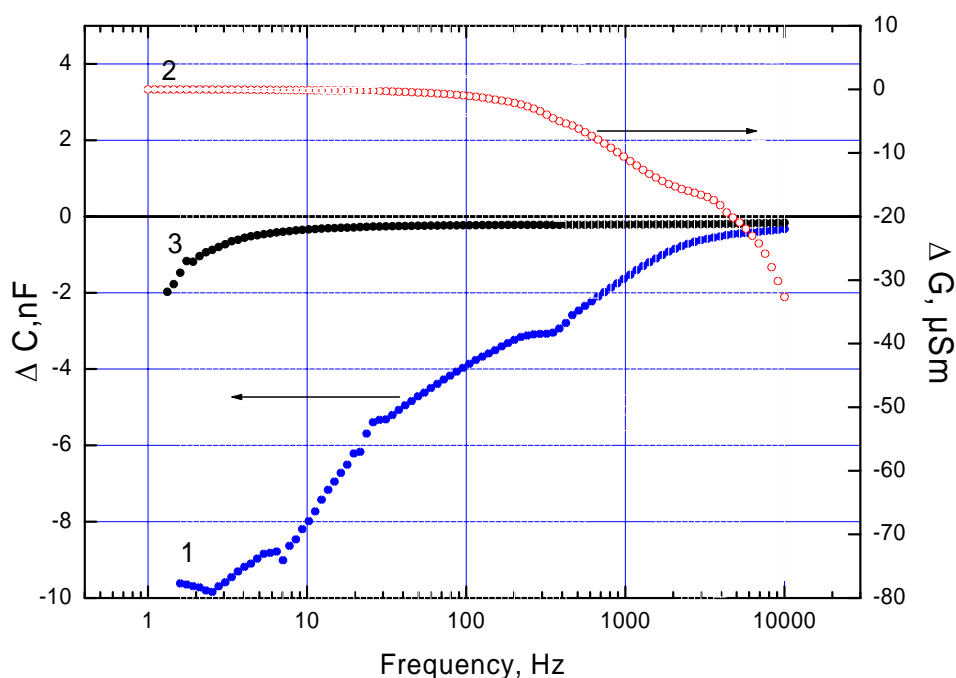


**FIGURE 5.27.** Difference in admittance of electrodes with adsorbed Na,K-ATPase due to ATP binding: 1, 3 - capacitance, 2 - conductance. The curve 1, 2 were measured on nanostructured electrodes with spreader-bars, the curve 3 was measured on non-structured electrode with hydrophobic surface.

The activity of this enzyme was higher on the surfaces with spreader-bars compared to non-structured surfaces coated by carboxy-alkanethiols. The lowest activity was found on surfaces of thiols with terminal methylene groups. If the membrane fragments were adsorbed on the gold electrode gold electrodes coated by hydrophobic alkanethiol, display only minor ATP-dependent changes of impedance spectra (figure 5.27, curve 3). It can be explained by the assumption that a water filled compartment between the support and membrane fragment is necessary for functioning of this ion pump: the tight contact of membrane fragments and hydrophobic alkylthiols block the activity of Na,K-ATPase (figure 5.28).

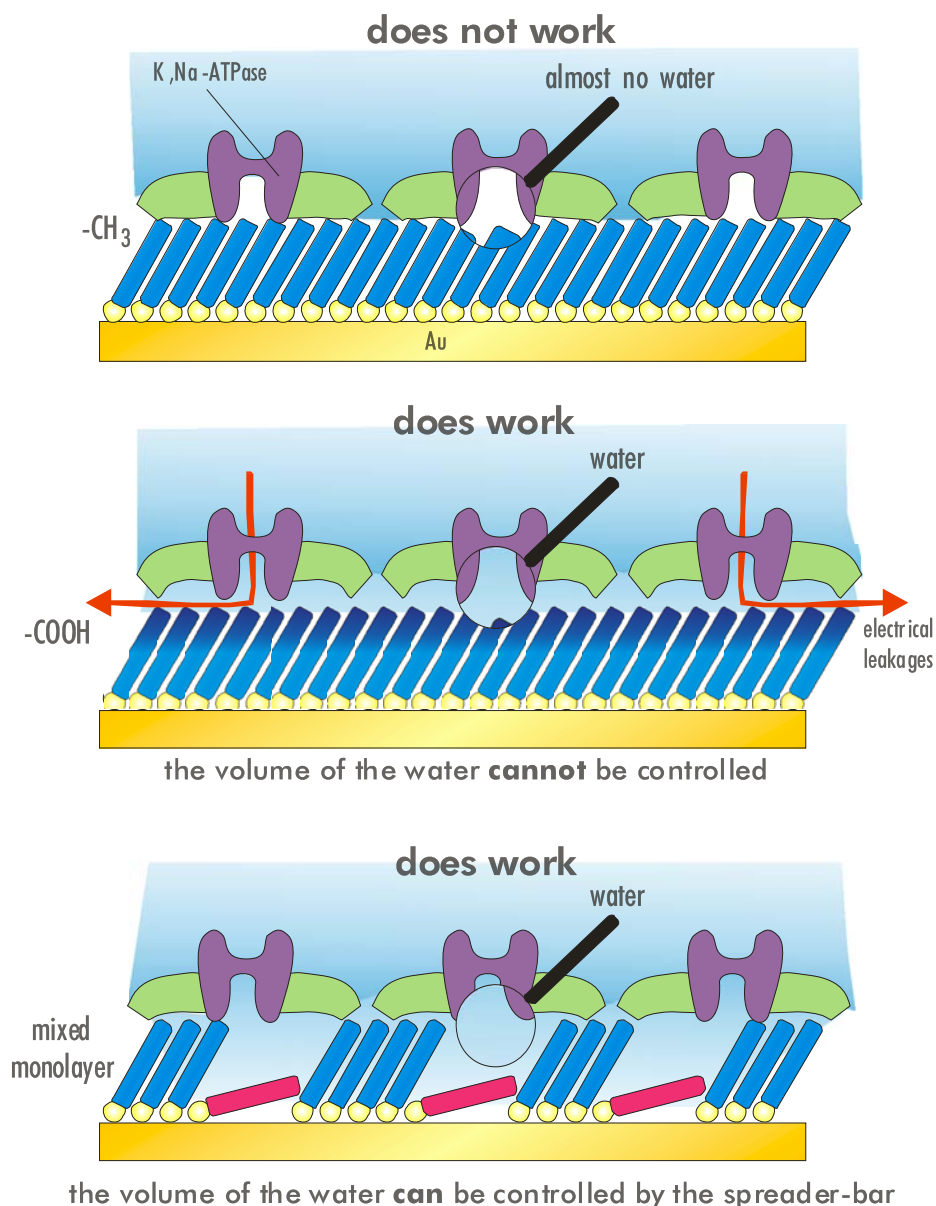


**FIGURE 5.28.** Possible explanation of increasing of detecting activity of Na,K,ATPase adsorbed on nanostructured monolayers: microvolumes of water between membrane fragments and electrode provides natural-like environment for the ion pump but block electrical leakages.

The surfaces with nanostructures and with carboxy-groups provide these aqueous cavities which are necessary for the functioning of the Na,K-ATPase. However, even in this case the nanostructured electrodes have an advantage that the lateral leakages of electrical current are blocked; it lead to minimization of artifacts in quantitative investigations. Additional advantage of the latter system is that it allows us to vary the size and the density of these cavities to reach the optimal conditions of the Na,K-ATPase function.

### 5.3 References

- [1] Xia, Y.; Zhao, X.-M.; Whitesides, G. M.; *Microelectron. Eng.* **1996**, *32*, 255 - 268.
- [2] Xia, Y.; Kim, E.; Whitesides, G.M.; *J. Electrochem. Soc* **1996**, *143*, 1070 - 1079.
- [3] Jeon, N. L.; Clem, P. G.; Payne, A. A.; Nuzzo, R. G.; *Langmuir* **1996**, *12*, 5350 - 5355.
- [4] Jeon, N. L.; Finnie, K.; Branshaw, K.; Nuzzo, R. G.; *Langmuir* **1997**, *13*, 3382 - 3391.
- [5] Wang, D.; Thomas, S. G.; Wang, K. L.; Xia, Y.; Whitesides, G. M.; *Appl. Phys. Lett.* **1979**, *70*, 1593 - 1595.
- [6] Jeon, N. L.; Nuzzo, R. G.; Xia, Y.; Mrksisch, M; Whitesides, G. M.; *Langmuir* **1995**, *11*, 3024 - 3026.
- [7] Hidber, P. C.; Helbig, W.; Kim, E.; Whitesides, G. M.; *Langmuir* **1996**, *12*, 1375 - 1380.
- [8] Xia, Y.; Whitesides, G. M.; *Annu. Rev. Mater. Sci.* **1998**, *28*, 153 - 184.
- [9] Rogers, J. A.; Paul, K. E.; Jackman, R. J.; Whitesides, G. M.; *Appl. Phys. Lett.* **1997**, *70*, 2658 - 2660.
- [10] Schmid, H.; Biebuyck, H. B.; Michel, B.; Martin, O. J. F.; *Appl. Phys. Lett.* **1998**, *72*, 2379 - 2381.
- [11] Rogers, J. A.; Paul, K. E.; Whitesides, G. M.; *J. Vac. Sci. Technol. B.* **1998**, *16*, 88 - 98.
- [12] Paul, K. E.; Breen, T. L.; Aizenberg, J.; Whitesides, G. M.; *Appl. Phys. Lett.* **1998**, *73*, 2893 - 2895.
- [13] Gibson, J. M.; *Phys. Today* **1997**, 56 - 61.
- [14] Pease, R. F. W.; *J. Vac. Sci. Technol. B* **1992**, *10*, 278 - 285.
- [15] Dagata, J. A.; *Science* **1995**, *270*, 1625 - 1626.
- [16] Binnig, G.; Rohrer, H.; Gerber, C.; Weibel, E.; *Appl. Phys. Lett.* **1982**, *40*, 178 - 181.
- [17] Sohn, L. L.; Willet, R. L.; *Appl. Phys. Lett.* **1995**, *67*, 1552 - 1554.
- [18] Wilder, K.; Quate, C. F.; Adderton, D.; Bernstein, R.; Elings, V.; *Appl. Phys. Lett.* **1998**, *73*, 2527 - 2529.

- [19] Muller, W.T.; Klein, D. L.; Lee, T.; Clarke, J.; McEuen, P. L.; Schultz, P. G.; *Science* **1995**, *268*, 272 - 273.
- [20] Stockman, L.; Neuttiens, G.; van Haesendonck, C.; Bruynseraede, Y.; *Appl. Phys. Lett.* **1993**, *62*, 2935 - 2937.
- [21] Sawaguchi, T.; Mizutani, F.; Taniguchi, I.; *Langmuir* **1998**, *14*, 3565 - 3569.
- [22] Tao, Y. T.; Wu, C. C.; Eu, J. Y.; Lin, W. L.; Wu, K. C.; Chen, C. H.; *Langmuir* **1997**, *13*, 4018 - 4023.
- [23] Boland, T.; Ratner, B. D.; *Langmuir* **1994**, *10*, 3845 - 3852.
- [24] Madueño, R.; Garcia-Raya, D.; Viudez, A. J., Sevilla, J. M.; Pineda, T.; Blázquez, M.; *Langmuir* **2007**, *23*, 11027 - 11033.
- [25] Bain, C. D.; Whitesides, G. M.; *Angew. Chem. Int. Ed. Engl.* **1989**, *28*, 506 - 512.
- [26] Folkers, J. P.; Laibinis, P. E.; Whitesides, G. M.; *Langmuir* **1992**, *8*, 1330 - 1341.
- [27] Bain, C. D.; Whitesides, G. M.; *J. Am. Chem. Soc.* **1989**, *111*, 7164 - 7175.
- [28] Schlenoff, J. B.; Li, M.; Ly, H.; *J. Am. Chem. Soc.* **1995**, *117*, 12528 - 12536.
- [29] Li, G.; Fudickar, W.; Skupin, M.; Klyszcz, A.; Draeger, C.; Lauer, M.; Fuhrhop, J.-H.; *Angew. Chem. Int. Ed. Engl.* **2002**, *11*, 1828 -1852.
- [30] Stöhr, J.; *NEXAFS Spectroscopy, Springer Series in Surface Science 25*, **1992**, Springer-Verlag, Berlin.
- [31] Lamont, C. L. A.; Wilkes, J.; *Langmuir* **1999**, *15*, 2037 - 2042.
- [32] Yanagi, H.; Kouzeki, T.; Ashida, M.; *J. Appl. Phys.* **1993**, *73*, 3812 - 3819.
- [33] Osso, J. O.; Schreiber, F.; Kruppa, V.; Dosch, H.; Garriega, M.; Alonso, M. I.; Cerdeira, F.; *Adv. Func. Mater.* **2002**, *12*, 455 - 458.
- [34] Osso, J. O.; Schreiber, F.; Alonso, M. I.; Garriega, M.; Barrena, E.; Dosch, H.; *Org. Electr.* **2004**, *5*, 135 - 140.
- [35] Leznoff, C. C., Lever, A. B. P.; *Phthalocyanines: Properties and Applications*, **1989**, VCH, New York.
- [36] Weber, A.; Reinöhl, U.; Bertagnolli, H.; *Bessy Jahresbericht*, **1998**, BESSY GmbH, Berlin.

- [37] Shi, Z.; Lipkowski, J.; *J. Electroanal. Chem.* **1994**, 364, 289 - 294.
- [38] Love, J. C.; Estroff, L. A.; Kriebel, J. K.; Nuzzo, R. G.; Whitesides, G. M.; *Chem. Rev.* **2005**, 105, 1103 - 1169.
- [39] Heister, K.; Zharnikov, M.; Grunze, M.; Johansson, L. S. O.; *J. Phys. Chem. B* **2001**, 105, 4058 - 4061.
- [40] Heister, K.; Johansson, L. S. O.; Grunze, M.; Zharnikov, M.; *Surf. Sci.* **2003**, 529, 36 - 46.
- [41] Sponer, J.; Leszczynski, J.; Hobza, P.; *J. Chem. Phys.* **1996**, 100, 5590 - 5596.
- [42] Tenenbaum, J. B.; de Silva, V. ; Langford, J. C.; *Science* **2000**, 290, 2319 - 2323.
- [43] Mirsky, V. M.; *TrAC Trends Anal. Chem.* **2002**, 21, 439 - 450.

## 6. Summary

Thiol modified purines and pyrimidines (spreader-bar) co-adsorbed with 1-dodecanethiols (matrix) onto a gold surface form self-assembled nanostructured monolayers showing recognition properties towards different purines and pyrimidines, depending on the type of the spreader-bar used. The structures were investigated by FTIR spectroscopy, contact angle measurements, ellipsometry, impedance spectroscopy and voltammetry. The results show that the coating conditions optimized for affinity properties correspond to a narrow range of the spreader-bar/matrix ratio in the coating solution leading to the presence of both types of molecule on the surface.

An array consisting of five receptors formed by thiolated derivatives of adenine, thymine, uracil, guanine and cytosine as spreader-bars, allows one to recognize different purines and pyrimidines. The results show that in spite of limited selectivity of every single sensor element, the sensor array can be used for

recognition of bases of nucleic acids as well as caffeine and uric acid. This first application of the spreader bar technology in sensor arrays illustrates its high potential in creation of large variety of chemoreceptors with different selectivity, thus fitting the main requirement in the development of modern analytical systems based on pattern recognition.

Chiroselective binding sites have been created by application of the spreader-bar approach. Impedometric techniques and surface plasmon resonance were applied to detect binding. (R)-(+)-1,1'-binaphthyl-2,2'-diol (R-BNOH) and (S)-(-)-1,1'-binaphthyl-2,2'-diol (S-BNOH) were used as model analytes. The artificial receptors were prepared by co-adsorption of 1-hexadecanethiol with a thiol-modified chiral selector (conjugates of D,L-thioctic acid and (R)-(+)- or (S)-(-) 1,1'-binaphthyl-2,2'-diamine). Different concentration ratios of the matrix and spreader-bar were tested. No chiral selectivity of surfaces formed by either the matrix or the spreader-bars alone was observed. The gold electrodes coated by the spreader-bar technique displayed an enantioselectivity of up to 4.76.

The nanostructured monolayers of different types of spreader-bars with different size were investigated thoroughly by ellipsometry, photoelectron spectroscopy, near-edge X-ray adsorption fine structure spectroscopy, infrared adsorption spectroscopy, atomic force microscopy, contact angle measurements, voltammetry and electrochemical impedance spectroscopy. The results confirmed high-stability of monolayers, nanostructured by means of the spreader-bar technique within several months. Then the resulting complex materials formed by nanostructured monolayers were successfully used as chemical receptors and as molecular templates for electrochemical preparation of metallic nanoparticles.

It has been demonstrated that spreader-bar stabilized nanostructures can be used for reconstitution of biological membrane proteins (this is important for applications in drug discovery) and for template-defined synthesis of nanoparticles (can be important for development of chemo- and biosensors, electrocatalysers, organic electronic devices).



---

The laterally organized surfaces obtained by this technology, could be of importance for applications in many fields of biology and medicine, including, for example, development of new bioanalytical methods and new biocompatible surfaces, new approaches for investigation of biological ion pumps and high-throughput screening of chemical compounds. Not surprisingly, our first article where the concept of the spreader-bar system was presented was cited in over 30 articles and more than 20 reviews up to now.

## 7. Zusammenfassung

Thiolmodifizierte Purine und Pyrimidine, sogenannte *spreader-bar* Moleküle, bilden zusammen mit langkettigen Alkylthiolmolekülen (Matrixmoleküle) durch Selbstorganisation nanostrukturierte Monoschichten mit Rezeptoreigenschaften. Die Rezeptoreigenschaften können durch die Wahl des *spreader-bar* Moleküls gezielt gesteuert werden. Die so erzeugten Strukturen wurden mit den Techniken der Infrarotspektroskopie, Kontaktwinkelmessungen, Ellipsometrie, Impedanzspektroskopie und der zyklischen Voltammetrie eingehend charakterisiert. Es wurde gezeigt, dass die Bedingungen für die Erzeugung von künstlichen Rezeptoren mittels *spreader-bar* Technik nur einen kleinen Variationsbereich des *Spreader-bar*-/Matrixmoleküle Mischungsverhältnisses in der Beschichtungslösung zulassen. Nur dann befinden sich beide Molekülarten nach dem Beschichten auf der Goldoberfläche.

Ein Array bestehend aus fünf künstlichen Rezeptoren mit thiolmodifizierten Derivaten aus Adenin, Cytosin, Guanin, Thymin und Uracil als spreader-bar Moleküle erlaubte die Detektion verschiedener Purine und Pyrimidine. Die Ergebnisse zeigten, dass trotz geringer Selektivität eines einzelnen Rezeptors, ein Sensoren Array aufgebaut werden kann, der die zielsichere Erkennung der Basen der Nukleinsäuren, sowie von Coffein und Harnsäure benutzt werden kann. Diese erste Anwendung der spreader-bar Technologie zeigt deren Potential in der einfachen Erzeugung einer Vielzahl an Chemorezeptoren mit verschiedener Selektivität, die mit Hilfe der Mustererkennung in der Entwicklung von Sensoren hilfreich sein können.

Die spreader-bar Technik konnte auch benutzt werden um chiroselektive Rezeptoren zu erzeugen. Mittels Impedanzmessungen und SPR-Messungen wurde die Analytbindung detektiert. (R)-(+)-1,1'-Binaphthyl-2,2'-diol (R-BNOH) und (S)-(-)-1,1'-Binaphthyl-2,2'-diol (S-BNOH) dienten hierbei als Modellanalyten. Die künstlichen Rezeptoren wurden durch Coadsorption von 1-Hexadecanthiol zusammen mit einem thiol modifizierten chiralen Selektor (Konjugat aus D,L- $\alpha$ -Liponsäure und (R)-(+)- oder (S)-(-)-1,1'-Binaphthyl-2,2'-diamine) hergestellt. Verschiedene Mischungsverhältnisse von Matrixmoleküle und spreader-bar Molekülen wurden getestet. Monoschichten die nur aus Matrix- oder spreader-bar-Molekülen bestanden zeigten keinerlei chirale Selektivität. Mit gemischten Monoschichten bestehend aus beiden Molekültypen konnten künstliche Rezeptoroberflächen mit einer Enantioselektivität von bis zu 4.76 erhalten werden.

Eine grundlegende Charakterisierung verschiedener spreader-bar Systeme mittels XPS, Ellipsometrie, elektrochemischer Untersuchungen, NEXAFS, Kontaktwinkelmessungen und AFM zum besseren Verständnis der erzeugten Nanostrukturen wurde durchgeführt. Dabei konnte gezeigt werden, dass der Weg der Nanostrukturierung mittels Selbstorganisation vielversprechend und perspektiv ist, denn die erzeugten Strukturen konnten eine hohe zeitliche Stabilität und Funktionalität über Monate vorweisen. Die entstandenen komplexen Materialien, selbst organisierter monomolekularer Schichten haben sich

nicht nur modellhaft als Rezeptorelemente sondern auch als Templatstruktur zur Erzeugung von metallischen Nanopartikeln bewährt.

So konnte gezeigt werden dass spreader-bar stabilisierte Nanostrukturen erfolgreich für die Rekonstitution von biologischen Membranproteinen eingesetzt werden können. Dies kann z.B. in der Medikamentenentwicklung von Interesse sein. Ein Einsatz der erzeugten metallischen Nanopartikel nicht nur zur Entwicklung neuer Chemo- und Biosensoren, sondern auch im Bereich der Elektrokatalyse oder für den Aufbau organischer Elektronik ist denkbar.

Zusammenfassend kann festgestellt werden, dass die lateral organisierten Oberflächen, die mittels spreader-bar Technik erzeugt wurden, in vielen Bereichen, wie der Biologie, und Medizin, als auch zur Entwicklung bioanalytischer Methoden oder neuer biokompatibler Oberflächen, der Grundlagenforschung zum Verständnis biologischer Ionenpumpen, oder im Hochdurchsatz Screening chemischer Substanzen eingesetzt werden kann. Dass das Konzept der spreader-bar-Technologie Beachtung findet, zeigt sich in der Zitierung unseres ersten Artikels in über 30 Veröffentlichungen und über 20 Übersichtsartikeln in den letzten Jahren.

## **8. Experimental methods**

### **8.1 Sample preparation**

#### **8.1.1 Materials**

The gold substrates used as electrodes were fabricated by evaporation of 150 nm of gold on a silicon oxide layer of a silicon wafer previously coated by a Ti/Pd adhesion layer (25 nm). These gold electrodes, obtained from Bosch (Stuttgart, Germany) have a shape of a circle with a diameter of 700  $\mu\text{m}$  and they are connected by a line of 10  $\mu\text{m}$  width and 7 mm length to a contact pad of the size of 2 mm<sup>2</sup>. This geometry provides an active surface area of 0.38 mm<sup>2</sup>. The change in

the surface area by different height of the liquid in the measurement cell can be neglected [1].

For study of AFM also substrates of mica was used. Gold was evaporated with a thickness of 200 nm on mica previously by a Ti adhesion layer of 5 nm. These substrates were produced by University of Heidelberg.

Gold substrates used for SPR measurements were made out of glass with a refractive index of 1.61 and a thickness of 1 mm. The size was 20 mm x 20 mm. On an adhesion layer of chromium with a thickness of 5 nm a gold layer with thickness of 50 nm was evaporated. The gold coated glass slides for SPR were obtained from Mivitec (Regensburg, Germany).

Before using, all gold surfaces were cleaned by ultrasonication in chloroform and ethanol, followed by dipping in hot piranha solution (1:3 (v:v) mixture of H<sub>2</sub>O<sub>2</sub> 30% and sulfuric acid 96%). **Caution:** *piranha solution reacts very violently with organic material* [2]. After rinsing with water and drying in a stream of nitrogen, the gold substrates were dried and stored in a desiccator under reduced pressure.

## 8.1.2 Preparation of monolayers on gold

### 8.1.2.1 Monolayer consisting of purines or pyrimidines and alkanethiols

Monolayers were assembled by immersing the fresh cleaned gold substrates for three days in an ethanolic solution containing the thiol compounds. The adsorption was followed by rinsing with ethanol and drying in a stream of nitrogen. In the case of monolayers with GSH, the immersing solution consisted of saturated solution of GSH and 100  $\mu\text{mol}\cdot\text{L}^{-1}$  dodecanethiol. For other mixed monolayers, the immersing solution consisted of 10  $\text{mmol}\cdot\text{L}^{-1}$  thiol modified purines or pyrimidines and 100  $\mu\text{mol}\cdot\text{L}^{-1}$  dodecanethiol. Pure monolayers of dodecanethiol, ASH, CSH, THS and USH, respectively, were prepared by 12 h incubation at room temperature in ethanol solution containing 100  $\mu\text{mol}\cdot\text{L}^{-1}$  of the corresponding compound.

### **8.1.2.1 Monolayer consisting of chiroselectors and alkanethiols**

Artificial binding sites for R-BNOH and S-BNOH were created on fresh cleaned gold surfaces. For the preparation of the artificial receptors by the spreader-bar technique, the electrodes were immersed into a solution of 16-mercaptohexadecane and R- or S-conjugate in a 9:1 (v:v) mixture of ethanol and dioxane for 72 h at room temperature, then rinsed with ethanol, and dried under nitrogen [11]. Self-assembled monolayers of thioctic acid, R-conjugate, S-conjugate or 1-hexadecanethiol, were formed on the gold electrodes from a  $1 \text{ mmol}\cdot\text{L}^{-1}$  solution in ethanol (or in a 1:1 (v:v) mixture of ethanol and dioxane, in the case of R- or S-conjugates) for 12 h at room temperature, then rinsed with ethanol and dried under nitrogen. A statistical deviation of the initial capacitance of coated electrodes prepared in the same conditions was typically within 10%.

### **8.1.2.1 Monolayer consisting of porphyrines or phthalocyanines and alkanethiols**

The monolayers were prepared at room temperature by immersing the fresh cleaned gold substrates for 72 h in an ethanolic solution containing C12 and TMPP. The TMPP concentration in the solution was varied between  $15 \text{ }\mu\text{mol}\cdot\text{L}^{-1}$  and  $15 \text{ mmol}\cdot\text{L}^{-1}$  while the C12 concentration was kept constant at  $1.5 \text{ }\mu\text{mol}\cdot\text{L}^{-1}$ .

For the formation of the nanostructured templates for the metal deposition the TMPP concentration was  $1.5 \text{ mmol}\cdot\text{L}^{-1}$ .

The mixed monolayers of C16 and AlPC were prepared at room temperature by immersing the fresh cleaned gold substrates in an ethanolic solution of for 72 h. The concentration of AlPC in the solution was kept constant at  $250 \text{ }\mu\text{mol}\cdot\text{L}^{-1}$  while that of C16 was varied, being either  $25 \text{ }\mu\text{mol}\cdot\text{L}^{-1}$  (C16:AlPC =1:10) or  $2.5 \text{ }\mu\text{mol}\cdot\text{L}^{-1}$  (C16:AlPC =1:100). An increase of the Al-PC concentration above  $250 \text{ }\mu\text{mol}\cdot\text{L}^{-1}$  was not possible because of the solubility limitation.

### 8.1.3 Electrodeposition of platinum

Electrodeposition of platinum on spreader-bar coated electrodes was performed at constant potential of -25 mV vs. SCE from 2.5 mmol·L<sup>-1</sup> of hexachloroplatinic acid in 50 mmol·L<sup>-1</sup> KCl. The electrodeposition was carried out by AutoLab-PG-stat-12 Electrochemical Workplace (EcoChemie, Utrecht, TheNetherlands).

## 8.2 Analytical methods

### 8.2.1 Contact angle measurements

Contact angles were measured with a ERMA 20676 goniometer (Shinbunsha, Tokyo, Japan). It is important to have always the same volume of the droplet; therefore a syringe with high precision in the range of micro liters was used. The needle had a hypodermic flat end to form perfect round drops. When the drop was on the end of the needle the syringe was lowered until the drop has touched the surface. The needle is kept in the droplet (captive drop) and the contact angle was read immediately. When the drop was added the advancing contact angle ( $\theta_{advancing}$ ), when the drop was withdrawn, the receding contact angle ( $\theta_{receding}$ ) was measured.

If the drop has fallen from the needle, the obtained contact angles were significant smaller than by the method described above. Mechanical vibrations may cause this difference. It was not possible to get sufficient reproducibility for this second method. All values presented in this work were obtained by measuring with the needle remaining in the droplet.

Measurements of contact angles of non polar solvents like hexadecane were not taken into account. Because of the high wettability of the spreader-bar surfaces it was not possible to measure such small values precisely.



## 8.2.2 Electrochemical measurements

### 8.2.2.1 Capacitance Measurements

The electrode capacitance was measured by recording electrical current with a phase shift of 90° by means of a lock-in amplifier. In this work lock-in amplifiers from the type Stanford DSP 850 (Stanford Research, Sunnyvale, USA), Ithaco Dynatrac 391 A (DL Instruments, Ithaco, USA), PAR 121 (Princeton Applied Research Corp., Oak Ridge, USA) or Femto LIA-BV 150 (Femto Messtechnik, Berlin, Germany) was used.

For the measurements of the receptive properties in a sensor array, a set of five gold electrodes covered with different spreader bar molecules were put into a glass cell containing 3.5 mL of 10 mmol·L<sup>-1</sup> phosphate and 100 mmol·L<sup>-1</sup> KCl adjusted to pH 7.4. A homemade Ag/AgCl electrode (area more than 50 mm<sup>2</sup>) was used as a reference electrode. Binding events were detected as changes in capacitive current. It was measured in two-electrode configuration by parallel registration of the 90° component of the electrode current by means of 5 parallel lock-in amplifiers (Femto, Germany) at 80 Hz. Internal current amplifiers of these lock-in amplifiers were used. The current amplifiers were modified to provide an application of DC potential to gold electrodes. During the measurements, this potential was +300 mV (gold electrodes vs. Ag/AgCl). The amplitude of the sine voltage on the electrodes was 20 mV; an internal oscillator of one of the lock-in amplifiers was used. The measurement system was controlled by LabView software. Signal changes presented in the figures, were recalculated as relative decrease of the capacitive current, i.e.  $C = (i_{c0} - i_c) / i_{c0}$ , where  $i_{c0}$  is an initial value of the capacitive current, and  $i_c$  is this capacitive current after addition of purines or pyrimidines. The analyte concentration was increased step by step up to 440 μmol·L<sup>-1</sup>. All measurements were performed at 30°C.

All capacitive measurements for detection of the enantioselective binding properties of spreader-bar systems were performed with the same setup. As

electrolyte a solution of 15 mmol·L<sup>-1</sup> phosphate and 50 mmol·L<sup>-1</sup> KCl with *pH* 7.3 was used. The measurements were performed at room temperature.

#### **8.2.2.2 Impedance spectroscopy**

Impedance spectroscopy experiments were performed with the Frequency Response Analyzer 2 (PGSTAT12/FRA2, Eco Chemie, Utrecht, The Netherlands) in a three-electrode cell under quiescent conditions in the presence of 10 mmol·L<sup>-1</sup> ferricyanide in 50 mmol·L<sup>-1</sup> KCl, *pH* 7.2 as supporting electrolyte. A gold electrode was used as a working electrode, a saturated calomel electrode as a reference electrode, and a platinum wire as an auxiliary electrode. The impedance spectra were recorded in the frequency range from 1 Hz to 100 kHz by using a sinusoidal excitation signal. The DC potential was 0.3 V. Excitation amplitude of 10 mV was used.

#### **8.2.2.3 Cyclic voltammetry**

Cyclic voltammetry was measured with AutoLab-PG-stat-12 Electrochemical Workplace (EcoChemie, Utrecht, The Netherlands) in a three electrode configuration with a gold electrode used as a working electrode, a saturated calomel electrode as reference electrode, and a platinum wire as auxiliary electrode. The scan rate was 100 mV·s<sup>-1</sup>. All measurements were carried out in a buffer solution of 10 mmol·L<sup>-1</sup> phosphate, 100 mmol·L<sup>-1</sup> KCl, 10 mmol·L<sup>-1</sup> ferricyanide, *pH* 7.2, or in the same buffer containing 10 mmol·L<sup>-1</sup> rutheniumhexammin instead of ferricyanide. Before measurement, the solution was degassed in vacuum, and during measurement, the solution was bubbled with argon.

#### **8.2.3 SPR measurements**

Surface plasmon resonance (SPR) experiments were carried-out with the BIOSUPLAR-2 SPR-spectrometer (Analytical  $\mu$ -Systems, Germany) onto gold coated glass slides that had been coated via the above procedure.

All capacitive measurements were performed in 15 mmol·L<sup>-1</sup> phosphate, 50 mmol·L<sup>-1</sup> KCl, pH 7.3 at room temperature.

#### 8.2.4 NEXFAS, XPS Studies

Scanning electron microscopy (SEM) was done with a LEO SUPRA35 (Germany). The film characterization by XPS, NEXAFS spectroscopy was performed at room temperature and under UHV conditions (at base pressure better than 1.5·10<sup>-9</sup> mbar). The XPS and NEXAFS measurements were carried out at the HE-SGM beamline of the synchrotron storage ring BESSY II in Berlin, Germany. The energy resolution was 0.40 eV. The XPS spectra were acquired in normal emission geometry with a VG CLAM 2 analyzer. As an X-ray source, synchrotron light was used; the photon energy was chosen between 350 and 650 eV. The energy scale was referenced to the Au 4f<sub>7/2</sub> peak at a binding energy of 84.0 eV. The NEXAFS spectra were collected at the carbon K-edge in the partial electron yield mode with a retarding voltage of -150 V. Linear polarized synchrotron light with a polarization factor of 82% was used. The incidence angle of the light was varied to monitor the orientational order within the TMPP/C12 films. The raw NEXAFS spectra were normalized to the incident photon flux by division through a spectrum of a clean, freshly sputtered gold sample. The energy scale was referenced to the pronounced  $\pi_1^*$  resonance of highly oriented pyrolytic graphite (HOPG) at 285.38 eV. The spectromicroscopic characterization of the SAMs was performed at a microscopy branch (7.3.1.1) of the beamline 7.3.1 at the Advanced Light Source in Berkeley, USA, using an X-ray photoelectron emission microscope (X-PEEM), which operates in the total electron yield (TEY) acquisition mode and provides a spatial resolution of typically 50-100 nm for elemental contrast imaging. Other experimental details are described elsewhere [3 - 9].

### 8.2.5 Other techniques

All atomic force microscopy measurements were carried out at the Institute of Physical and Theoretical Chemistry at the University of Regensburg with an Autoprobe CP scanning probe microscope from Park Scientific Instruments (Sunnyvale, USA). The experimental setup is described in [10].

FTIR spectra and ellipsometric data were obtained at the Department of Physics and Measurement Technology at Linköping University in Sweden. A Bruker IFS 66 system (Billerica, USA) was used to measure the FTIR spectra at grazing angle of 85° and a liquid-nitrogen-cooled MCT detector [11]. The experimental details for ellipsometry are depicted in [12].

Scanning electron microscopy was done at the Institute of Experimental and Applied Physics at University of Regensburg, with a Topcon SM-510 microscope (Tokyo, Japan).

Optical microscopy was performed with a Leica DMRE microscope (Wetzlar, Germany).

## 8.3 Chemicals

All alkanethiols and AIPC were purchased from Sigma-Aldrich and used without further purification.

(R)-(+)-1,1'-binaphthyl-2,2'-diol (R-BNOH), (S)-(-)-1,1'-binaphthyl-2,2'-diol (S-BNOH), (R)-(+)-1,1'-binaphthyl-2,2'-diamine, (S)-(-)-1,1'-binaphthyl-2,2'-diamine, L-phenylalanine, D-phenylalanine and D,L-thioctic acid were purchased from Sigma. N,N'-dicyclohexyl-carbodiimide and N-hydroxysuccinimide were obtained from Aldrich.

Deionized water was additionally purified by passing it through a Millipore-Milli-Q system, the final resistivity being at least 18 M $\Omega$ ·cm<sup>-1</sup>. 'Milli-Q' (Millipore) water was used throughout.

Conjugates were prepared by mixing of 0.4 mmol·L<sup>-1</sup> DL-thioctic acid, 30 mmol·L<sup>-1</sup> of N,N'-dicyclohexyl carbodiimide, 30 mmol·L<sup>-1</sup> of N-hydroxysuccinimide and 0.2 mmol·L<sup>-1</sup> S- or R-BNH in dioxane (all the concentrations are referred to the final solution) and stirred for 5 days at room temperature. Then the mixture was centrifuged to remove the precipitate. A formation of the conjugates was indicated by thin layer chromatography (chloroform/methanol/water : 65/25/10 (v/v/v)) as an extra spots, besides that of S- or R-BNH, which was positive to both ELLMANN'S reagent and ninhydrin.

TMPP was fabricated from a precursor, 5,10,15,20-Tetrakis-(4-sulfonatophenyl)-porphyrin, which was purchased from Porphyrins Systems, a derivative of 5,10,15,20-tetrakis(4-sulfonatophenyl)-porphyrin. The sulfonato-groups of the latter compound were chemically reduced to thiol-groups by triphenylphosphine and iodine [13]; XPS detected two thiol groups pro resulting TMPP molecule.

Adenine, cytosine, guanine, thymine, uric acid, ATP were purchased from Aldrich. Caffeine was obtained from Avocado and uracil from Fluka. All chemicals were used as received. The alkanethiols and spreader bar compounds were dissolved in absolute ethanol (Baker) for preparing the SAM on the electrodes.

All other chemicals were from Merck or Aldrich with quality of analytical grade.

## 8.4 References

- [1] Riepl, M.; *New capacitive (bio)sensors based on self-assembled monolayers on gold and palladium*, **2000**, Dissertation, Universität Regensburg.
- [2] Dobbs, D. A.; Bergman, R. G.; Theopold, K. H.; *Chem. Eng. News* **1990**, 68 (17), 2 - 5.
- [3] Mirsky, V. M.; Hirsch, T.; Piletsky, S. A.; Wolfbeis, O. S.; *Angew. Chem. Int. Ed.*, **1999**, 38, 1108 - 1110.
- [4] Prodromidis, M. I.; Hirsch, T.; Mirsky, V. M.; Wolfbeis, O. S.; *Electroanalysis*, **2003**, 15, 1795 - 1798.
- [5] Stöhr, J.; *NEXAFS Spectroscopy*; Springer Series in Surface Science 25, **1992**, Springer-Verlag, Berlin.
- [6] Moulder, J. F.; Stickle, W. E.; Sobol, P. E.; Bomben, K. D. *Handbook of X-ray Photoelectron Spectroscopy*, **1992**, Chastian, J., Ed.; Perkin-Elmer Corp., Eden Prairie.
- [7] Batson, P. E.; *Phys. Rev. B* **1993**, 48, 2608 - 2610.
- [8] Zharnikov, M.; Grunze, M.; *J. Phys. Condens. Matter*. **2001**, 13, 11333 - 11365.
- [9] Zharnikov, M.; Ouchi, Y.; Hasegawa, M.; Scholl, A.; *J. Phys. Chem. B* **2004**, 108, 859 - 863.
- [10] Schnell, E.; *Rasterkraftmikroskopie als Methode zur Charakterisierung amphiphiler Strukturen*, **2002**, Dissertation, Universität Regensburg.
- [11] Valiokas, R.; Svedhem, S.; Östblom, M.; Svensson, S. C. T.; Liedberg, B.; *J. Phys. Chem. B* **2001**, 105, 5459 - 5469.
- [12] Tengvall, P.; Lundström, I.; Liedberg, B.; *Biomaterials* **1998**, 19, 407 - 422.
- [13] T. Oae, *Bull. Chem. Soc. Jpn.* **1984**, 57, 232 - 237.

## 9. Appendix

### 9.1 Fundamental physical constants

$c$	Speed of light in vacuum	$299792458 \text{ m}\cdot\text{s}^{-1}$
$e$	Elementary charge	$1.60217733\cdot 10^{-19} \text{ C}$
$F$	Faraday constant	$96485.309 \text{ C}\cdot\text{mol}^{-1}$
$h$	Planck constant	$6.6260755\cdot 10^{-34} \text{ J}\cdot\text{s}$
$R$	Molar gas constant	$8.314510 \text{ J}\cdot\text{mol}^{-1}\cdot\text{K}^{-1}$

*Non-SI units:*

$\text{eV}$	Electron volt	$1.60217733\cdot 10^{-19} \text{ J}$
-------------	---------------	--------------------------------------

### 9.2 Symbols

$\alpha$	Phase angle
$\gamma$	Angle between X-ray beam and electron beam
$\gamma$	Surface free energy
$\Delta$	Ellipsometric angle
$\theta$	Contact angle
$\theta_c$	Critical angle
$\theta_i$	Angle of incidence
$\lambda$	Mean free path length
$\mu$	Reduced mass

---

$\nu$	Frequency
$\nu$	Vibration quantum number
$\bar{E}$	Molar fraction
$\sigma_X^e$	Cross section for electron e of atom X
$\sigma$	Warburg impedance
$\phi$	Phase angle
$\Psi$	Ellipsometric angle
$\omega$	Angular frequency
$A$	Area
$B$	Instrumental constant
$C$	Capacitance
$c$	Concentration
$D$	Diffusion coefficient
$E$	Energy
$E$	Potential
$f$	Frequency
$G$	Admittance
$I$	Current
$I$	Intensity
$i$	Current
$k$	Spring constant
$L$	Angular asymmetry factor
$L$	Inductance
$N$	Atomic density
$n$	Refractive index
$R$	Resistance



---

<i>R</i>	Reflectance
<i>t</i>	Time
<i>W</i>	Work
<i>x</i>	Molar fraction
<i>Z</i>	Impedance

### 9.3 Abbreviations

AC	Alternating current
AFM	Atomic force microscopy
Al-PC	Aluminum 2,3-naphthophthalocyanine chloride
ASH	6-Mercaptopurine
ATP	Adenosine triphosphate
ATR	Attenuated total reflection
BNOH	1,1-Binaphthyl-2,2-diol
BNTA	1,1'-Binaphthyl-2,2'-diamin conjugated to DL-6,8-thioctic acid
BSE	Back-scattered electrons
C4	1-Butanethiol
C6	1-Hexanethiol
C8	1-Octanethiol
C12	1-Dodecanethiol
C14	1-Tetradecanethiol
C16	1-Hexadecanethiol
C18	1-Octadecanethiol
CPE	Constant phase element
CSH	4-Amino-2-mercapto-pyrimidine

---

CVD	Chemical vapor deposition
DC	Direct current
EIS	Electrochemical impedance spectroscopy
ESCA	Electron spectroscopy for chemical analysis
FTIR	Fourier transform infrared
GSH	2-Amino-6-purinethiol
IR	Infrared
LB-Film	Langmuir-Blodgett-Film
MBE	Molecular beam epitaxy
MP	6-Mercaptopurine
$\mu$ -CP	Microcontact printing
NEXAFS	Edge X-ray absorption fine structure
OTS	Octadecyltrichlorsilane
Phe	Phenylalanine
PVD	Physical vapor deposition
QCM	Quartz crystal microbalance
SA	Self assembly
SAM	Self assembled monolayer
SCE	Saturated calomel electrode
SE	Secondary electrons
SEM	Scanning electron microscope
SI	International Systems of Units
SPR	Surface plasmon resonance
STM	Scanning tunneling microscopy
TBA	2-Thiobarbituric acid
TCA	Thiocyanuric acid
TE	Transverse electric

---

TM	Transverse magnetic
TMPP	5,10,15,20-Tetrakis(4-sulfonatophenyl)-porphyrin partially thiol modified
TPD	Temperature programmed desorption
TSH	4-Hydroxy-5-methyl-2-mercaptopyrimidine
TUA	Thiouric acid
UHV	Ultra high vacuum
UPS	Ultraviolet photoelectron spectroscopy
USH	4-Hydroxy-2-mercaptopyrimidin
XAM	X-ray absorption spectromicroscopy
XPS	X-ray photoelectron spectroscopy

## 10. Curriculum Vitae

**Persönliche Angaben:** Geburtsort: Griesbach im Rottal, Landkreis Passau  
Geburtstag: 14. 01. 1969  
Familienstand: ledig

**Schulbildung:**

1989 Abitur, Wilhelm Diess Gymnasium Pocking

**Wehrdienst:**

1989 - 1990 3. Panzerbataillons 241, Kirchham

**Ausbildung:**

1990 - 1998 Studium der Chemie an der Universität Regensburg  
Diplomarbeit: *Neuartige künstliche Chemosensoren durch molekulare Architektur auf Goldoberflächen.*

1999 - 2001, 2003 - 2004, 2007 - 2008 Anfertigung der Dissertation am Institut für Analytische Chemie, Chemo- und Biosensorik an der Universität Regensburg  
Thema: *Nanostrukturierung selbstorganisierender Alkylthiol-Monoschichten auf Goldoberflächen.*

**bisherige Tätigkeiten:**

2001 - 2002, 2004 - 2006 freiberuflich tätig, als WebDesigner

**Kongressteilnahmen:**

Trends and New Applications of Thin Films 1998, Regensburg  
International Symposium on the Separation and Analysis of Proteins, Peptides and Polynucleotides Symposium of 1998, Wien  
ANAKON 1999, Konstanz  
Dt. BioSensor Symposium 2001, Tübingen  
Dt. BioSensor Symposium 2003, Potsdam  
XVII. EuroSensors 2003, Guimaraes, Portugal

**Patente:**

Mirsky, V. M.; Hirsch, T.;  
*Molecular imprinting with retaining the template molecule for applications as electrodes and other affinity surfaces.*  
PCT Int. Appl. (1999), WO: 9928047  
Mirsky, V.; Kettenberger, H.; Goedke, C.; Hirsch, T.;  
*Procedure and apparatus for degassing of liquid media.*  
Ger. Offen. (2003), DE 10163083 A1

## 11. List of publications

*Monomolecular Films of Phthalocyanines: Formation, Characterization, and Expelling by Alkanethiols.*

Hirsch, Thomas; Shaporenko, Andrey; Mirsky, Vladimir M.; Zharnikov, Michael;  
*Langmuir* **2007**, 23(8), 4373 - 4377.

*Size-controlled electrochemical synthesis of metal nanoparticles on monomolecular templates.*

Hirsch, Thomas; Zharnikov, Michael; Shaporenko, Andrey; Stahl, Joachim; Weiss, Dieter;  
Wolfbeis, Otto S.; Mirsky, Vladimir M.;  
*Angewandte Chemie, International Edition* **2005**, 44(41), 6775 - 6778.

*Enantioselective artificial receptors formed by the spreader-bar technique.*

Prodromidis, Mamas I.; Hirsch, Thomas; Mirsky, Vladimir M.; Wolfbeis, Otto S.;  
*Electroanalysis* **2003**, 15(22), 1795 - 1798.

*A simple strategy for preparation of sensor arrays: molecularly structured monolayers as recognition elements.*

Hirsch, Thomas; Kettenberger, Hubert; Wolfbeis, Otto S.; Mirsky, Vladimir M.;  
*Chemical Communications* **2003**, 3, 432 - 433.

*Capacitive detection of analyte binding in thin film chemo- and biosensors.*

Mirsky, Vladimir M.; Riepl, Michael; Mass, Markus; Hirsch, Thomas; Schweiss, Ruediger;  
Wolfbeis, Otto S.;  
*Advances in Science and Technology* **1999**, 26, 441 - 448.

*Intelligent nanostructures for biosensors and sensor arrays.*

Mirsky, Vladimir M.; Wrobel, Nadia; Riepl, Michael; Hirsch, Thomas; Wolfbeis, Otto S.;  
*BioTec* **1999**, 10(4), 28, 31 - 32.

*A spreader-bar approach to molecular architecture: formation of stable artificial chemoreceptors.*

Mirsky, Vladimir M.; Hirsch, Thomas; Piletsky, Sergey A.; Wolfbeis, Otto S.;  
*Angewandte Chemie, International Edition* **1999**, 38(8), 1108 - 1110.

**In preparation:**

*Spreader-bar structures as artificial receptors.*

Hirsch, Thomas; in *Artificial Receptors for Chemical Sensors*, Eds.: Mirsky, Vladimir M.; Yatsimirsky, Anatoly K.; **2009**, Wiley - VCH, Weinheim.

*Kinetic Investigation of spreader-bar systems: experiments and theoretical models.*

Portnov, Vladimir I.; Hirsch, Thomas; Mirsky, Vladimir, M.

*Kinetics of microcontact printing.*

Stempfhuber, Thomas; Hirsch, Thomas; Mirsky, Vladimir M.